Final Master Thesis

Màster Universitari d'Enginyeria Industrial (MUEI)

Technical Design and Business Plan for a Light Energy Generation Module

Author: Jordi Sarradell Laguna
Director: Emilio Hernández Chiva
Date :   September 2019

ETSEIB

Escola Tècnica Superior
d'Enginyeria Industrial de Barcelona

Universitat Politècnica de Catalunya

UPC

Abstract

The aim of this project is to design a solar charger to be used in places where the access to electricity is limited or non-existent and there is a great need to provide electricity to electronic devices such as smartphones, tablets or laptops.

This paper presents the basic theoretical principles and equations to model the main components of the solar portable generator, as well as the power electronics needed to perform quality battery charges without damaging the electronic devices. The paper also presents a selection of real components to build the solar charger, specifying sizes and materials used.

In addition to the technical design itself, a business plan is also developed in order to commercialize the portable solar charger through a digital platform (downloadable application). The business plan includes the value proposition, the business model, the strategic partners, the monetization policy, future revenue projections and the financial plan for the first three years of operation.

By delivering all these outcomes, the main purpose of the project is to set the fundamental bases for the creation of a start-up company dedicated to deliver energetical services using renewable energies in order to satisfy real life needs in a sustainable way.

Contents

ETSEIB

1. Nomenclature

Photoelectric Effect

$E\ [J] \rightarrow Energy\ of\ the\ absorbed\ photons$

$K_{max}\ [J] \rightarrow Maximum\ kinetic\ energy\ of\ the\ ejected\ photoelectrons$

$\phi\ [J] \rightarrow Work\ function.\ Amount\ of\ energy\ needed\ to\ lift\ an\ electron\ out\ of\ the\ surface$

$\nu\ [s^{-1}] \rightarrow Electromanetic\ frequency\ of\ the\ absorbed\ photons$

$\nu_0\ [s^{-1}] \rightarrow Threshold\ frequency$

$\lambda\ [m] \rightarrow Electromagnetic\ wavelength\ of\ the\ absorbed\ photons$

$\lambda_0\ [m] \rightarrow Threshold\ wavelegnth$

$V_0\ [V] \rightarrow Stopping\ voltage$

$h\ [Js] \rightarrow Planck\ constant$

$e\ [C] \rightarrow Electric\ charge\ of\ an\ electron$

$c\ [m/s] \rightarrow Speed\ of\ light$

Energy Band Theory and Semiconductors

$E_g\ [J] \rightarrow Energy\ gap\ (E_g \cong 1.12\ eV\ in\ silicon)$

$E_c\ [J] \rightarrow Lowest\ energy\ level\ in\ conduction\ band$

$E_v\ [J] \rightarrow Highest\ energy\ level\ in\ valence\ band$

$N_n(E)[m^{-3}] \rightarrow Density\ of\ states\ for\ free\ electrons\ in\ conduction\ band$

$N_p(E)[m^{-3}] \rightarrow Density\ of\ states\ for\ free\ holes\ in\ valence\ band$

$m_n^*, m_p^*[kg] \rightarrow Effective\ mass\ of\ the\ electron\ anf\ hole, respectively$

$k\ [JK^{-1}] \rightarrow Boltzmann\ constant$

$E\ [J] \rightarrow Energy\ level\ of\ the\ state$

$E_F [J] \rightarrow Fermi\ Energy\ Level$

$T\ [K] \rightarrow absolute\ temperature\ of\ the\ thermodynamic\ state$

$f_C(E) \rightarrow probability\ of\ occupation\ of\ an\ electron\ (negative\ charge\ carrier)$

$f_V(E) \rightarrow probabilty\ of\ occupation\ of\ a\ hole\ (positive\ charge\ carrier)$

$n\ [m^{-3}] \rightarrow concentration\ of\ electrons\ in\ conduction\ band\ (electrons\ density)$

$p\ [m^{-3}] \rightarrow concentration\ of\ holes\ in\ valence\ band\ (holes\ density)$

$n_i\ [m^{-3}] \rightarrow intrinsic\ concentration\ of\ carriers\ (intrinsic\ carriers\ density)$

$N_A^-\ [m^{-3}] \rightarrow concentration\ of\ acceptor\ impurities$

$N_D^+\ [m^{-3}] \rightarrow concentration\ of\ donor\ impurites$

The p-n junction

$J_{df,n}, J_{df,p}\ [Am^{-2}] \rightarrow diffusion\ current\ density\ of\ the\ charge\ carriers$

$J_{dr,n}, J_{dr,p}\ [Am^{-2}] \rightarrow drift\ current\ density\ of\ the\ charge\ carriers$

$D\ [m^2/s] \rightarrow diffusion\ coefficient\ or\ diffusivity$

$V_t\ [V] \rightarrow voltage\ equivalent\ of\ temperature$

$\mu\ [ms^{-1}V^{-1}] \rightarrow electron\ mobility\ in\ the\ medium$

$E_{bi}\ [V/m] \rightarrow built-in\ electric\ field$

$V_{bi}\ [V] \rightarrow built-in\ voltage$

$\sigma_n, \sigma_p\ [S/m \equiv A/V] \rightarrow conductivity\ of\ the\ charge\ carriers$

$W\ [m] \rightarrow depletion's\ layer\ width$

$V_{bias}[V] \rightarrow external\ voltage\ applied\ to\ a\ p-n\ junction$

$\varepsilon_{SC}\ [F/m] \rightarrow permittivity\ of\ the\ semiconductor\ material$

PV Solar Cell

$\alpha \ [m^{-1}] \rightarrow absortion \ coefficient$

$x \ [m] \rightarrow depth \ in \ the \ solar \ cell$

$G_L \ [m^{-3}] \rightarrow photo \ generation \ rate$

$N_0 \ [m^{-2}s^{-1}] \rightarrow photon \ flux \ at \ the \ surface$

$I_{ph} \ [A] \rightarrow photo \ generated \ current$

$I_d \ [A] \rightarrow direct \ current \ in \ the \ diode$

$I_{sh} \ [A] \rightarrow leakage \ current \ (losses \ in \ the \ parallel \ branch)$

$R_s \ , R_{sh} \ [\Omega] \rightarrow respectively, series \ and \ shunt \ resistance$

$G, G_{ref}, G_n \ [W/m^2] \rightarrow real, reference \ and \ normal \ irradiances$

$T_c, T_{c,ref}, T_{c,n} \ [K] \rightarrow real, reference \ and \ normal \ cell \ operation \ temperatures$

$I_{sc} \ [A] \rightarrow short \ circuit \ current$

$V_{oc} \ [V] \rightarrow open \ circuit \ voltage$

$K_{ti} \ [A/K] \ , K_{tv} \ [V/K] \rightarrow respectively, temperature \ coefficients \ for \ I_{sc} \ and \ V_{oc}$

$I_o \ , I_{o,ref} \ [A] \rightarrow respectively, real \ and \ reference \ inverse \ saturation \ current \ in \ the \ diode$

$\eta_d \ [adim.] \rightarrow ideality \ factor \ of \ the \ diode$

$(V_{mp} \ [V] \ , I_{mp} \ [A]) \rightarrow maximum \ power \ point \ (MPP)$

$P_{mp} \ [W] \rightarrow maximum \ power$

$FF \ [adim.] \rightarrow Fill \ Factor$

$\eta \ [admi.] \rightarrow solar \ cell \ efficiency$

$A \ [m^2] \rightarrow area \ of \ the \ solar \ cell \ surface$

$N_p \ [adim.] \rightarrow number \ of \ cells \ connected \ in \ parallel \ in \ a \ module$

$N_s \ [adim.] \rightarrow number \ of \ cells \ connected \ in \ series \ in \ a \ module$

Lithium-ion batteries

C_n [Ah] → $nominal\ capacity\ of\ the\ battery$

V_{REG} [V] → $constant\ voltage\ applied\ during\ the\ absortion\ phase\ (cut-off\ voltage)$

I_{REG} [A] → $constant\ current\ applied\ during\ the\ bulk\ phase$

SOC [$\%$] → $state\ of\ charge$

Power electronics

V_{PV} [V], I_{PV} [A] → $voltage\ and\ current\ provided\ by\ the\ PV\ array$

V_{in} [V], I_{in} [A] → $input\ voltage\ and\ current\ of\ DC/DC\ converter$

V_{out} [V], I_{out} [A] → $output\ voltage\ and\ current\ of\ DC/DC\ converter$

D [$adim.$] → $duty\ cycle$

t_{ON} [s] → $time\ when\ the\ transistor\ is\ ON\ in\ a\ commutation\ period$

T_c [s] → $commutation\ period\ in\ a\ DC/DC\ converter$

N_{USB} [$adim.$] → $number\ of\ USB\ outlets\ in\ the\ solar\ charger$

ETSEIB

2. Preface

2.1. Origin of the Project and Motivations

Since I started my studies in engineering, I have been developing an increasing interest in renewable energy systems. My first approach to the renewable energy generation systems was in February 2016, when I started a project directed by professor Oriol Gomis Bellmunt which consisted in the design of an autonomous microgrid based in wind power generation and a pump-turbine hydroelectric storage system in an isolated island located in the Cabo Verde archipelago. This project wasn't as detailed as I would like in the technical aspects because I had only been studying renewable energy systems for three months, but it was a good way to introduce myself in this field of knowledge.

After that, I moved to the Netherlands and I started a group project in the TU Delft University about modeling an autonomous solar powered microgrid for 50 households and simulate its behavior under different conditions. Thanks to that project I developed advanced skills in power systems simulation using the *Matlab-Simulink* software package, among others.

I decided to do my Bachelor Final Thesis about the design and simulation of a grid connected microgrid with solar generation, batteries and a Low Voltage Direct Current (LVDC) generation system, which introduced me in the field of advanced power electronics. Finished my bachelor, I decided to specialize in Energy.

While doing my MSc in engineering, I also enrolled in a postgraduate course about business applied to technology and I worked in an Electric Supply Company for seven months, getting in touch with the real application in the market of the technologies that I had been previously studying. That experiences made me increase my interest in real and innovative business applications, so I decided to focus my Master Final Thesis on developing a business model around a renewable energy generation system in order to solve a real need.

My idea fitted perfectly with the topic that professor Emilio Hernández had proposed, so I decided to pick it and start to work on it.

2.2. Required knowledge and skills

In order to do this project, I have applied the background knowledge acquired during my studies in engineering and in business development. The fundamental topics are:

- Photovoltaic systems

- Power electronics and converters

- Dynamical systems and controllers

- Energy, electronic and control systems simulation (Matlab-Simulink, HOMER, OrCAD, LTspice)

- Business and financial planning

- Future Revenue Projections

3. Introduction

This idea of this project is born after the identification of a real problem which creates a need in the market that can be solved with photovoltaic technology, generating a business opportunity. The introduction aims to define that problem and stablish the objectives and the scope of the project.

3.1. Definition of the problem and Objectives

Problem:

The problem to be solved in this project was identified from my own experience and after asking for the opinion of 15 different young people (age between 20-28 years old) about it. What they all had in common was the fact that they often go to music festivals or other outdoor activities that last several days, like motorsport events.

If you go to an outdoor activity that lasts more than two or three days, you are at high risk that your electronic devices (smartphones, tablets, laptops) run out of battery. This is due to the difficult access to electricity that these places have and to the short battery life of these devices, which rarely exceed 24 hours even if excessive use is not made. This fact can be a serious problem since someone may need to use the electronic device for something important or urgent (for example: getting lost, looking for a specific friend or others).

This problem creates a clear need in the people involved in these situations: charging their smartphones (or other electronic devices) as soon as possible without connecting them to the electric grid. Photovoltaic energy is a good solution to solve this problem, satisfying the need.

Objective:

The main objective of this project is to create a start-up company that can satisfy the need of charging electronic devices in places without access to the electric grid in a short period of time by using a photovoltaic energy generation system, making life easier for the clients that use our service.

Like all private companies, another principal objective is to create a business which is economically viable, can deliver value to their clients and can have a positive net profit in the medium term.

3.2. Scope

The scope of the project stablishes which tasks are going to be made and which ones are not. It is very important to define the scope precisely in order to determine the time and resources needed.

In scope:
- Detailed explanation of the theoretical background of a solar charger
- Design and simulation of a Minimum Viable Product (MVP) for the solar charger:
    o Design the general electric scheme
    o Identify and select the components
    o Design the simulation model for the power electronics
    o Simulate the system under different conditions
- Qualitative explanation of the subsequent improvements to be made in the MVP in order to develop the Final Product.
- Business Plan:
    o Business Model and Value Proposition (brand creation, key partnerships, monetization policy, etc)
    o Future Revenue Projection – Economic study of the project
- Environmental Impact

Out of scope:
- Product external design – 3D modelling of the solar charger
- Build the prototype of the solar charger
- Develop the digital platform for the commercialization of the product/service
- Set the company, contact the strategic partners, fundraising

4. State of the Art

4.1. Photovoltaic Principles

Definition of photovoltaic: adj. Providing a source of electric current under the influence of light or similar radiation. [1]

4.1.1. The Photoelectric Effect (from Becquerel to Einstein)

Edmond Becquerel appears to have been the first to experience the photoelectric effect. In 1839, he generated electricity by illuminating Pt electrodes with different types of light. Best results were obtained with blue or ultraviolet light and when electrodes were coated with light sensitive material such as AgCl. As it can be observed in *Figure 4.1*, the electrodes were submerged in a conductive acidic solution and, when illuminated, voltage and current was generated. [2].
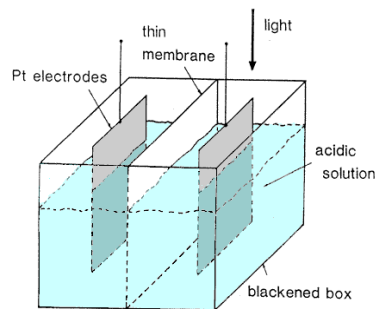

Figure 4.1. Diagram of "apparatus" described by Becquerel

In 1877, Adams and Day observed the photoelectric effect in an all solid-state system by running the next experiment [*Figure 4.2*]. They pushed two heated platinum contacts into opposite ends of small cylinders of vitreous selenium, tucked into a vacuum glass tube. Their intention was to prove that it was possible to create a current in the selenium merely by the action of light, and the result was positive. [1]
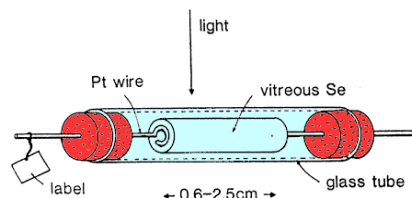

Figure 4.2. Sample geometry used by Adam and Day for the experiment.

In 1887, soon after discovering radio waves, Heinrich Hertz observed that when ultraviolet light from the sparks of his radio wave generator fell on the negative electrode of his radio wave detector, they induced a flow of electricity in the gap between the electrodes. He finally discovered that light of sufficiently short wavelength causes the emission of charge from a metal surface, but he didn't try to explain this effect. [3]

In 1897, Joseph John Thompson discovered the electron by experimenting with a cathode ray tube [*Figure 4.3*], demonstrating that cathode rays were negatively charged. He discovered this by applying electric field in the path of cathode ray and observing that the ray was deflected towards positively charged plate. Hence cathode ray consists of negatively charged particles. Thomson was also able to determine the charge-to-mass ratio of the electron. Today, the accepted value of e/m is $1,7588196 \cdot 10^{11}$ C/kg. [3]
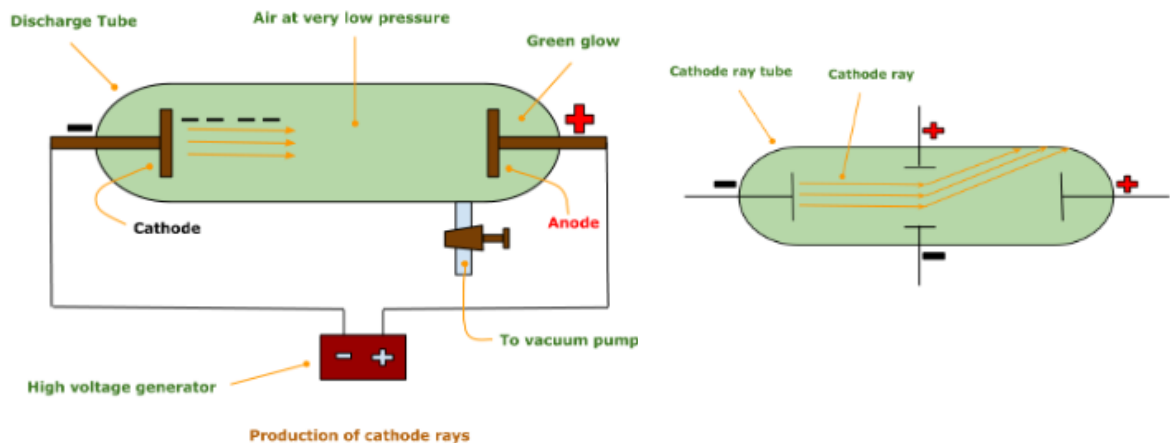

Figure 4.3. Cathode ray tube. Left, without deflection. Right, rays deflected by an electric field

.

Philipp Lenard, an assistant of Hertz who continued with his work, discovered in 1902 that charge-to-mass (e/m) ratio of the emitted charge from a metal surface when it was illuminated was identical to that of the electrons which has recently been discovered by J. J. Thompson. [ref. The Photoelectric Effect, MIT] He proved it by running the next experiment [Figure 4.4]. He used metal surfaces that were held under a vacuum. The metal sample (photoemissive) was housed in an evacuated glass tube with a second metal plate (photoreceptive) mounted at the opposite end. The tube was then positioned in some manner so that light would only shine on the first metal plate. Such a tube is called a photocell. Lenard connected his photocell to a circuit with a variable power supply, voltmeter, and microammeter. He then illuminated the photoemissive surface with light of differing frequencies and intensities. Knocking electrons free from the photoemissive plate

would give it a slight positive charge. Since the second plate was connected to the first by the wiring of the circuit, it too would become positive, which would then attract the photoelectrons floating freely through the vacuum where they would land and return to the plate from which they started.
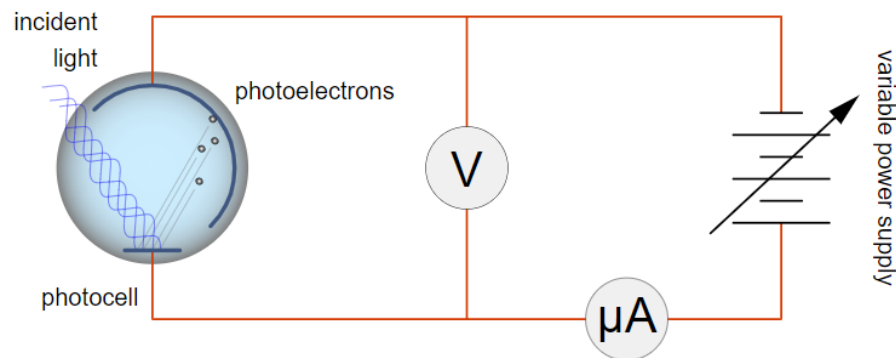

Figure 4.4. Lenard's photocell diagram

Lenard concluded that electrically charged particles are liberated from a metal surface when it is illuminated and that these particles are identical to electrons (also called photoelectrons in this case). [4]

The next relevant discovery about the photoelectric effect was made in 1914 by Robert Millikan. He found that light with frequencies below a certain cutoff value, called the *threshold frequency* (which depends on the material), would not eject photoelectrons from the metal surface no matter how bright the source was [*Figure 4.5*]. These results were unexpected for classical physicists. Given that it is possible to move electrons with light and given that the energy in a beam of light is related to its intensity, classical physics would predict that a more intense beam of light would eject electrons with greater energy than a less intense beam no matter what the frequency. This was not the case. [4]
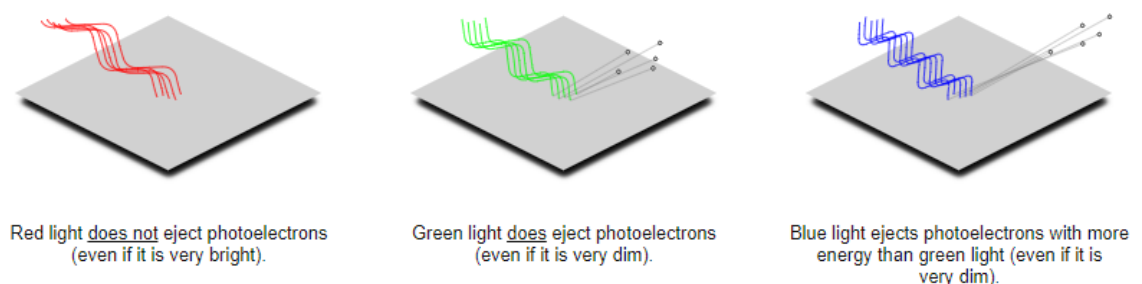

Red light does not eject photoelectrons (even if it is very bright).

Green light does eject photoelectrons (even if it is very dim).

Blue light ejects photoelectrons with more energy than green light (even if it is very dim).

Figure 4.5. Milikan's Discovery

After Milikan's discovery, classical physics was not able to explain the photoelectric effect anymore because the classical model of light as a transverse, electromagnetic wave was not applicable to these next two facts:

- Maximum kinetic energy of the released electrons did not vary with the intensity of the light, but was proportional instead to the frequency of the light.

- There was virtually no time lag between the arrival of radiation and the emission of electrons.

In 1900, German theoretical physicist Max Planck revolutionized the field of physics by discovering that energy does not flow continuously but is instead released in discrete packets. His discovery ended the primacy of what many people now call "classical physics" in favor of the study of quantum physics.

Planck's hypothesis: "*the energy associated with the radiation of a given frequency takes only multiple values of an elementary quantum that is proportional to the frequency of the radiation.*" The proportionality constant between the frequency of the radiation and its elementary is known as Planck's constant (h)

This hypothesis was used by Albert Einstein to discover the "*the law of photoelectric effect*" in 1905. If Planck's hypothesis is taken as a given, it means that matter radiates its energy in quanta of energy ($E = h \cdot \nu$). Einstein postulated that light delivers its energy to an absorber in quanta with energy ($E = h \cdot \nu$). Thus, if it takes an amount of energy to lift an electron out of the surface and away from its image charge (also called work function, ϕ), then the maximum kinetic energy (K_{max}) of the ejected electron is:

$$K_{max} = E - \phi = h \cdot \nu - \phi = h \cdot (\nu - \nu_0) \; [eq.1]$$

Being $E = h \cdot \nu$ the energy of the absorbed photons with frequency ν, being $\phi = h \cdot \nu_0$ the work function with threshold frequency ν_0 and being $h \cong 6{,}626 \cdot 10^{34} \, Js$ the Planck's constant.

Using fundamental equations from electrostatics and electromagnetic radiation:

$$c = \nu \cdot \lambda \; [eq.2] \qquad \Delta V \cdot q = W \rightarrow V_0 \cdot e = K_{max} \; [eq.3]$$

We can express *eq.1* like:

$$V_0 = \frac{h}{e} \cdot (\nu - \nu_0) = \frac{h \cdot c}{e} \cdot \left(\frac{1}{\lambda} - \frac{1}{\lambda_0} \right) \; [eq.4]$$

Being $q = e = -1{,}6 \cdot 10^{-19} \, C$ the electric charge of an electron, $c \cong 3 \cdot 10^8 \, m/s$ the speed of light, λ and λ_0 the wavelength of the absorbed photons and the threshold wavelength, respectively. Also being V_0 the stopping potential (the potential necessary to stop any electron, even the one with the most kinetic energy, from reaching the other side). If we apply

a negative potential on the photoemissive plate, the electrons will not approach so easily. Only the electrons with sufficient energy and hence, velocity, will be able to surpass this opposing potential (also called retarding potential) of the plate. If we keep on increasing this negative retarding potential, there will be one point when no more electrons reach this plate and thus, no electron flows through the circuit. Thus, current flow through the circuit stops [*Figure 4.6*].
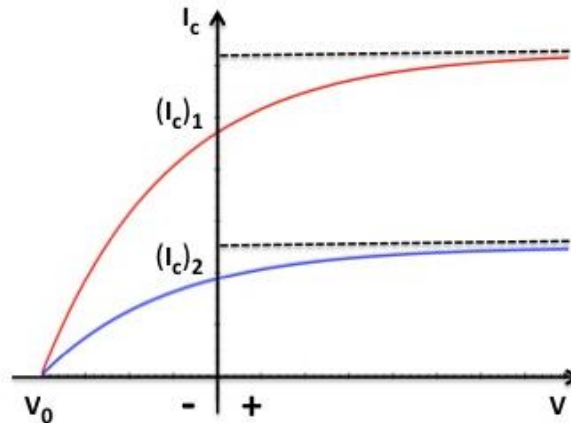

Figure 4.6. Evolution of the current flow for different voltage values in a photocell circuit. V_o is the stopping potential, so no current is generated for higher negative values of V. The light intensity of the red curve is higher that the light intensity of the blue curve.

In 1916, Robert Millikan verified Einstein's equation and showed with high precision that the value of Einstein's constant h was the same as Planck's constant. [3] [4]

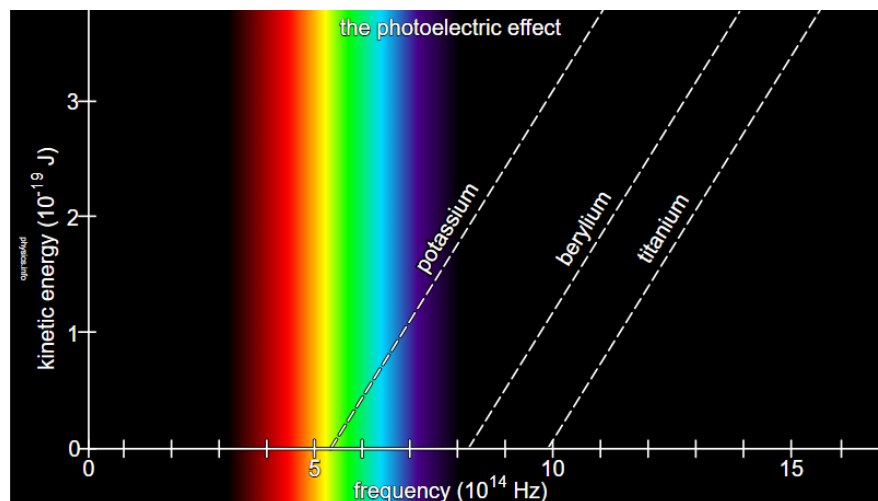The photoelectric effect is summarized in [*Figure 4.7*][4]

Figure 4.7. Kinetic energy of the photoelectrons ejected for different frequency values. Different materials have different threshold frequency values. The gradient of the curve equals the Planck's constant.

The photoelectric effect is the fundamental theory for the direct conversion of solar energy

into electricity, so it is the basis of photovoltaic technology.

4.1.2.   Semiconductor materials

Bohr Atomic Model

In 1911, Ernest Rutherford provided conclusive proof of the inadequacy of the Thompson atomic atom based on the results of a series of experiments carried out by Hans Geiger and Ernest Madsen. The most relevant experiment is the one in which a collimated beam (parallel rays, so minimum dispersion of the rays as they propagate) of alpha particles ($\alpha = He_2^4$) strike a gold foil. They found that few alpha particles were scattered at large angles. Rutherford concluded that instead of being spread throughout the atom, the positive charge is in fact concentrated in a very small region at the center of the atom called nucleus, around which the negatively charged electrons (much lighter) circulate in orbits. [5]
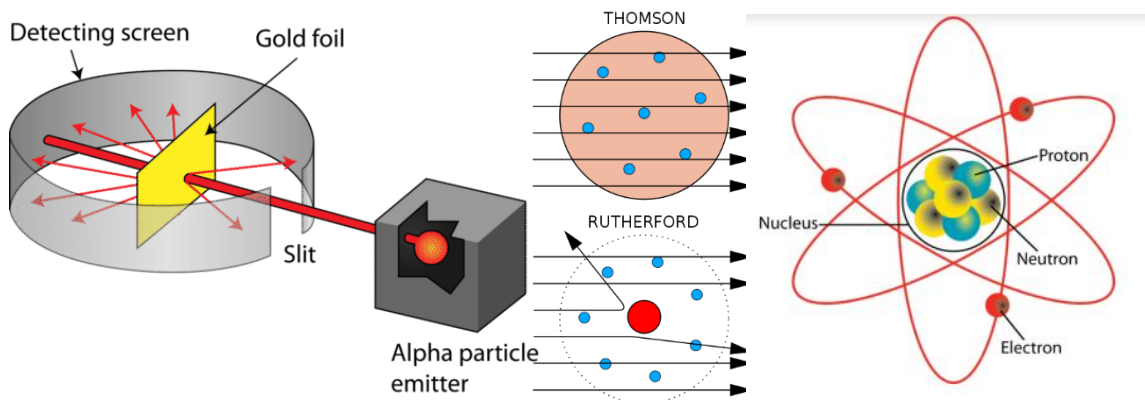

Figure 4.8. Left, gold foil experiment. Middle, Thompson vs. Rutherform model. Right, Rutherford planetary model of the atom.

The Rutherford atomic model had one major problem; the atoms were unstable because the negatively charged electron could fall into the nucleus. Thus, an atom would rapidly collapse to nuclear dimension. In 1913, Niels Bohr applied Planck and Einstein's quantum physics to Rutherford model and came up with a simple model of atomic structure.

Bohr model is based in the next four postulates:

1- Atomic electron move in circular orbits about a massive nucleus under the influence of the Coloumb attraction between the electron and the nucleous, obeying laws of classical mechanics. → based in Rutherford model
2- Instead of the infinity of orbits which would be possible in classical mechanics, an electron can in fact only move in an orbit for which its angular momentum L is quantized (integral multiple of an elementary energy state) → based in Planck's quantum hypothesis.

3- Electrons can only gain or lose energy by jumping from one allowed orbit to another, absorbing or emitting eectromagnetic radiation with frequency v, determined by the energy difference of the level [*eq. 5*] → based in Einstein's postulate.

$$\Delta E = E_f - E_i = h \cdot v \ [eq. 5]$$

4- An electron moving in such an allowed orbit does not radiate electromagnetic energy → Bohr's original postulate

Since the Bohr model could well explain the spectra of atoms with one valence electron, it had a domain of applicability. So, it could not be entirely wrong and would have to correspond in some way with another, possibly more successful theory. [5]
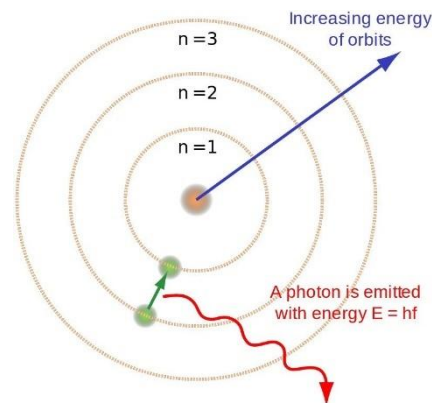

Figure 4.9. Bohr Atomic Model

Energy Band Theory

Between 1915 and 1930, several important discoveries were made in the fields of quantum physics:

- 1916: Arnold Sommerfield postulates the Sommerfield Atomic Model based on Bohr Model
- 1924: Louis-Victor de Broglie postulates the Wave-Particle duality theory
- 1925: Wolfgang Pauli postulates the Pauli Exclusion Principle
- 1925: Erwin Schrödinger postulates the Schrödinger equation, which describes the wave function of a mechanical system.
- 1926: Erwin Schrödinger postulates the Schrödinger Atomic Model.
- 1926: Enrico Fermi and Paul Dirac postulate Fermi-Dirac quantum statistics.
- 1927: Enrico Pauli corrects Schrödinger equation and Atomic Model, postulating Schrödinger-Pauli equation and Atomic Model.
- 1927: Werner Heisenberg postulates Heisenberg Uncertainty Principle

This theoretical framework is soon applied to solid-state physics:

- 1927: Arnold Sommerfield postulates the Free Electron Model, which explains the behavior of charge carriers in a metallic solid.

- Free Electron Model evolves to Nearly Free Electron Model, which enables understanding and calculating the electronic band structure of especially metals.

The basis for discussing transport in semiconductors is the underlying electronic band structure of the material arising from the solution of the Schrödinger equation. In isolated atoms, the electrons are orbiting around their nuclei with certain energy levels. When isolated atoms are brought together, to form a solid, various interactions (due to attraction and repulsion forces) occur between neighboring atoms. As a consequence of these interactions, the energy levels of individual atoms are transformed into common energy bands. The energy band structure of a solid describes ranges of energy that an electron is forbidden or allowed to have. [6]

As the electron clouds of individual atoms in a solid are overlapped, electrons of higher energies are no longer belonging to a specific atom (free electrons). In contrast, the electrons that are found in the lower energy levels are somewhat tightly bound to their nuclei (non-free electrons). In fact, the original discrete energy levels of such electrons are split into dense groups of adjacent levels that we called energy bands. These dense groups of levels (or energy bands) are belonging to the crystal rather than to individual atoms. Usually, these energy bands are separated by successive forbidden regions, that we call energy gaps *[Figure 4.10]*. [6]
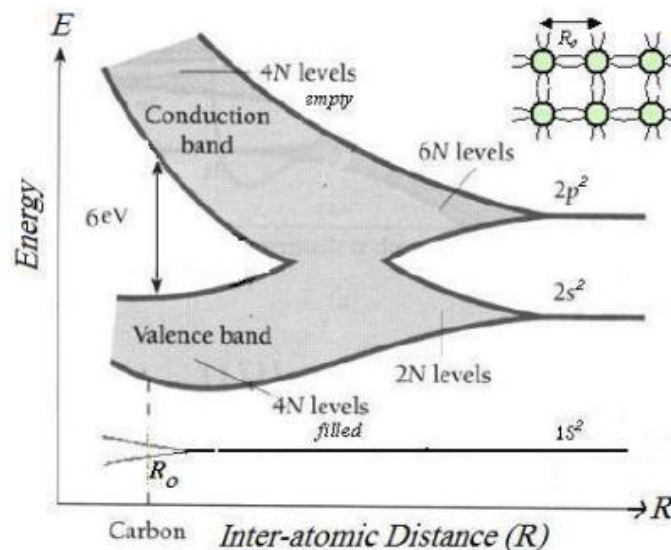

Figure 4.10. Schematic of energy level splitting and formation of energy bands in a diamond crystal of N atoms as a function of interatomic distance R. The distance R_0 is the interatomic separation at the state of equilibrium between atomic forces. For high R values, atoms are isolated and have discrete energy levels.

The highest filled energy band, in the energy band diagram, is usually called: valence band. Also, the energy band just above the valence band is called the conduction band. The

valence and conduction band are separated by a region called the energy gap (E_g). The height of the energy gap is given by:

$$E_g = E_c - E_v \ [eq.\,6]$$

Being E_c the lowest energy level in the conduction band and E_v the highest energy level in the valence band. [6]
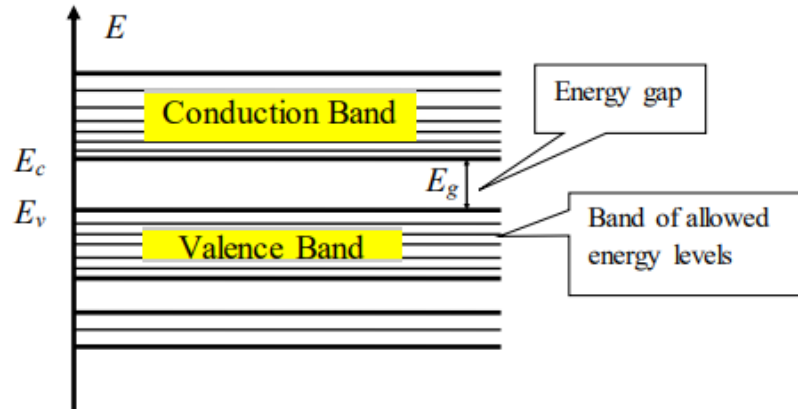

Figure 4.11. Schematic of the energy band diagram (versus crystal spatial position).

Conductors, Semiconductors and Insulators

The classification of the crystalline solid depends on the configuration of its band structure [Figure 4.12]:

- Conductors: Metals are conductors. There is no band gap between their valence and conduction bands, since they overlap. There is a continuous availability of electrons in these closely spaced orbitals. → charge carriers: electrons
- Semiconductors: Semiconductors have a small energy gap between the valence band and the conduction band. Electrons can make the jump up to the conduction band, but not with the same ease as they do in conductors. → charge carriers: electrons and holes
- In insulators, the band gap between the valence band and the conduction band is so large that electrons cannot make the energy jump from the valence band to the conduction band. → charge carriers: none [7]
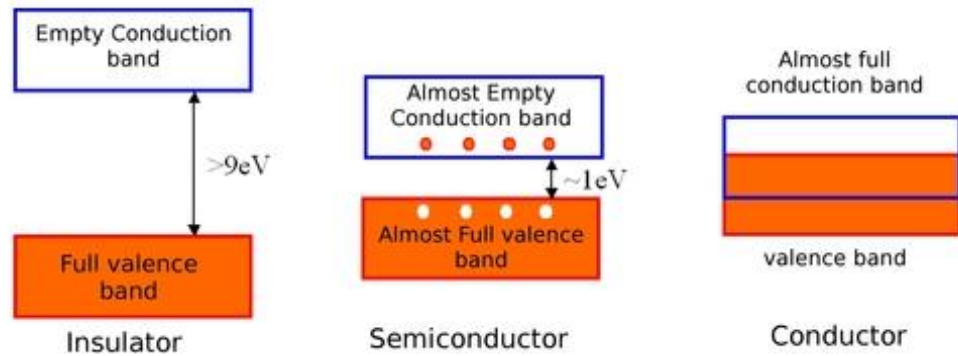
ETSEIB

Figure 4.12. Type of crystalline solid depending on its band structure.

Charge Carriers

A charge carrier is a particle or quasiparticle that is free to move, carrying an electric charge. Examples are electrons, ions and holes. In a conducting medium, an electric field can exert force on these free particles, causing a net motion of the particles through the medium; this is what constitutes an electric current. [7]

The electrical conductivity of a material depends on the number of charge carriers (i.e., free electrons and free holes) per unit volume (charge carrier density) and on the rate at which these carriers move under the influence of an electric field. [8]

To determine the charge carrier density, it is necessary to define two solid-state physics concepts: density of states and probability of occupation.

- Density of states (DOS): describes the number of states that are available to be occupied by the system at each level of energy, and it is noted as a function $N(E)$. For a crystalline semiconductor the functions are:

$$N_n(E) = \frac{\pi}{2}\left(\frac{8m_n^*}{h^2}\right)^{3/2}\sqrt{E - E_C} \ [eq.7] \qquad N_p(E) = \frac{\pi}{2}\left(\frac{8m_p^*}{h^2}\right)^{3/2}\sqrt{E_V - E} \ [eq.8]$$

   Being $N_n(E), N_p(E)$ the density of states for electrons and holes, respectively. m^* is the effective mass of the charge carrier.

- Probability of occupation: show how likely it is for a given energy level to be occupied by a fermion (electrons and holes are fermions because they follow the Pauli Exclusion Principle). It follows the Fermi-Dirac $f(E)$ distribution:

$$f_C(E) = f(E) = \frac{1}{e^{\frac{E-E_F}{k \cdot T}} + 1} \ [eq.9] \qquad f_V(E) = 1 - f(E) \ [eq.10]$$

   $f_C(E), f_V(E)$ are the probability of occupation of an electron and a hole, respectively. Being $k = 1,3806 \cdot 10^{-23} \ JK^{-1}$ the Boltzmann constant; T and E the absolute temperature and energy of the state, respectively. E_F is the Fermi level (the energy

level such that, at thermodynamic equilibrium, have a 50% probability of being occupied at any given time).

Defined these two concepts, the charge carrier density functions can be defined as:

$$n(E) = N_n(E) \cdot f(E) \; [eq. 11] \qquad p(E) = N_p(E) \cdot [1 - f(E)] \; [eq. 12]$$

Being $n(E)$ the density of electrons and $p(E)$ the density of holes.

In [*Figure 4.13*] all the described functions are plotted both for electrons and holes $N_n(E), N_p(E), f_C(E), f_V(E), n(E), p(E)$.
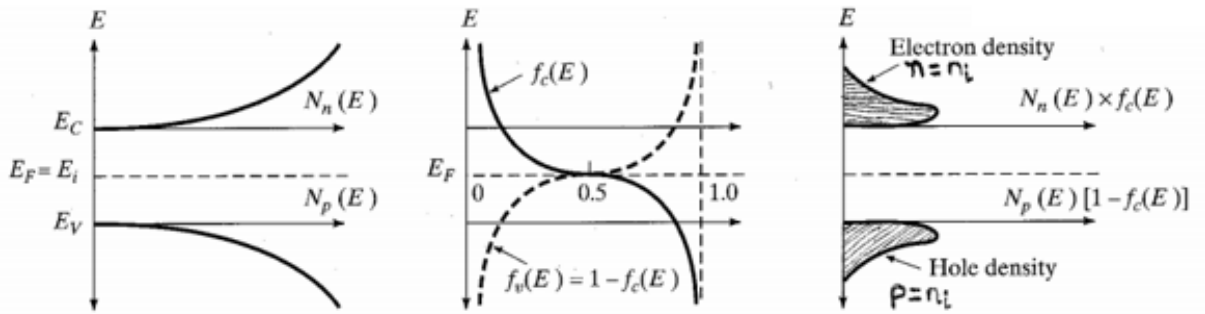

Figure 4.13. Density of state functions, probability of occupation functions and charge carrier density functions for electron and holes.

To find the value of the concentration of electrons and the concentrations of holes (charge carrier density) the functions $n(E), p(E)$ must be integrated as follows:

$$n = \int_{E_c}^{\infty} N_n(E) \cdot f_C(E) \cdot dE = \cdots = N_C \cdot e^{-\left(\frac{E_C - E_F}{kT}\right)} \; ; \; N_C = 2\left(\frac{2\pi m_n^* kT}{h^2}\right)^{3/2} \; [eq. 13]$$

$$p = \int_{-\infty}^{E_v} N_p(E) \cdot f_V(E) \cdot dE = \cdots = N_V \cdot e^{-\left(\frac{E_F - E_V}{kT}\right)} \; ; \; N_V = 2\left(\frac{2\pi m_p^* kT}{h^2}\right)^{3/2} \; [eq. 14]$$

Being N_C the effective density of states in the conduction band and N_V the effective density of states in the valence band.

For solving this integration, the Boltzmann approximation [*eq. 15*][*eq.16*] has been used. This approximation is valid when $|E - E_F| \gg kT$.

$$f_C(E) = f(E) \cong e^{-\frac{(E - E_F)}{kT}} \; ; (E - E_F) > 3kT \; [eq. 15]$$

$$f_V(E) = 1 - f(E) \cong e^{-\frac{(E_F - E)}{kT}} \; ; (E_F - E) > 3kT \; [eq. 16]$$

The Fermi level can be expressed with the next equation:

$$E_F = \frac{E_C + E_V}{2} + \frac{kT}{2} ln\left(\frac{N_V}{N_C}\right) \ [eq.\,17]$$

[9]

Intrinsic and Extrinsic Semiconductors

An intrinsic semiconductor is a pure semiconductor. This means that holes in the valence band are vacancies created by electrons that have been thermally excited to the conduction band (Si, Ge, GaAs), as opposed to doped semiconductors where holes or electrons are supplied by a "foreign" atom acting as an impurity.

In an intrinsic semiconductor there exists an equal number of free electrons and free holes [*eq. 18*] [*Figure 4.14*]. The electrons and holes, however, have different mobilities (that is to say, they move with different velocities in an electric field). For example, for intrinsic silicon at room temperature, the electron mobility is $1500 \ cm^2/Vs$ (an electron will move at a velocity of 1500 centimetres per second under an electric field of one volt per centimeter) while the hole mobility is $500 \ cm^2/Vs$. The mobilities of a given semiconductor generally decrease with increasing temperature or with increased impurity concentration. [10]
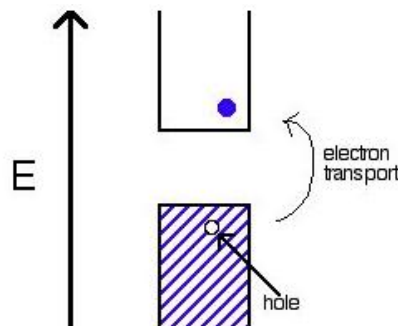
$$n = p = n_i \ [eq.\,18]$$

Figure 4.14. Intrinsic semiconductor material.

From [*eq. 18*] the law of mass action is deduced for intrinsic semiconductors:

$$n \cdot p = n_i^2 = N_C N_V \cdot e^{-\frac{(E_C - E_V)}{kT}} = N_C N_V \cdot e^{-\frac{E_g}{kT}} \ [eq.\,19]$$

Applying [*eq. 13*] and [*eq. 14*] to [*eq. 19*] we get the expression of the intrinsic carrier density:

$$n_i = 2\left(\frac{2\pi kT}{h^2}\right)^{3/2} (m_n^* m_p^*)^{3/4} \cdot e^{-\left(\frac{E_g}{2kT}\right)} \ [eq.\,20]$$
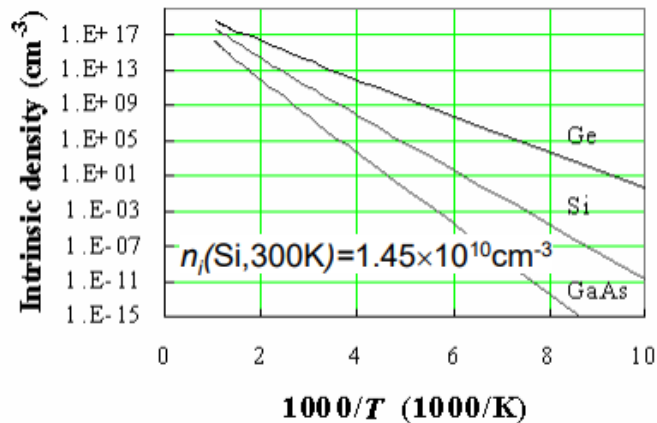
Figure 4.15. Plot of the intrinsic density versus a T function for three different semiconductor materials.

Electrical conduction in intrinsic semiconductors is quite poor at room temperature. To produce higher conduction, one can intentionally introduce impurities (typically to a concentration of one part per million host atoms). This is the so-called doping process. The doped semiconductor materials are called extrinsic semiconductors.

In extrinsic semiconductors, the number of holes will not equal the number of electrons jumped. There are two different kinds of extrinsic semiconductors, p-type (positive charge doped) and n-type (negative charge doped).

p-type: doped with III group elements (B, Al, In, Ga), with only three electrons in their valence band. When introduced to the crystalline structure it will tend to capture an electron in the valence band, generating additional holes in the semiconductor. Holes are the principal carriers

n-type: doped with V group elements (P, As), with five electrons in their valence band. When introduced. When introduced to the crystalline structure it will tend to donate an electron to the conduction band, generating additional electrons in the semiconductor. Electrons are the principal carriers
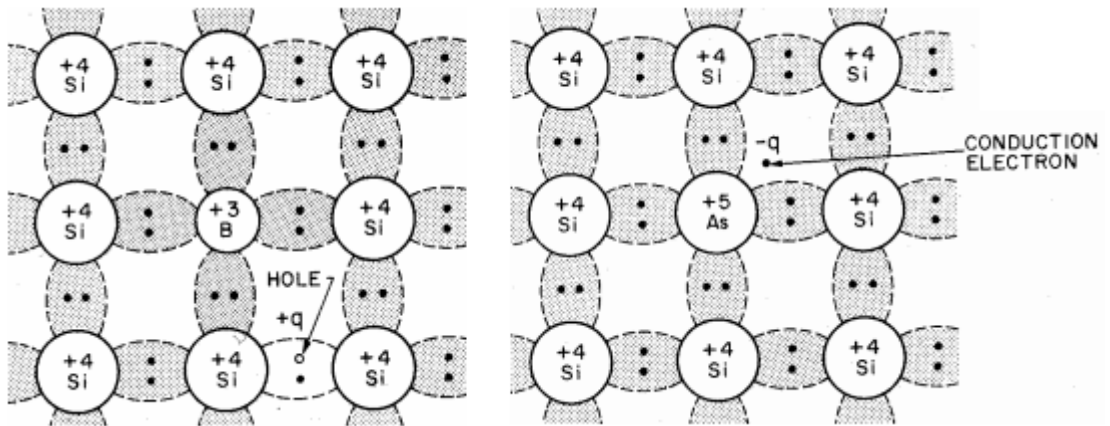
Figure 4.16. Left, p-type SC doped with B atoms. Right, n-type SC doped with As atoms.
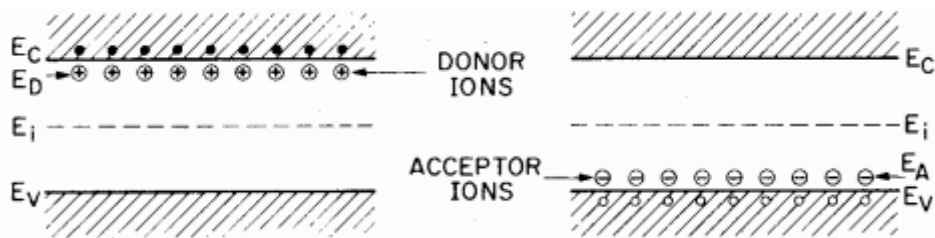

Figure 4.17. Left, energy band structure of n-type SC. Right, energy band structure of p-type SC

Mass action law and charge neutrality law for extrinsic semiconductors in thermic equilibrium:

$$\begin{cases} n \cdot p = n_i^2 \\ n + N_A^- = p + N_D^+ \end{cases} \quad [eq.\,21]$$

Where N_A^-, N_D^+ are the concentration of ionized acceptor and donator impurities, respectively.

For a n-type SC: $N_D \gg N_A$; $N_D \gg n_i$, hence:

$$n \cong N_D \;\; ; \;\; p \cong {n_i^2}/{N_D} \quad [eq.\,22]$$

For a p-type SC: $N_A \gg N_D$; $N_A \gg n_i$, hence:

$$p \cong N_A \;\; ; \;\; n \cong {n_i^2}/{N_A} \quad [eq.\,23]$$

The carrier concentration varies with temperature as shown in [Figure 4.18], showing three different regions: partial ionization, extrinsic, intrinsic.
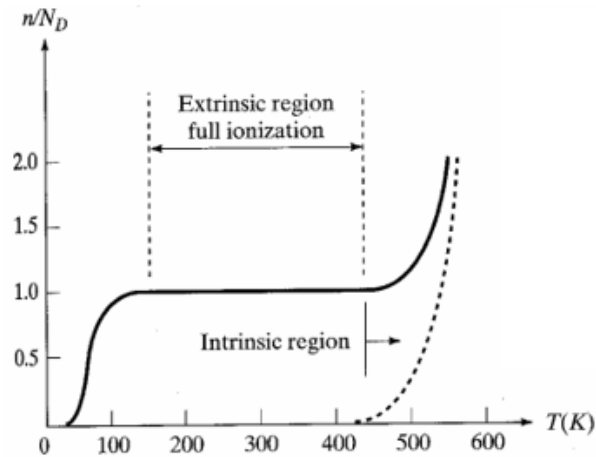
Figure 4.18. electron density vs. temperature in a n-type SC. Three regions are shown.

Other interesting topics: Hall effect, generation and recombination of charge carriers, diffusion currents in an extrinsic semiconductor. [9] [10]

4.1.3. The p-n junction

In the photovoltaic effect, a voltage is generated when the electrons freed by the incident light are separated from the holes that are generated, producing a difference in electrical potential. This is typically done by using a *p-n* junction rather than a pure semiconductor. A *p-n* junction occurs at the juncture between *p*-type (positive) and *n*-type (negative) semiconductors. Illumination frees electrons and holes on opposite sides of the junction to produce a voltage across the junction that can generate current, thereby converting light into electrical power. [10]

p-n junction in thermal equilibrium

Thermal equilibrium: defined by a constant temperature distribution and no electrical, optical, mechanical or chemical excitation is applied from the outside world. (also called zero bias)

Before forming the junction, there are two different doped regions (one is n-type and the other is p-type) which are electrically neutral. Each region has a large number of majority carriers (nearly as many as ionized impurities or dopants) and a very small number of minority carriers. Applying *[eq. 21]* we get:

For p-region: $p_p - n_p - N_A = 0$ [$eq.\,24$]
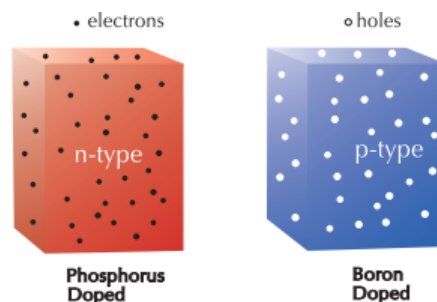
For n-region: $p_n - n_n - N_D = 0$ [$eq.\,25$]

Figure 4.19. Doped silicon. Electrically neutral.

Now, both regions are brought in contact:

1- Diffusion mechanism: A huge gradient of the carrier concentration appears at the border of the two regions. Consequently, and obeying the Fick's first law [*eq. 26*], an enormous carrier flux of electrons and holes turns up in such a way that the carriers tend to generate a uniform distribution of the concentration of each carrier inside the structure. Hence, a current density is generated in the material ($J_{df,n}$, $J_{df,p}$).

$$J_{df,n} = e \cdot D_n \frac{dn}{dx} \ ; \ J_{df,p} = -e \cdot D_p \frac{dp}{dx} \ \ [eq. 26]$$

Where D is the diffusion coefficient (or diffusivity) which, according to Einstein relation on electrical mobility, can be expressed as a relation of the electron mobility coefficient (μ) and the volt equivalent of temperature (V_t):

$$D = \mu V_t = \mu \left({kT}/{e} \right) [eq. 27]$$

2- Built-in electric field: As the electrons in the n-type material diffuse across towards the p-type side, they leave behind positively charged phosphorus ions, near the interface between the n and p regions. Similarly, the positive holes in the p-type region diffuse towards the n-type side and leave behind negatively charged boron ions. These fixed ions set up an electric field right at the junction between the n-type and p-type material. This electric field points from the positively charged ions in the n-type material to the negatively charged ions in the p-type material.

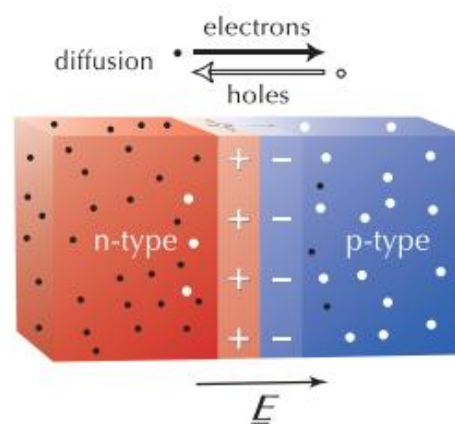

Figure 4.20. Diffusion stablishes a built-in electric field.

3- Junction Equilibrium: Thus, the "built-in" electric field causes some of the electrons and holes to flow in the opposite direction to the flow caused by diffusion. These opposing

flows eventually reach a stable equilibrium with the number of electrons flowing due to diffusion exactly balancing the number of electrons flowing back due to the electric field. The net flow of electrons across the junction is zero and the net flow of holes across the junction is also zero.
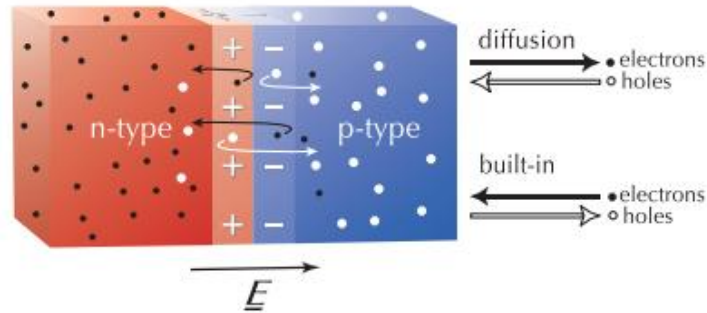

Figure 4.21. Motion of mobile electrons and holes due to diffusion and the built-in electric field.

Although there is no net flow of current across the junction there has been established an electric field at the junction and it is this electric field that is the basis of the operation of diodes, transistors and solar cells. [11] [12]

So, a drift current density $\left(J_{dr,n} \ , \ J_{dr,p}\right)$ is created because of the built-in electric field, following the Ohm's law:

$$J_{dr,n} = \sigma_n E_{bi} \ ; \ J_{dr,p} = \sigma_p E_{bi} \ [eq. 28]$$

Being σ the electrical conductivity of charge carriers defined as:

$$\sigma_n = en\mu_n \ ; \ \ \sigma_p = ep\mu_p \ [eq. 29]$$

We can also express the built-in electric field as a linear voltage gradient:

$$E_{bi}(x) = -\frac{dV_{bi}(x)}{dx} \ [eq. 30]$$

Considering that, in equilibrium, there is no net flow of electrons across the junction (so there is no net current density):

$$J_p = J_{df,p} + J_{dr,p} = 0 \ [eq. 31]$$

Applying [*eq. 26*][*eq.28*][*eq.29*] to [*eq.31*] we get the next expression:

$$J_p(x) = e \left[\mu_p p(x) E_{bi}(x) - D_p \frac{dp(x)}{dx}\right] = 0 \ \rightarrow \ \frac{\mu_p}{D_p} E_{bi}(x) = \frac{1}{p(x)} \frac{dp(x)}{x} \ [eq. 32]$$

Hence, applying [*eq. 27*][*eq. 30*] to [*eq.32*] we get:

$$-\frac{e}{kT} \frac{dV_{bi}(x)}{dx} = \frac{1}{p(x)} \frac{dp(x)}{dx} \ \rightarrow \ dV_{bi} = -\frac{kT}{e} \frac{dp(x)}{p(x)} \ [eq. 33]$$

Integrating from P to N region we get the expression of the built-in voltage:

$$V_{bi} = \frac{kT}{e} ln\left(\frac{p_p}{p_n}\right) \ [eq.34]$$

Finally, applying [*eq.22*][*eq.23*] to [*eq.33*] we get a better expression for built-in voltage:

$$V_{bi} = \frac{kT}{e} ln\left(\frac{N_A N_D}{n_i^2}\right) \ [eq.35]$$

4- Depletion region: Within the depletion region, there are very few mobile electrons and holes. It is "depleted" of mobile charges, leaving only the fixed charges associated with the dopant atoms. As a result, the depletion region is highly resistive and now behaves as if it were pure crystalline silicon: as a nearly perfect insulator.

Depletion layer's width (W) depends on the built-in voltage and can be modified by adding an external electric field, which is also called bias. The depletion region can therefore be considered to operate as a voltage-controlled resistor.

It is possible to deduce the width function of the depletion layer using Poisson's equation, getting the next expression:

$$W(V) = \sqrt{\frac{2\varepsilon_{SC}}{e} \cdot \frac{N_D + N_A}{N_D N_A} \cdot V} \ [eq.36]$$

Being ε_{SC} the permittivity of the semiconductor material.

If the p-n junction is in equilibrium the voltage V will be the built-in voltage V_{bi}, but if there is an external electric field the new voltage will be: [11] [12]
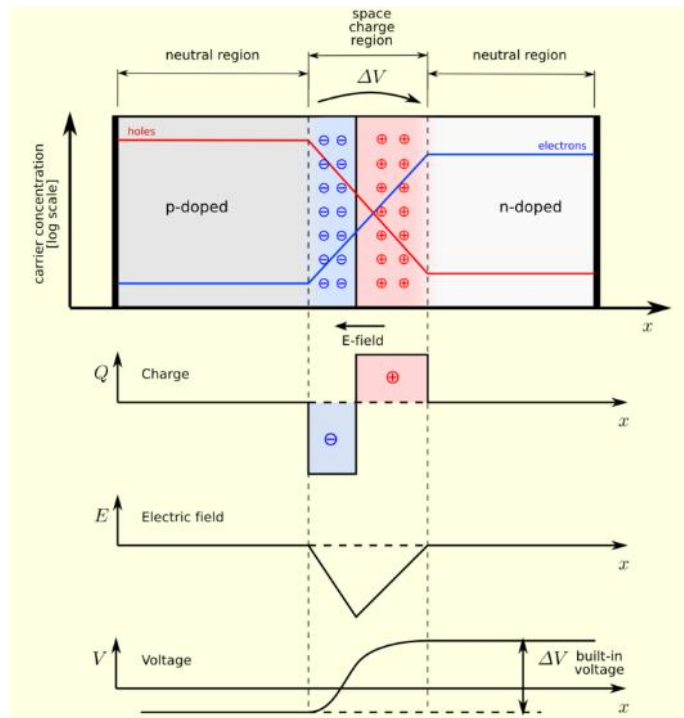
$$V = V_{bi} - V_{bias} \ [eq.37]$$

Figure 4.23. Depletion region behavior.

p-n junction with forward and reverse bias

At the p-n junction, the "built-in" electric field and the applied electric field are in opposite directions. So, forward bias reduces the resultant field at the junction and reverse bias

increases it, as shown in [*eq.37*].

If a positive voltage is applied to the p-type side and a negative voltage to the n-type side, current can flow (depending upon the magnitude of the applied voltage). This configuration is called "Forward Biased". This results in a thinner, less resistive depletion region. If the applied voltage is large enough, the depletion region's resistance becomes negligible [*Figure 4.25*]. In silicon, this occurs at about 0.7 volts forward bias. From 0 to 0.7 volts, there is still considerable resistance due to the depletion region. Above 0.7 volts, the depletion region's resistance is very small and current flows virtually unimpeded.

If a negative voltage is applied to the p-type side and a positive voltage to the n-type side, no (or exceptionally small) current flows. This configuration is called "Reverse Biased". This creates a thicker, more resistive depletion region. In reality, some current will still flow through this resistance, but it may be considered to be zero [*Figure 4.25*]. As the applied reverse bias voltage becomes larger, the current flow will saturate at a constant but very small value (around -20 µA in Silicon) [11]

$$W_{rev,bias} > W_{bi} > W_{for,bias} \; [eq. 38]$$
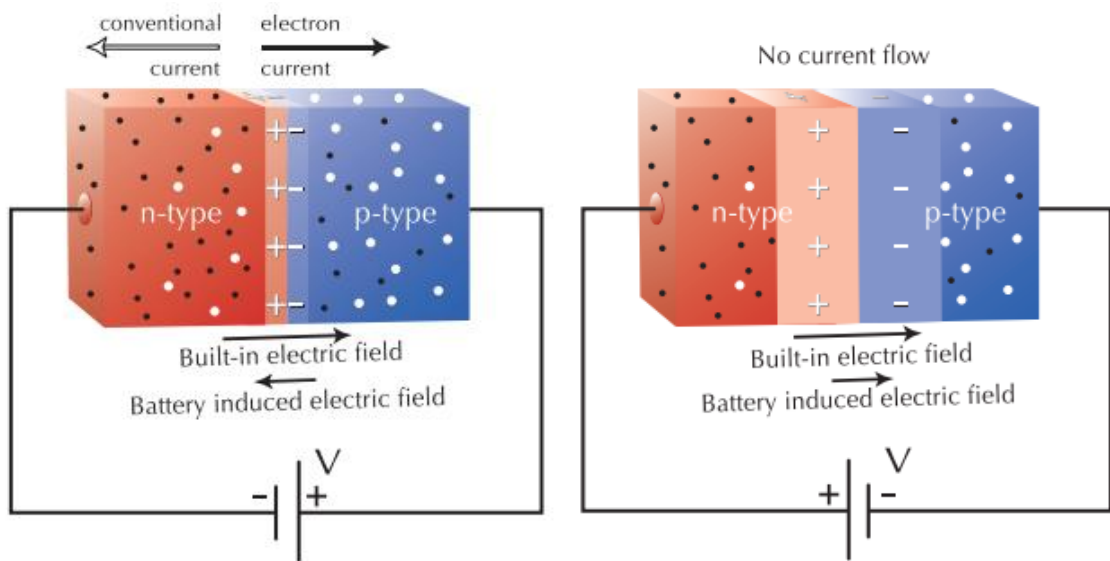
Figure 4.24. Left, forwarded biased p-n junction. Right, reverse biased p-n junction.

Characteristic curve

As it can be seen in [Figure 4.25], if reverse bias voltage becomes too large then the junction will break down and the current will flow. This is called Avalanche Breakdown and it happens because, as the magnitude of the reverse voltage increases, the kinetic energy of the minority charge carriers also increases. These fast moving electrons collide with the other atoms to release some more electrons from them, by breaking the covalent bonds.
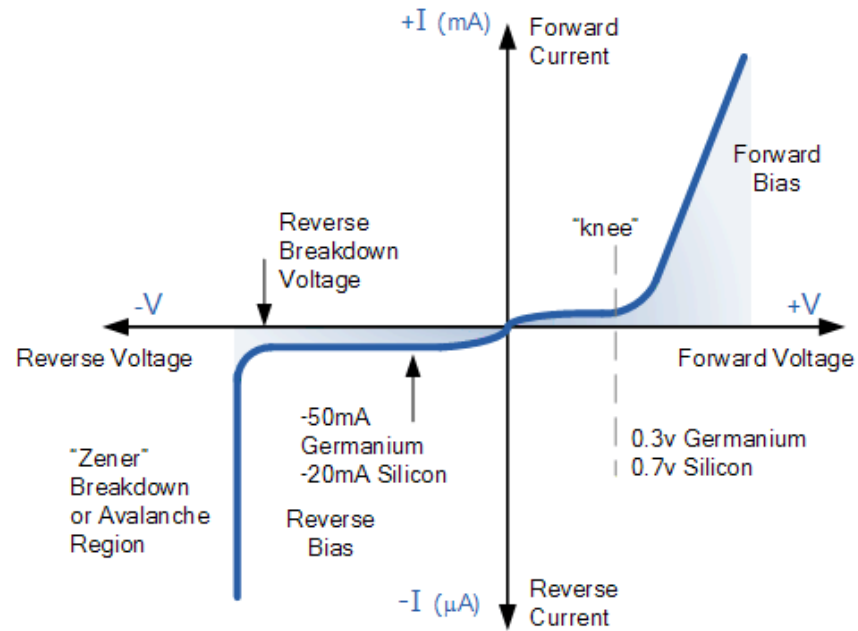
Figure 4.25. Characteristic V-I curve of p-n junction.

4.1.4. PV Solar Cell

PV cell is considered the fundamental power conversion unit of a PV-based power system.

Description

PV cell is basically a semiconductor p-n junction-based photodiode [*Figure 4.26*]. This semiconductor photodiode generates electrical power when exposed to light.

Figure 4.26. Photodiode symbol.

Solar cells are made of different layers of materials [*Figure 4.27*]. They have a protective glass plate, thin films as moisture barriers and the actual solar cells which convert the energy.

Figure 4.27. Schematic representation of a silicon solar cell. The blue layer is an anti-reflective and protective layer, the grey layers are the cathode and anode, the yellow layer is the n-type semiconductor and the brown layer is the p-type semiconductor.
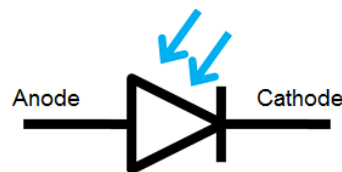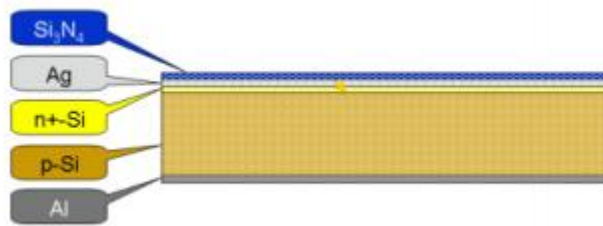
Crystalline Silicon (Si) is the most used semiconductor material in solar cells. Both monocrystalline and polycrystalline Silicon are common in the industry. [13]

PV Cell Operation

The principle of operation of a PV cell is based on the basic principle of photoelectric effect [*Chapter 4.1.1*]. So, in a PV cell, when sunlight strikes its surface, some portion of the solar energy is absorbed in the semiconductor material. If the absorbed energy is greater than the band gap energy of the semiconductor, the electron from the valence band jumps to the conduction band. By this, additional charge carrier are created as pairs of hole-electron in the illuminated region of the semiconductor [*Chapter 4.1.2*]. The electrons thus created in the conduction band are now free to move. These free electrons are forced to move in a particular direction by the action of the electric field presented in the PV cells [*Chapter 4.1.3*]. These flowing electrons constitute current and can be drawn for external use by connecting a metal plate on top and bottom of PV cells. Current and voltage (created because of its built-in electric field) generate electric power. [14]

Because of the built-in electric field, the electrons are attracted towards the positive charge on the n-type material side. Similarly, the holes are attracted to the negative charge on the p-type material side. This separation of charges causes a current to flow across the junction. The direction of the current flow (conventional current) is the same as the motion of the holes (as they are positively charged). That is, the current flows across the junction from the n-type side to the p-type side. [11]
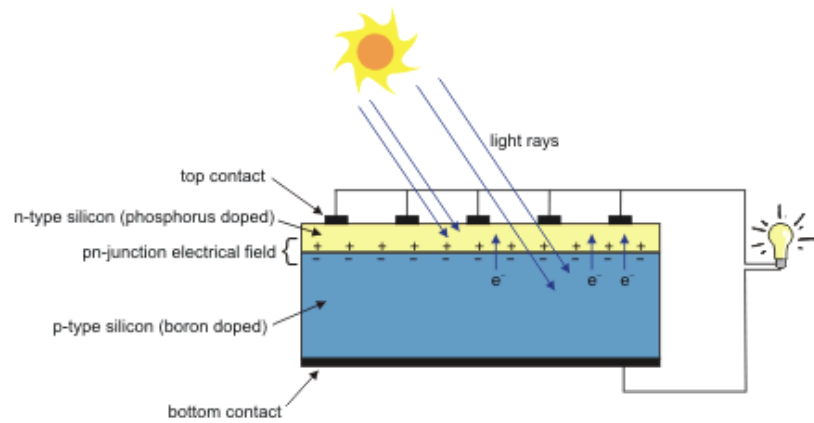
Figure 4.28. PV Cell operation diagram.

The amount of light which is absorbed by a material depends on the absorption coefficient α, (which depends on the material and on the wavelength of light, as seen in [*Figure 4.28*]) and the thickness of the absorbing metal.
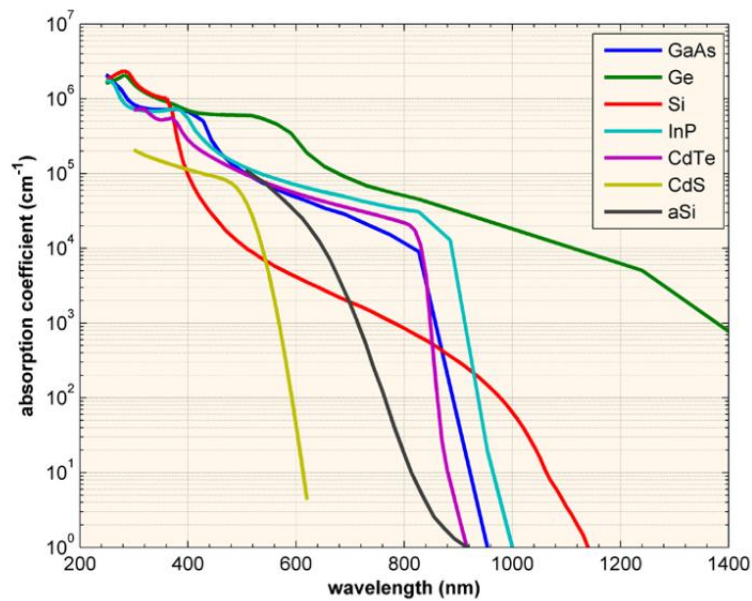
Figure 4.29. Absorption coefficient vs. wavelength for different semiconductor materials.

The intensity of light (absorption of photons rate) at any point in the device can be calculated according to [*eq 39*]:

$$I_x(x) = I_0 \cdot e^{-\alpha(\lambda)x} \ [eq.\,39]$$

Being I_0 the light intensity in the surface of the material and x the depth at which light intensity is calculated.

The decrease in light intensity is related to the generation of electron-hole pairs by differentiating [*eq.39*]:

$$G_L(x) = \alpha(\lambda)N_0 \cdot e^{-\alpha(\lambda)x} \; [eq.\,40]$$

Where N_0 is the photon flux at the surface. [*eq. 40*] shows that the generation rate is highest at the surface, where the intensity is highest. The generation rate varies for different wavelengths. Short wavelength photons (blue light, high energy) have small absorption depths and are absorbed first, large wavelength photons (red light, lower energy) are absorbed at greater depths [*Figure 4.30*].
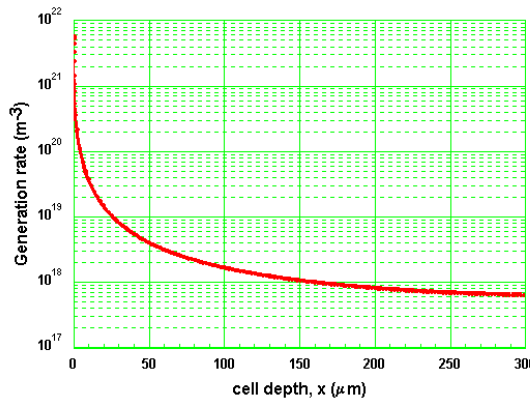
Figure 4.30. Generation rate vs. solar cell depth for a wavelength of light around 800 nm.

The collection probability is the probability that a carrier will be collected by the junction and contributes to the current. For a carrier generated in the depletion region, the collection probability is one since the electron-hole pair are instantly separated by the electric field and are collected in the junction. Away from the depletion region, this probability drops. [14]
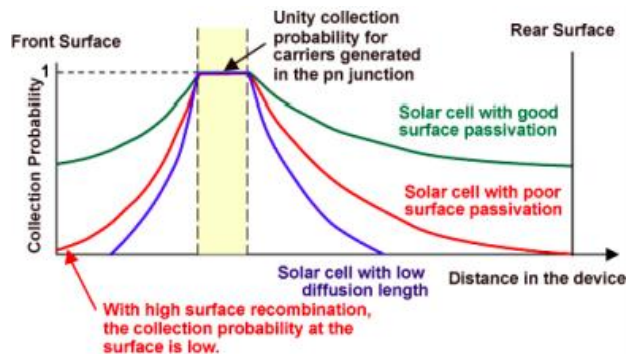
Figure 4.31. Illustration of the collection probability against the depth in the solar cell.

Electric equivalent circuit and Mathematical model

As shown in [*Fig. 4.32*], the equivalent circuit of the general model is composed of photo current source, diode, parallel resistor expressing the leakage current, and series resistor describing the internal resistance to the current flow.
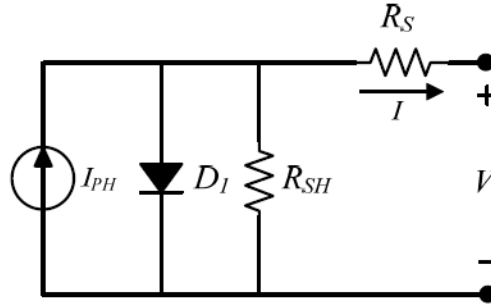
Figure 4.32. The equivalent circuit of a PV cell.

Being I_{ph} the photogenerated current (which depend on the irradiance and the temperature of the cell), I_d the direct current in the diode and I_{sh} the losses in the parallel branch, the output current of the cell can be expressed as:

$$I = I_{ph} - I_d - I_{sh} \ [eq. 41]$$

The equation for the photogenerated current is:

$$I_{ph} = \frac{G}{G_{ref}} [I_{sc} + K_{ti}(T_c - T_{c,ref})] \ [eq. 42]$$

Where $G_{ref} = 1000 \ W/m^2$ is the reference irradiance (standard conditions), $T_{c,ref} = 25 \ °C$ is the reference cell temperature (standard conditions), I_{sc} is the short-circuit current at $T_{c,ref}$ and G_{ref}, and K_{ti} is the cell short-circuit current temperature coefficient.

The equation for the direct current in the diode is:

$$I_d = I_o \left(\exp\left[\frac{V + IR_s}{\eta_d V_t} \right] - 1 \right) \ [eq. 43]$$

$$V_t = \frac{kT_c}{e} \ [eq. 44]$$

$$I_o = I_{o,ref} \left(\frac{T_c}{T_{c,ref}} \right)^3 exp\left[eE_g \frac{\left(\frac{1}{T_{c,ref}} - \frac{1}{T_c} \right)}{\eta_d k} \right] \ [eq. 45]$$

$$I_{o,ref} = \frac{I_{sc}}{e^{V_{oc}/V_t} - 1} \ [eq. 46]$$

Where I_o is the reverse saturation current of the diode, $I_{o,ref}$ is the reference reverse saturation current (standard conditions), η_d is the ideality factor of the diode (which models

the mismatch of the real semiconductor material with the mathematical equations), V_{oc} is the open-circuit voltage at G_{ref} and $T_{c,ref}$ (standard conditions).

The equation for the losses in the parallel branch is:

$$I_{sh} = \frac{V + IR_s}{R_{sh}} \; [eq. 47]$$

[14]

Performance and Characteristic curve

The performance of a solar cell is indicated by four parameters. These are the open-circuit voltage V_{oc}, the short-circuit current I_{sc}, the fill factor FF and the maximum power point P_{mp}.

The characteristic curve plots the measured current against the applied voltage over the solar cell. When there is no voltage applied to the solar cell the current is called the I_{sc} . When there is no net current flowing, the voltage is called V_{oc}, which is a property of the junction and the material itself.
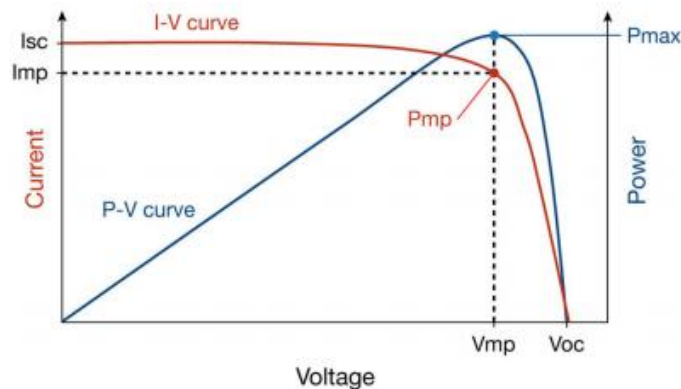
Figure 4.33. Example of V-I characteristic curve (red) and its corresponding power curve (blue).

From this curve, a power output can be plotted using [*eq.48*]. This curve has a maximum at $P_{max} \equiv P_{mp}$. The voltage corresponding to this point (V_{mp}) has to be applied for maximum power.

$$P = V \cdot I \rightarrow P_{mp} = V_{mp} \cdot I_{mp} \; [eq. 48]$$

The fill factor measures the squareness of the characteristic curve. The more the characteristic is rectangle-shaped, the bigger the fill factor is. Hence, higher efficiency.

$$FF = \frac{V_{mp} \cdot I_{mp}}{V_{oc} \cdot I_{sc}} \ [eq.\,49]$$

[13]

Efficiency

The efficiency of a solar cell is defined as the maximum power output divided by the total power of light that radiates on the solar cell:

$$\eta = \frac{P_{mp}}{P_{in}} = \frac{V_{mp} \cdot I_{mp}}{G \cdot A} = \frac{FF \cdot V_{oc} \cdot I_{sc}}{G \cdot A} \ [eq.\,50]$$

The maximum efficiency that could be reached is limited by the Shockley-Queisser (SQ) limit [*Figure 4.34*]. This is a theoretical limit to the maximum achievable efficiency of a solar cell with a single p-n junction. The losses of energy which cannot be converted into electrical power are caused by different factors:

- Photons below the band gap energy cannot be absorbed.
- Radiative recombination of electron-hole pairs. It releases a photon and thus energy.
- Photons with high energies excite electrons too much, so the surplus energy ($> E_g$) is lost in form of heat.
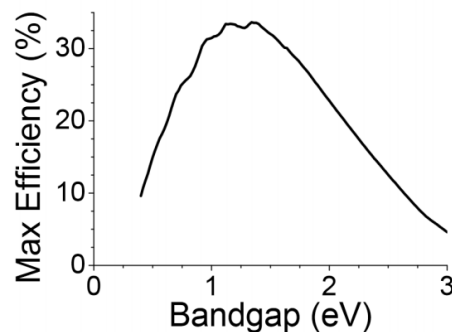
Figure 4.34. Shockley-Queisser limit vs. bandgap of the material. Maximum efficiency is placed around 33.7% assuming a single p-n junction band gap of 1.4 eV. Solar radiation is modelled as 6000 K blackbody radiation.

At outdoor operating conditions, there are three main parameters which influence the efficiency of a solar cell: Intensity, temperature and spectral shape:

- Light Intensity (or Irradiance) → When G increases its value:
  - P_{in} increases linearly with irradiance ($P_{in} = G \cdot A \ [eq.\,51]$)
  - I_{sc} increases linearly with G. V_{oc} increases logarithmically with G.
  - $P_{mp} = FF \cdot V_{oc} \cdot I_{sc}$ increases logarithmically with G in operation range.
  - Hence, efficiency η increases in the operation range.

- Temperature → When T_c increases its values the band gap narrows ($E_g' < E_g$):
    - P_{in} stays the same.
    - V_{oc} decreases logarithmically. I_{sc} increases linearly with T_c.
    - P_{mp} decreases logarithmically in the operation range.
    - Hence, efficiency η decreases its value in the operation range.
- Spectral shape → If the spectral shape has more high energy photons (high v such that $h \cdot v \geq E_g$) a larger part of the spectrum can excite electrons, increasing η.

[13] [15]

PV Modules

Since a PV cell produces very low power, the cell should be arranged in series-parallel configuration modules to produce enough power. Photovoltaic modules are the fundamental building blocks of PV systems.

The equivalent circuit for a PV module arranged in N_p parallel and N_s series cells is shown in [*Fig. 4.35*]. The terminal equation for the current and voltage of the array becomes as follows [*eq.52*]:
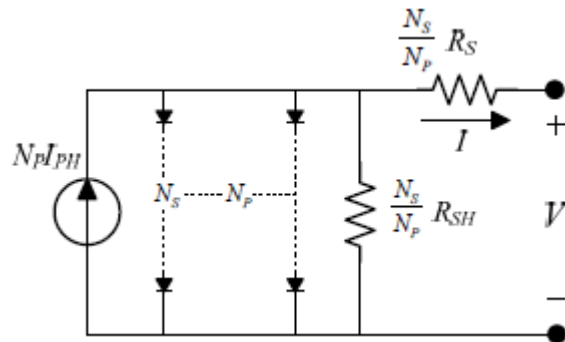
Figure 4.35. Generalized module model

$$I = N_p I_{ph} - N_p I_0 \left[exp \left(\frac{\frac{V}{N_s} + \frac{IR_s}{N_p}}{V_t \eta_d} \right) - 1 \right] - \frac{\left(\frac{N_p}{N_s} V + IR_s \right)}{R_{sh}} \quad [eq.52]$$

Series connection increases the open circuit voltage of the final module and parallel connection increases its short circuit current. Considering that all the solar cells are exactly the same, we can express:

$$V_{oc,mod} = \sum_{i=1}^{N_s} V_{oc,i} = N_s \cdot V_{oc} \; [eq.\,53] \qquad I_{sc,mod} = \sum_{j=1}^{N_p} I_{sc,j} = N_p \cdot I_{sc} \; [eq.\,54]$$

[*eq.53*] and [*eq.54*] can also be applied for the maximum power point ($V_{mp,mod}$, $I_{mp,mod}$).
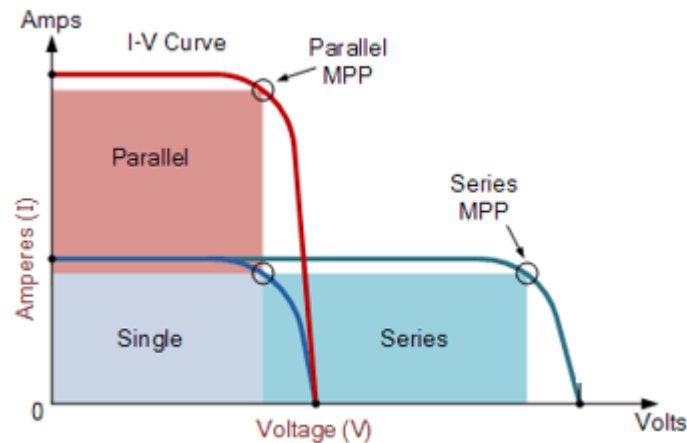
Figure 4.36. V-I characteristic curve for series vs. parallel connection

[14]

<u>Mismatch effect</u>

Even when working with identical PV Cells, mismatch losses are caused by the interconnection of solar cells which experience different conditions from one another (for example, when some regions of the module are shaded). The characteristic curve of the PV module is affected decisively when solar cells are irradiated at different levels, decreasing its power output [*Figure 4.37*]. The shaded cell acts as load, dissipating power on itself which may lead ultimately damage of the cells.

To prevent shadowed cells from narrowing the current path in a cell, downgrading the performance of other cells and reducing the power production of the whole module, bypass diodes are placed (reverse biased) to series connected cells and blocking diodes are placed to parallel connected cells. [*Figure 4.38*]

Bypass diodes will allow current to pass around shaded cells and thereby reduce the power losses through the module [*Figure 4.39*]. Blocking diodes prevent current from passing through the shadowed parallel branches, also reducing the power losses.

Figure 4.37. Mismatch effect due to partial shading of a module. This module is formed by 36 PV cells in series.
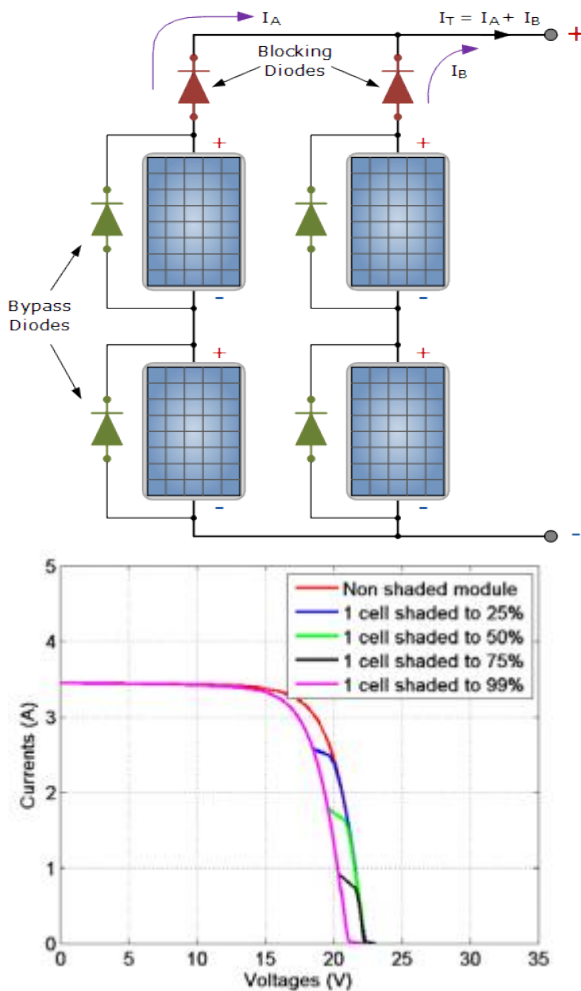
Figure 4.38. Bypass and blocking diodes in a PV array.   *Figure 4.39. Bypass diodes effect*

Normally, PV modules are made of series connected cells with bypass diodes placed in anti-

parallel to small groups of series connected cells.

PV arrays combines both series and parallel connected modules, using both bypass and blocking diodes properly. [16]

4.2. Solar Chargers

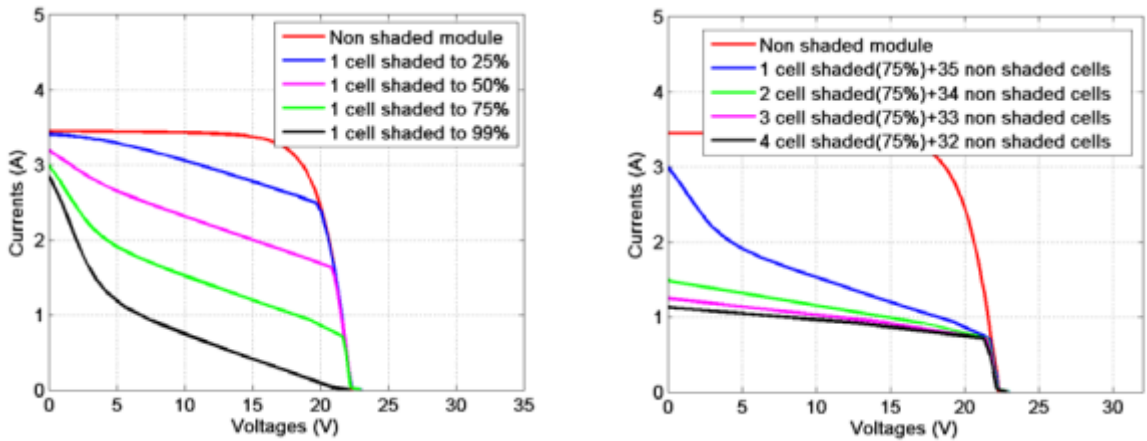A solar charger is a photovoltaic panel-based charging system which can be carried any place at any time. In addition, a good solar charger must be easy to use and must not affect negatively the performance and lifetime of the battery which is being charged.

Normally, solar chargers are used to charge low voltage electronic devices such as smartphones, tablets and laptops. These devices have lithium-ion batteries with charging nominal voltage from 5 V (smartphones, tablets) to 20 V (laptops).

Two main different types of solar chargers can be designed: direct chargers and indirect chargers. The main difference between them is the existence of an energy reservoir, as it will be explained later in this paper.
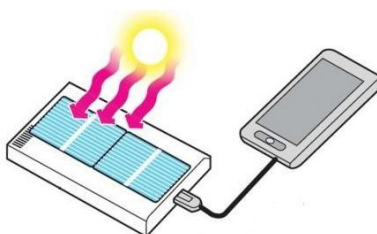
Figure 4.40. Solar charger conceptual idea.

4.2.1. Fundamentals and Technology

Lithium-ion battery charging

Li-ion batteries make use of a cathode (positive electrode) which is metal oxide (for example $LiCoO_2$), an anode (negative electrode) which is porous carbon (C), and an electrolyte. When the circuit is closed, the ions flow from the anode to the cathode during discharge, generating electricity. Charging reverses the direction of the ion flow [*Figure 4.41*], which make them rechargeable.

The battery capacity (C_n) represents the maximum amount of energy that can be extracted

from the battery under certain specified conditions. However, the actual energy storage capabilities of the battery can vary significantly from the "nominal" rated capacity.

$$C_n = I \cdot t \ [eq. 55]$$

So, if a battery's nominal capacity is $C_n = 15 \ Ah$ it means that it can provide a constant discharge current of 1 A during 15 hours, or 5 A during 3 hours.

The charging/discharging rate (C-rate) refers to the rate at which battery is charged or discharged, related to its nominal capacity (for example, if the nominal capacity is rated at 4 A and C-rate is defined as 0.5C, charging nominal current will be 2 A.

A battery charges by applying DC for a limited time. This charge occurs in three phases. The first phase is a constant current charge (CC or bulk phase), when a constant current is applied to the battery and the voltage increases up to a determined value. The second phase is a constant voltage charge (CV or absorption phase), when the battery voltage is set at a constant value to continue the charge, and the current decreases to a minimum value (between 3~5% of its C-rate). In the third phase, if the charger is left connected to the battery, a periodic 'top up' charge is applied to counteract battery self-discharge. *[Figure 4.42]*
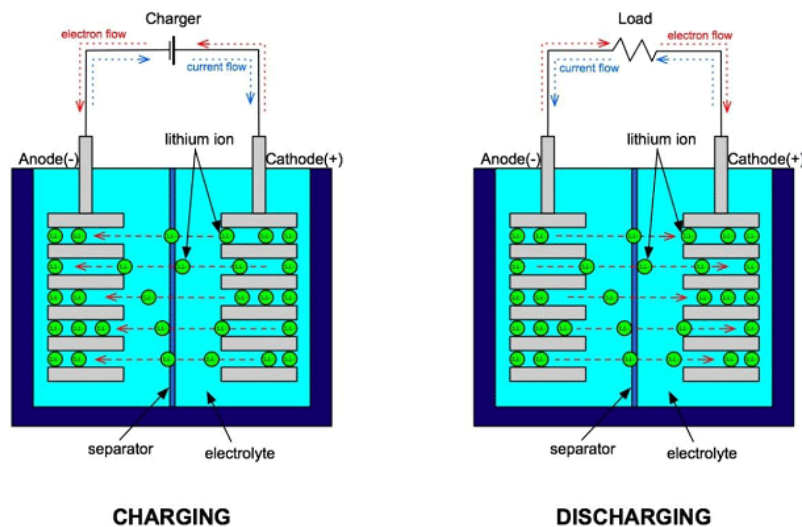
Figure 4.41. Lithium-ion battery charging and discharging operation.
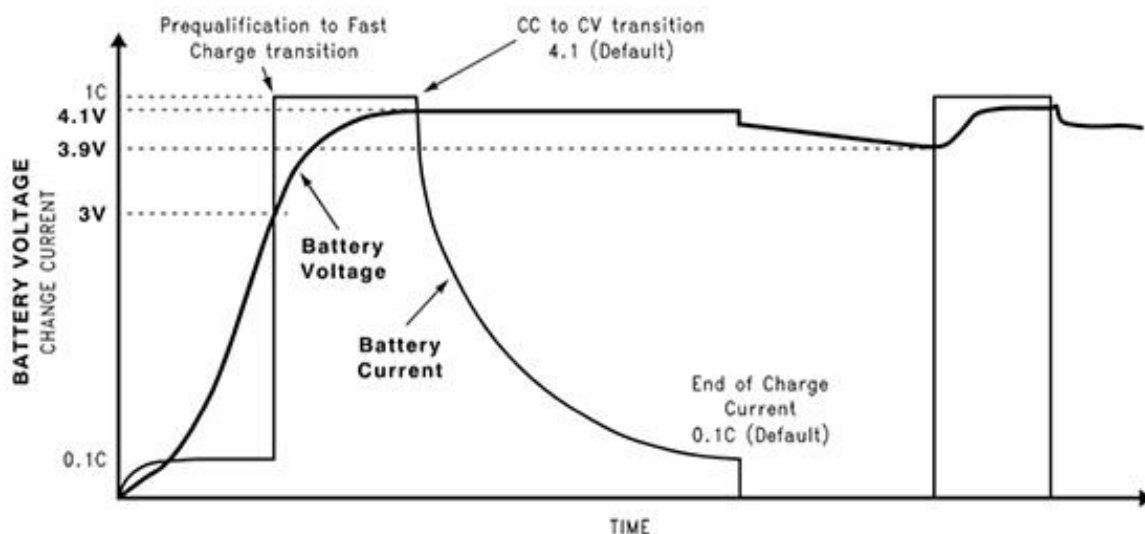
Figure 4.42. Voltage and current through the different stage of the charging process (Li-ion battery).

The advised charge rate of an Energy Cell is between 0.5C and 1C; the complete charge time is about 2–3 hours. Manufacturers of these cells recommend charging at 0.8C or less to prolong battery life. [17] [18]

Charge V/cell	Capacity at cut-off voltage	Charge time	Capacity with full saturation
3.80	~40%	120 min	~65%
3.90	~60%	135 min	~75%
4.00	~70%	150 min	~80%
4.10	~80%	165 min	~90%
4.20	~85%	180 min	100%

Table 4.1. Typical charge characteristics of lithium-ion batteries.

Components

The required components of a solar charger are:

1- Input voltage source → PV module
2- Output voltage regulator (power electronic systems) → MPPT + DC/DC

Converter
3- Charge controller (power electronic systems) → Linear or Switch-mode solutions
4- Auxiliary electronic systems → Charge termination system, top up charge system, temperature monitoring system, etc.
5- USB ports
6- External case
7- Optional: additional battery for energy supply when there is not enough sunlight (night, cloudy days)

Power electronics

The power electronics involved in the different technical solutions for a solar charger may vary between different chargers, but the most used solutions are exposed here.

MPPT (Maximum Power Point Tracking)

The maximum power point tracking is a technique used with photovoltaic arrays to maximize the power extraction regardless of the irradiance and temperature conditions. In this case, the MPPT algorithm tracks the maximum power point (V_{mp}, I_{mp}) and injects the maximum power to the DC bus through a DC/DC converter which converts the voltage from $V_{in} = V_{mp}(G, T_c)$ to the output voltage V_{out}. The MPPT algorithm computes the required duty cycle (D) for the DC/DC converter in order to guarantee maximum power. The most used and simplest algorithm for tracking the MPP is called "Perturbe and Observe (Hill-Climbing)". It is explained in the diagram of [*Figure 4.43*].
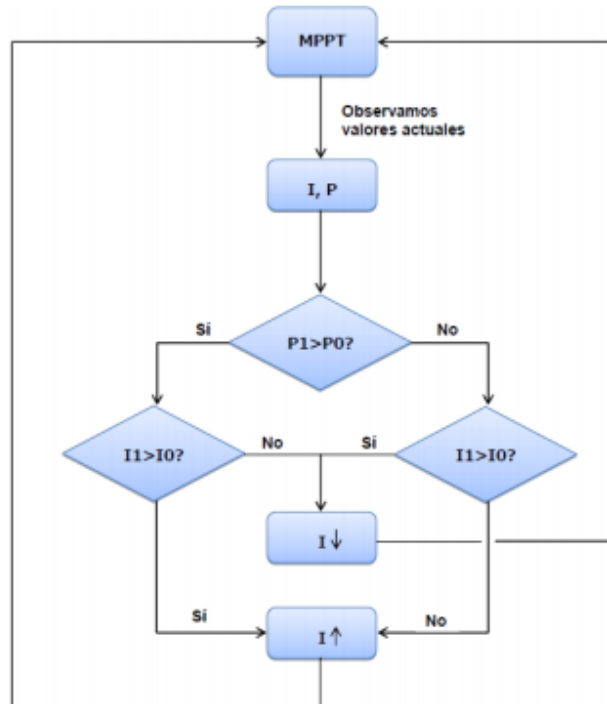
Figure 4.43. Diagram of Perturbe & Observe MPPT algorithm.

This algorithm compares the produced power in the instant (t) with the produced power in the previous instant $(t - \Delta t)$ and changes the duty cycle (D) of the converter in order to increase/decrease the value of the current (I_{PV}) as needed (some MPPT algorithms change the value of the voltage (V_{PV}) instead of the current). The power supplied by the PV array after the MPPT is always oscillating around the maximum power (Hill-Climbing concept).

Following the first algorithm (current controlled P&O MPPT), four possible cases (states) can be easily analyzed, which are summarized in [*Table 4.2*] and [*Figure 4.44*], taking into account the next equation:

$$D = \frac{t_{ON}}{T_c} \ [eq. 56]$$

Where t_{ON} is the time when the transistor is ON (ohmic region in MOSFETs and saturation region in BJTs) in a commutation period. T_c is the commutation period. [19]

state	$I_{PV}(t)$	$P_{PV}(t)$	$t_{ON}(t)$	$D(t)$	$I_{PV}(t + \Delta t)$
1	$< I_{PV}(t - \Delta t)$	$< P_{PV}(t - \Delta t)$	$increase$	$increase$	$> I_{PV}(t)$
2	$< I_{PV}(t - \Delta t)$	$> P_{PV}(t - \Delta t)$	$decrease$	$decrease$	$< I_{PV}(t)$

| 3 | $> I_{PV}(t - \Delta t)$ | $< P_{PV}(t - \Delta t)$ | *decrease* | *decrease* | $< I_{PV}(t)$ |
| 4 | $> I_{PV}(t - \Delta t)$ | $> P_{PV}(t - \Delta t)$ | *increase* | *increase* | $> I_{PV}(t)$ |

Table 4.2. States of the MPPT algorithm.
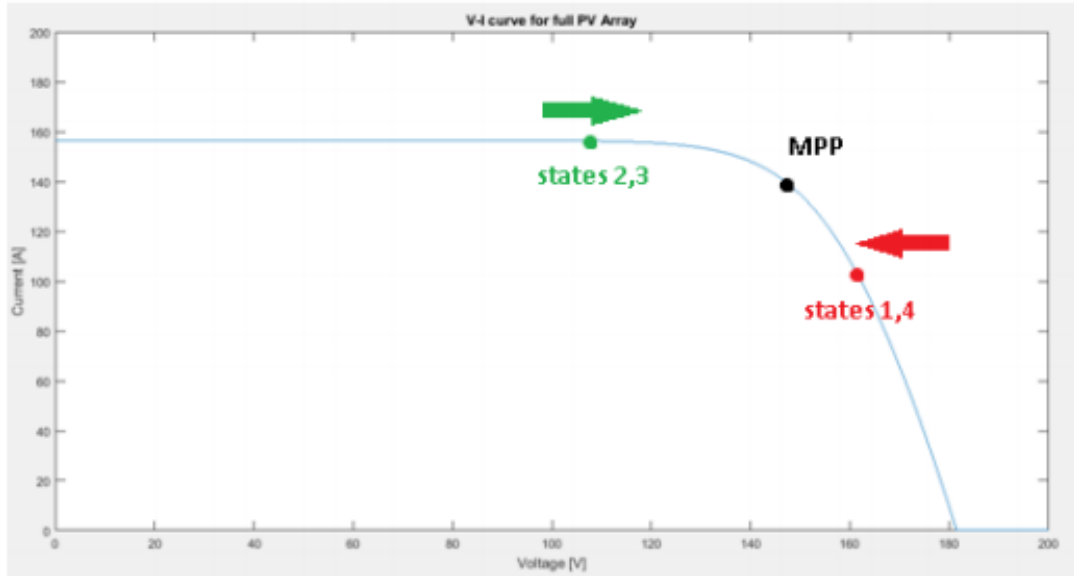
Figure 4.44. Response to the states of the MPPT algorithm. In states 1 and 4, current will increase in order to track the MPP. In states 2 and 3, current will decrease.

Buck converter

A buck converter (also called chopper) is a power electronic device which objective is to efficiently reduce the voltage of an electric signal without losing its power (losses are very little and can be neglected).

$$P_{in} = P_{out} \rightarrow V_{in} \cdot I_{in} = V_{out} \cdot I_{out} \ [eq.\,57]$$

The equivalent circuit for a buck converter is showed in [*Figure 4.45*] and it is composed of a switch which controls the flow of current from the source to the load, an inductor, a reverse-biased diode which allows the discharge of the inductor to the load and a capacitor which is used to filter the output voltage.
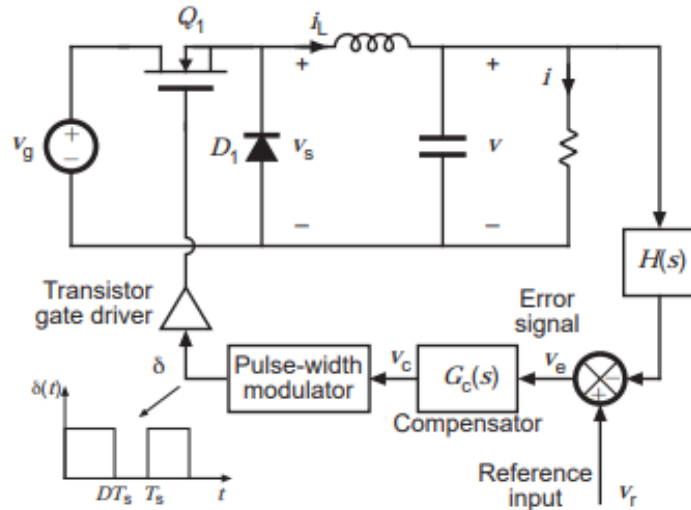
Figure 4.45. Buck converter schematic. A feedback loop is added for regulation of the output voltage.

The converter has two different states [*Figure 4.46*] depending on the position of the switch (which is in fact a MOSFET or BJT transistor). The time that the switch is ON (t_{ON}) defines the duty cycle of the converter and the output voltage, as defined in [*eq.56*][*eq.58*].

$$V_{out} = D \cdot V_{in} = \frac{t_{ON}}{T_c} \ [eq.58]$$

When the switch is ON, energy is being directly supplied to the load while the inductor is getting charged; when the switch is OFF the inductor is discharging the accumulated energy to the load through the diode.
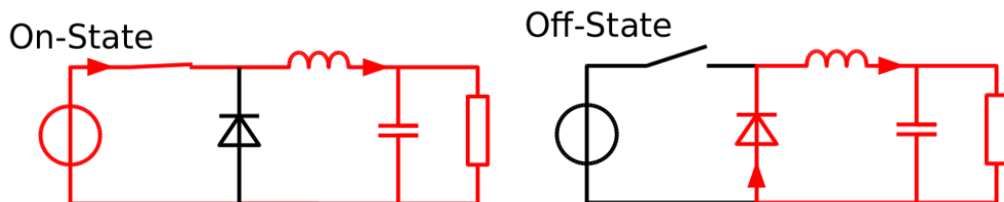
Figure 4.46. Two different states in a buck converter.

The output voltage is controlled by a feedback loop called Pulse Width Modulation (PWM) in order to make sure that the real output voltage gets the value of the reference output voltage. [18]

SEPIC

Another important power electronic device which is very useful for designing viable solar chargers is the Single-Ended Primary-Inductor Converter (SEPIC). It is a DC/DC converter which allows the output voltage to be greater than, less than, or equal to the input voltage. It

also maintains the same polarity from input to output.

This converter is also controlled by a PWM which alternates a switch (MOSFET or BJT transistor) between two states (ON an OFF), defining a duty cycle as described in [*eq.56*]. The output voltage depends on the duty cycle, as described in [*eq.59*].

$$V_{out} = \frac{D}{1-D} V_{in} \ [eq.59]$$

So, for $D = 0.5$ the output voltage is the same as the input voltage; for $D < 0.5$ the SEPIC acts as a buck converter ($V_{out} < V_{in}$); for $D > 0.5$ the SEPIC acts as a boost converter ($V_{out} > V_{in}$)

The equivalent circuit of an ideal SEPIC converter is more complex and have more components than the Buck converter circuit, as it is shown in [*Figure 4.47*]. It is made up of two capacitors, two inductors, a power switch (IGBT) and a diode.
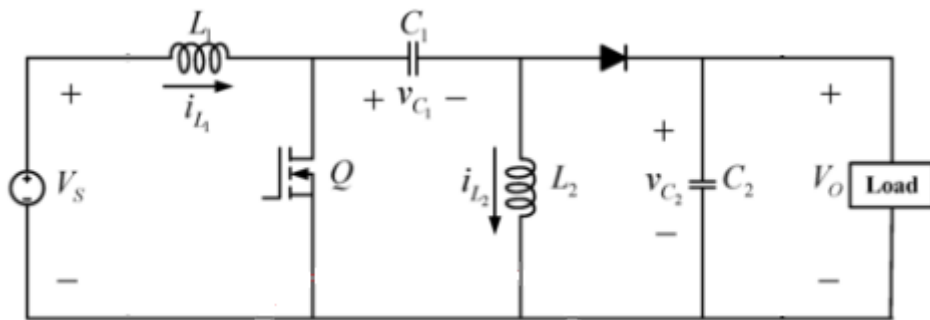
Figure 4.47. SEPIC converter schematic.

When the switch is ON: inductor 1 is charged by the input voltage, inductor 2 is charged by capacitor 1, the diode is OFF, and the output voltage is maintained by capacitor 2.

When the switch is OFF: inductors 1 and 2 discharge to the load through the diode (which is ON), and capacitors 1 and 2 are charged. [20]
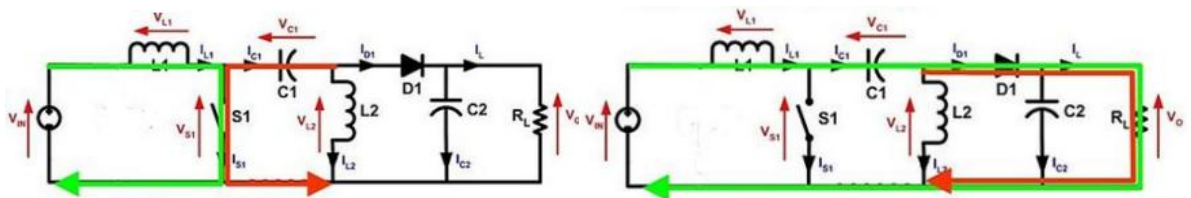
Figure 4.48. Left, SEPIC operation when the switch is ON. Right, SEPIC operation when the switch is OFF

Charge controller

When output voltage of the DC/DC converter is accurately regulated, an appropriate charge management system must be developed in order to charge the Lithium-ion batteries properly (as described in [*Figure 4.42*]).

There are two types of charge controllers for charging batteries application:

1- Linear solutions: linear charging solutions are employed when a well-regulated input source is available. Linear solutions, in these applications, offer advantages such as ease-of-use, size, and cost.
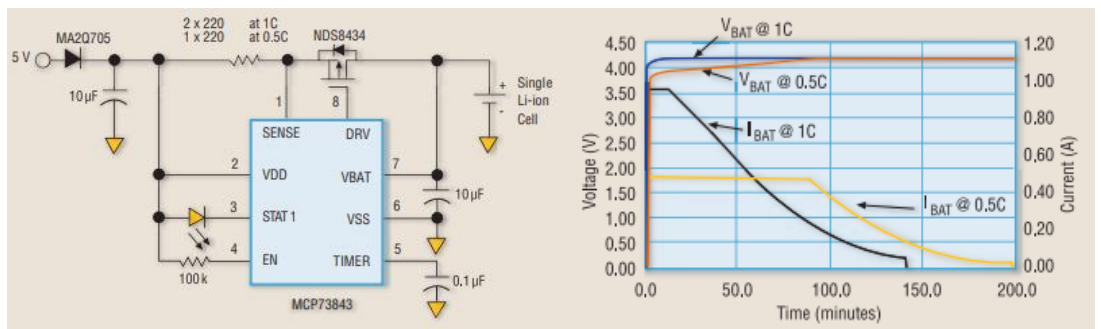
Figure 4.49. MCP73843 linear solution for a Lithium ion battery charger. Microchip Technology Inc.

2- Switch Mode Solutions: these solutions are often used when the input voltage range (which is actually the DC/DC converter's output voltage) is wide. Switching regulators lower the internal battery charger power dissipation to an acceptable level, having a better efficiency than linear solutions, but adding complexity to the system. The output signals are not continuous (smooth) as the ones in linear solutions, this is because the Pulse Width Modulation control (PWM).
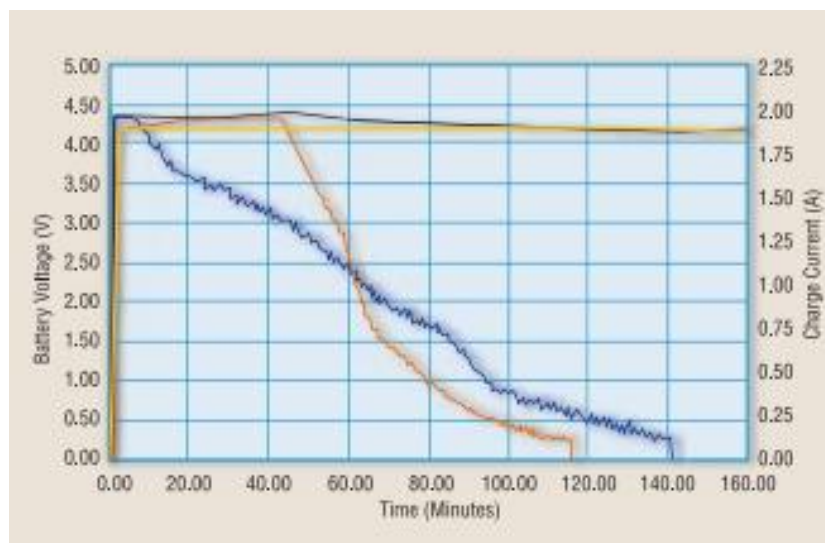
Figure 4.50. Switch mode charge cycle waveforms. Microchip Technology Inc.

[21]

4.2.2. Available solar chargers in the market

There are quite a lot of different solar chargers available in the market and several different brands that provide this product. Four solar chargers are described in this chapter; they have been selected because of their good characteristics, which make them stand out from others.

Big Blue 28W

- Price: $59.99 at Amazon
- Panel Nominal Power: 28 W
- USB outlets: 2
- Weight: 0.67 kg (23.4 oz)
- Pros: inexpensive, efficient, user-friendly, excels   in partly cloudy conditions
- Cons: bulky, heavy

Figure 4.51. Big Blue 28W

Renogy 15,000mAh

- Price: $34.99 at Amazon
- Panel Nominal Power: 2 W
- USB outlets: 2
- Weight: 0.27 kg (9.5 oz)
- Pros: lightweight, inexpensive, efficient
- Cons: Ineffective if relying only on solar power, not very durable

Figure 4.52. Renogy 15,000mAh

Voltaics Systems Arc 20W

- Price: $229 at Amazon
- Panel Nominal Power: 20 W
- USB outlets: 0

- Weight: 0.74 kg (26 oz)
- Pros: effective panel, external battery to charge large electronics like laptops
- Cons: expensive, heavy, useless for smartphone

Figure 4.53. Voltaics Systems Arc 20W

X-Dragon 40W

- Price: $114,99 at Amazon
- Panel Nominal Power: 40 W
- USB outlets: 1
- Weight: 1.05 kg (37 oz)
- Pros: powerful, works well in partial sun, can charge laptops, cheap compared to other laptop compatible solar chargers
- Cons: expensive: bulky, heavy, complicated adaptors for laptop charge

Figure 4.54. X-Dragon 40W

Unluckily, due to intellectual property policies it is not possible to know the internal characteristics of these chargers (which kind of charging solutions they use, which DC/DC converter topology they use, whether they have a MPPT algorithm or not, etc.).

4.3. Conventional Charging vs. Fast Charging

As Lithium-Ion batteries have been improved and high capacity batteries have been introduced in different smartphones, the charging technology has also evolved in order to increase the charging speed (decreasing the time that the smartphone has to be charging).

Conventional charging, or standard USB charge, are chargers that work at a 5V voltage and can send current values around 0.5 A, delivering a 2.5W of power.

Fast charging increases the current sent to the battery to fill up its capacity quicker, so it delivers higher power to the battery.

ETSEIB

USB Power Delivery (USB-PD) is the official fast charging specification (published in 2012). It augments the basic USB charging speeds for up to 100W of output power [*Table 4.3*]. The amount of available power is split into different power ratings, which operate at different voltages. The 7.5W+ and 15W+ modes are best for phones, while 27W and above are for laptops and other higher power devices.

The official Power Delivery specification, and the technology is supported in the vast majority of smartphones today.

Power output (Operating Voltage and Current)	0.5 - 15W	15 - 27W	27 - 45W	45 - 60W	60 - 100W
5V	0.1 – 3.0A	3.0A (15W cap)	3.0A (15W cap)	3.0A (15W cap)	3.0A (15W cap)
9V		1.67 – 3.0A	3.0A (27W cap)	3.0A (27W cap)	3.0A (27W cap)
15V			1.8 – 3.0A	3.0A (45W cap)	3.0A (45W cap)
20V				2.25 – 3.0A	3.0 – 5.0A

Table 4.3. USB-PD specifications

ETSEIB

5. Predesign

In this chapter, different technical options for the design of the solar charger are going to be discussed in order to find the best option. The objective is not to design the final deliverable product (which should have better characteristics than this prototype) but to design a Minimum Viable Product (MVP) which is capable of charging electronic devices properly without adding too much complexity to the hole system. The MVP should be simple enough to be simulated with Matlab/Simulink, and the subsequent improves to be added to the final product will also be qualitatively described (but not simulated).

The main variables to be considered in the MVP technical design solution are:

- Performance and quality (acceptable charge speed, low battery damage, good performance in partly cloudy conditions, etc.)
- Simplicity (use as few components as possible, use simple components, use components with linear solutions)

The improvements to be added to the final product have the objective of improving:

- Usability (can be used at night, can be used to charge larger electronic devices)
- Efficiency (reduce losses in the system)
- Economy (use cheap components)

5.1. Study of Electrical Consumptions - Nominal Power

The first thing to be defined before starting to design the product is the nominal power that the solar panel must provide to the load. This parameter is strictly related with the number and type of electronic devices that can be simultaneously charged.

The MVP for the solar charger will be focused in charging smartphones, so no larger electronic devices will be considered (such as laptops or tablets). The solar charger is designed for being able to charge any two smartphones at the same time under "normal" sun conditions.

Now, batteries in smartphones have nominal capacities from 1,891 mAh (iPhone 8 - Apple) to 5000 mAh (Moto G7 Power - Motorola, Moto E5 Plus – Motorola, Huawei Mate 20 X – Huawei, Zenfone Max Pro M1 – ASUS, Galaxy A40s – Samsung, etc.) or even more.

In order to define the nominal power provided by the solar generator, some high capacity smartphone batteries are going to be described:

Xiaomi Mi Max 3

Battery technical data:

- Nominal capacity: $C_n = 5500\ mAh$

- Minimum capacity: $C_{min} = 5400\ mAh$

- Normal and fast charge modes recommended by the manufacturer:
    - Normal charge: 5V 2A (10 W)
    - Fast Charge 3.0: 9V 2A (18 W)
    - C-rate around 0,37C

Figure 5.1. Xiomi Mi Max 3

Samsung Galaxy A40s

Battery technical data:

- Nominal capacity: $C_n = 5000\ mAh$

- Normal and fast charge modes recommended by the manufacturer:
    - Normal charge: 5V 2A (10 W)
    - Fast Charge 3.0: 5V 3A (15 W)
    - C-rate: between 0,4C and 0,6C

Figure 5.2. Samsung Galaxy A40s

So, considering the normal recommended range of charging voltages and currents in different smartphone batteries, the solar chargers available in the market and the highest capacity batteries available in the market, the design specifications for the MVP solar charger

are:

- Number of USB outlets: $N_{USB} = 2$
- Output voltage: $V_{out} = 5\ V$
- Charging current: $I_{out} = 2.4\ A$

So, the nominal power supply under "normal" sun conditions is:

$$P_{PV} = N_{USB} \cdot V_{out} \cdot I_{out} = 24\ W\ [eq.\,60]$$

A solar charger with these specifications can simultaneously charge two high capacity smartphone batteries in 2h - 2.3h (120min – 140min); even less if the capacity of the battery is lower.

5.2. Possible solutions - Discussion

In this chapter different design solution are described and the final solution for the MVP product is chosen considering the defined variables (performance, quality, simplicity).

- With auxiliary battery vs. without auxiliary battery:
  The first decision to be took is whether to add an auxiliary acid lead battery or not. The pros and cons of adding tare summarized in [*Table 5.1*].

pros	cons
Additional storage system, the solar charger can be used at night and in very cloudy days.	More complex system. Two converters needed.
Adds value to the product. Increase quality.	Increase of cost
	Less portability. Makes the product bulkier and heavier.

  Table 5.1. Pros and cons of adding a battery.

  Analyzing the pros and the cons described above, it has been considered that the MVP product will not have an auxiliary battery, but final product should have one in order to provide a better service.

- With MPPT algorithm vs without MPPT battery: pros and cons in [*Table 5.2*]

pros	cons
Power optimization	More complexity in computing the duty cycle of the converter.

Easier to control the output voltage	
More predictable system.	

Table 5.2. Pros and cons of MPPT algorithm.

The MVP solar charger will compute MPPT converter because it is an economical way to increase its quality.

- Buck converter vs. SEPIC converter
  Buck and SEPIC converters are two different topologies for DC/DC converters, as explained in [*Chapter 4.2.1*]. Their pros and cons are analyzed in [*Table 5.3*].

	pros	*cons*
BUCK	Simple	Only reduces voltage
	Economical	Can cause important damage to the system when sun power is low
SEPIC	Can reduce and increase voltage	More complex
	Works well when sun power is low	Increases the cost a little bit
	Better performance	

Table 5.3. Pros and cons of buck and SEPIC converters.

The final decision is to use a SEPIC as main converter in the MVP and add a buck converter after the battery in the final product.

- Linear charging solution vs. switch model charging solution: as explained in [*Chapter 4.2.1*], pros and cons of each are:

	pros	*cons*
LINEAR	Simplicity	Not very efficient. Thermal losses
	Smooth output signals	Voltage must be precisely controlled.
SWITCH MODE	Less losses	Not smooth output signals
	Works better when voltage is not well controlled (wide range)	Works with PWM control. Adds complexity.

Table 5.4. Pros and cons of linear and switch mode charging management solution.

In order to reduce complexity of the system and considering that the voltage will be correctly controlled, the charging solution will be linear.

5.3. Minimum Viable Product vs. Final Product

The electric diagram of the MVP product is described in [*Figure 5.3*] as defined in the previous chapter. The final product [*Figure 5.4*] will have an additional battery in order to store energy for charging smartphones at night.
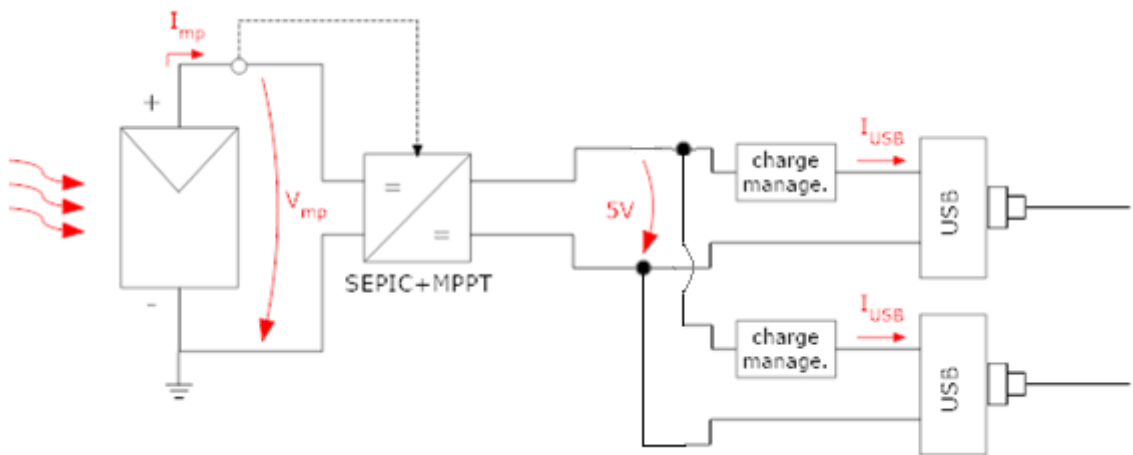
Figure 5.3. Minimum Viable Product electric diagram.
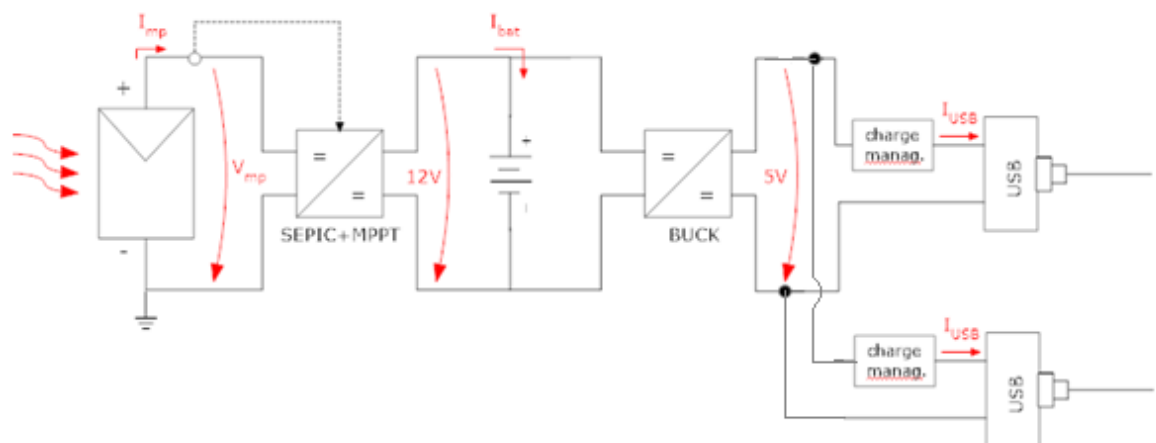
Figure 5.4. Final product electric diagram.

6. Design and simulation of the MVP

6.1. Solar Generator

6.1.1. Design conditions

As said in [*Chapter 5.1*], the solar generator is designed to deliver 24W of maximum power [*eq. 60*] under "normal" conditions. First, it's necessary to define what "normal" conditions are (they must not be confused with standard conditions).

Standard conditions are the irradiation ($G_{ref} = 1000 \ W/m^2$) and cell temperature ($T_{c,ref} = 25\ °C$) conditions used as a reference by manufacturers to define the characteristics of a solar module ($V_{oc}, I_{sc}, V_{mp}, I_{mp}, etc$).

Normal conditions are the design conditions under which the solar system is likely to operate, and they are not chosen by the manufacturer but by the engineer who designs the system. These conditions are chosen according to the location of the system and its average climate conditions. This portable system is designed to work at any place of the Iberian Peninsula so, after studying the average solar irradiance in Spain and Portugal [22] the next "normal" conditions have been set (below average conditions in order to work well in unfavorable situations):

$$G_n = 430 \ W/m^2 \qquad T_{c,n} = 20\ °C$$
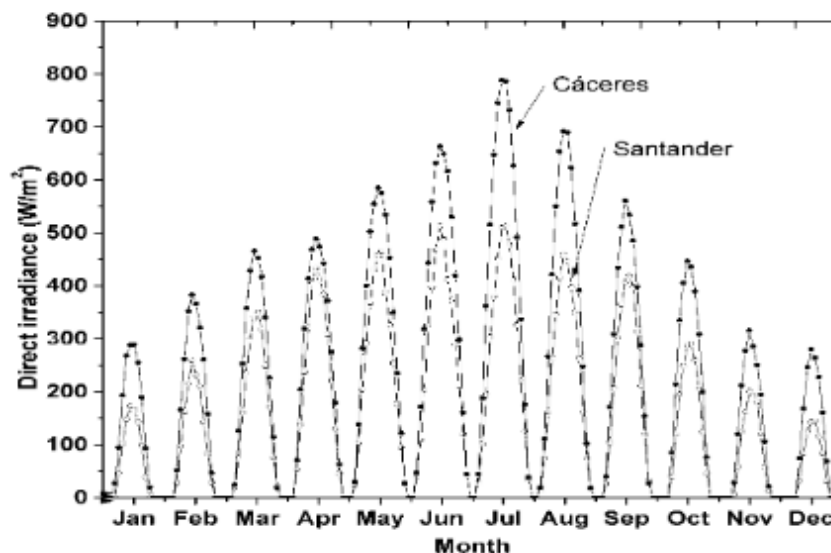
Figure 6.1. Annual evolution of the average solar irradiance in two Spanish cities. Cáceres (high

irradiance) and Santander (low irradiance).

6.1.2.   Material selection

There are three main types of solar cells: monocrystalline, polycrystalline and thin film PV cells. Although thin film cells are not as efficient as the other two types (because it's not such a mature technology) their mechanic and aesthetic characteristics make them perfect for this application because they are lighter, slighter, more flexible and manageable and more visually pleasant.

Figure 6.2. Three type of PV cells.

There are also four different type of thin film cell depending on the photovoltaic material used for its construction: amorph silicon (a-Si), cadmium telluride (CdTe), copper indium gallium selenide (CIGS) and gallium arsenide (GaAs). CIGS cells are preferable to the other three types because they have better efficiency rates (around 20%). [23]
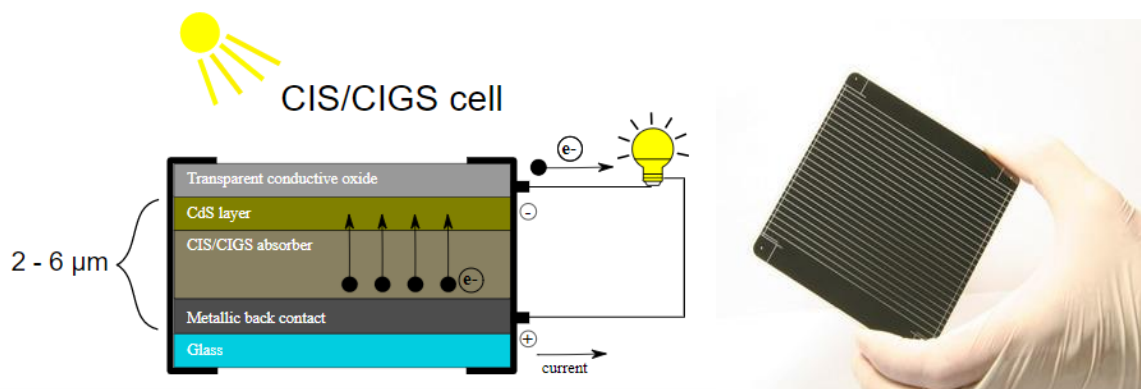
Figure 6.3. CIGS PV cell technology.

6.1.3. CIGS PV Module

After doing an extensive research about different CIGS PV modules which are already commercialized and can be applied in the solar charger, the Flisom-eFlex-1.6mFF60 has been finally selected because its characteristics fit perfectly with our requirements. The complete datasheet of this module is attached in [*Appendix A*]. In [*Table 6.1*] are described the main characteristics of the module, and some secondary characteristics are described in [*Table 6.2*].

V_{oc}	48 V
I_{sc}	1.91 A
V_{mp}	36 V
I_{mp}	1.66 A
P_{mp}	59.76 W ($\cong$ 60 W)
FF	0,652

Figure 6.4. Flisom - eFlex 1.6m FF60   *Table 6.1. Flisom eFlex 1.6 FF60 main characteristics.*

thermal charactersitics		*mechanical characteristics*	
K_{ti}	0.01 %/°C $\equiv 1.91 \cdot 10^{-4}$ A/K	*weight*	1.3 kg
K_{tv}	-0.3 %/°C $\equiv -0.144$ V/K	A	0.664 m^2

Table 6.2. Flisom eFlex 1.6 FF60 secondary characteristics.

Another important characteristic of this solar module is the intern configuration of its cells, which are connected in series with a by-pass diode for every set of 6 cells, as represented in [*Figure 6.5*]. This fact makes the module perform more efficiently when part of the surface is shadowed and reduces the risk of damage, as explained in [*Chapter 4.1.4*]. [24]
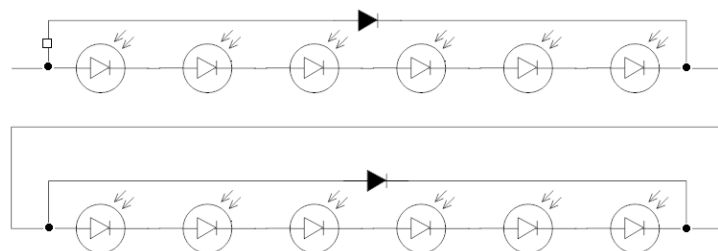
Figure 6.5. PV module intern configuration (PV cells and by-pass diodes)

6.1.4.   Simulation model

In order to simulate the characteristic curves and the power output of the selected PV module, a Matlab-Simulink block model has been designed following the mathematical model described in [*Chapter 4.1.4*], described by the equations [*eq.41*], [*eq.42*], [*eq.43*], [*eq.44*], [*eq.45*], [*eq.46*] and [*eq.47*]. The block model is represented in the next figures:

- [*Figure 6.6*]: photo-generated current
- [*Figure 6.7*]: temperature equivalent voltage
- [*Figure 6.8*]: reference reverse saturation current
- [*Figure 6.9*]: diode reverse saturation current
- [*Figure 6.10*]: diode direct current
- [*Figure 6.11*]: losses in parallel branch

All this block diagrams are put together to create the complete model of a PV module [*Figure 6.12*]. It is important to remark that the voltage data points have been generated with a ramp signal (sweep) in order to generate the characteristic curves; the model needs a feedback loop of the current signal in order to compute the curves iteratively.
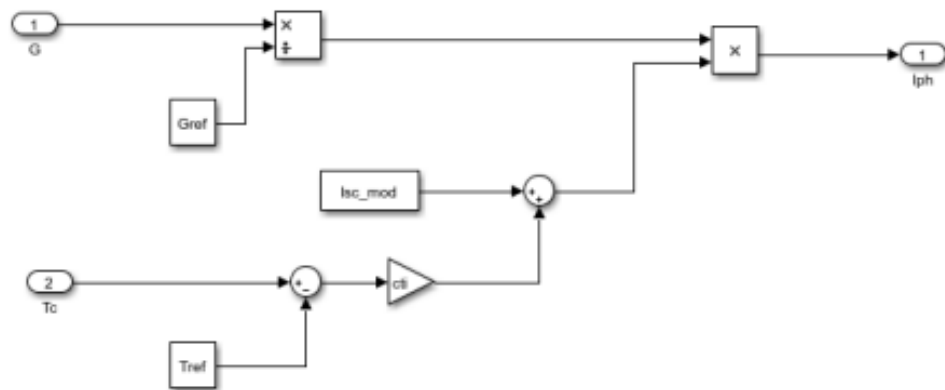
Figure 6.6. Photo-generated current. [eq.42]
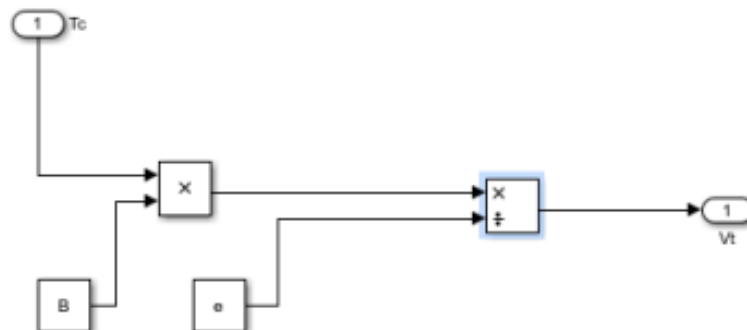
Figure 6.7. Temperature equivalent voltage. [eq.44]
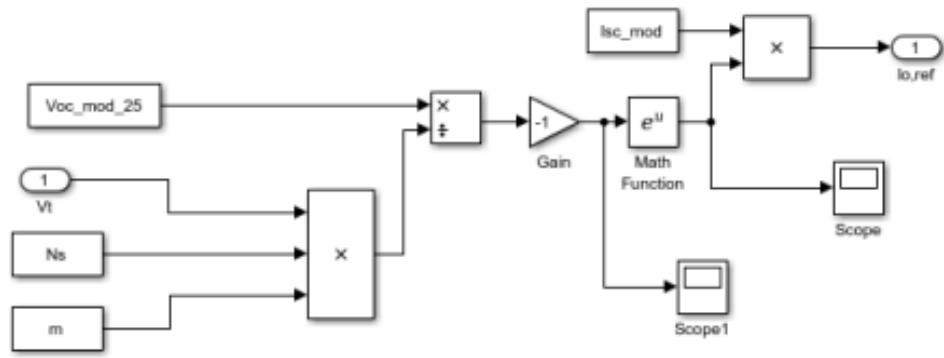
Figure 6.8. Reference reverse saturation current. [eq.46]
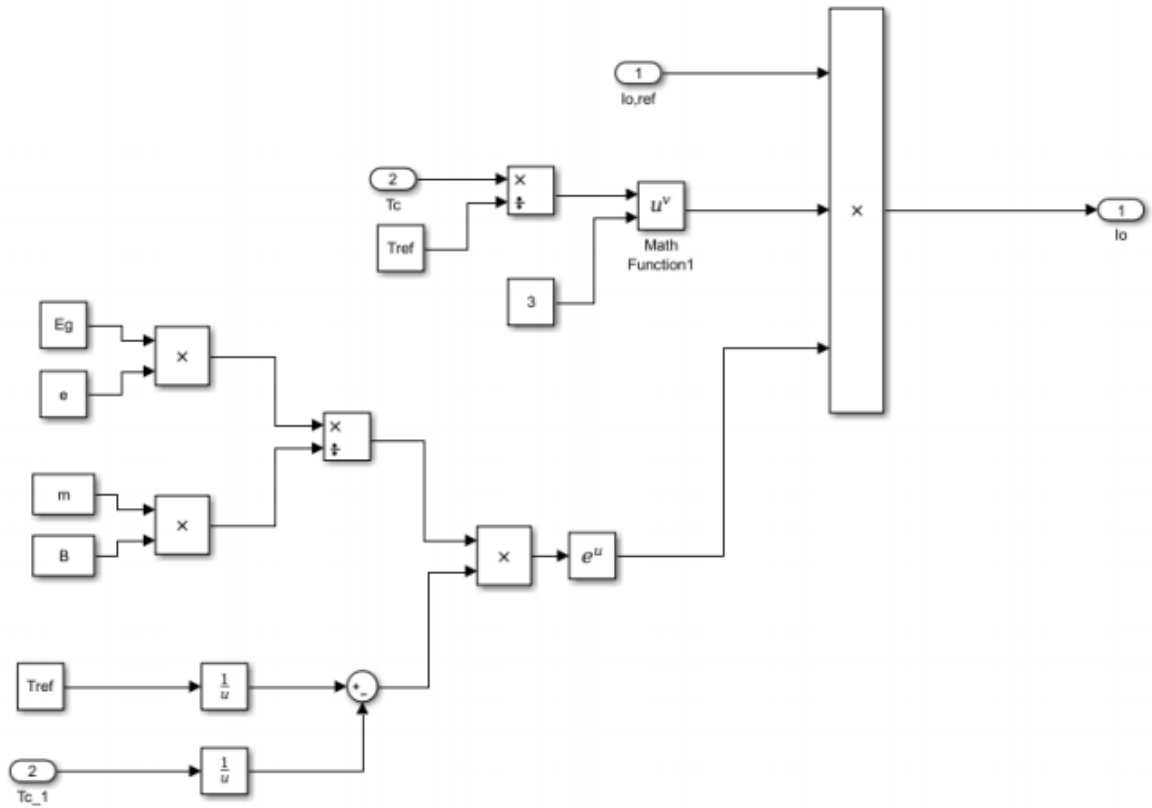
Figure 6.9. Diode reverse saturation current. [eq.45]
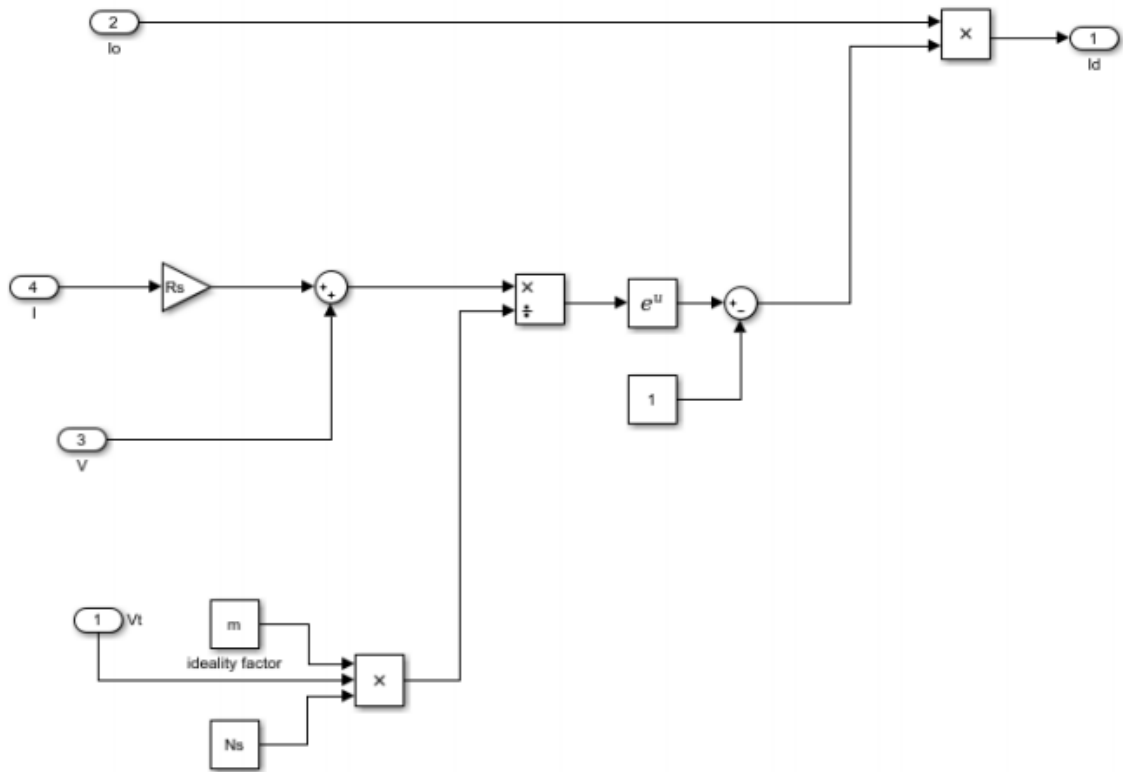
Figure 6.10. Diode direct current. [eq.43]
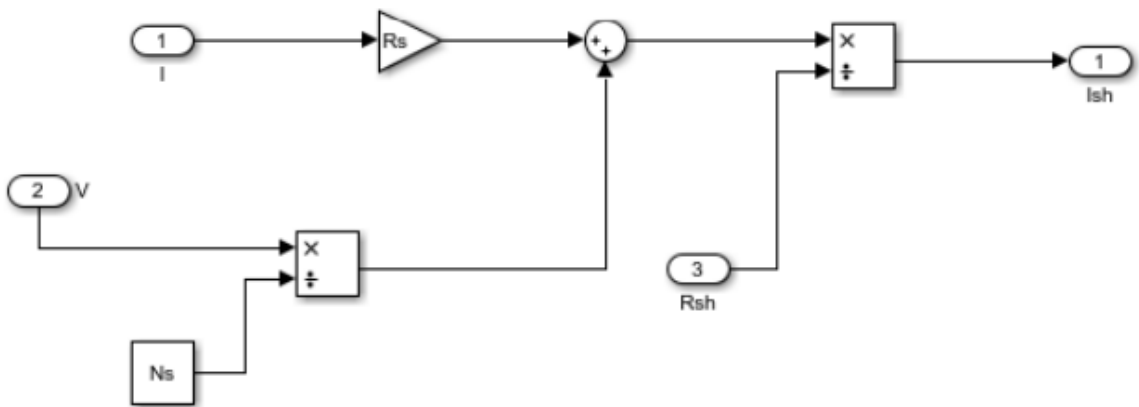
Figure 6.11. Losses in parallel branch. [eq.47]

ETSEIB
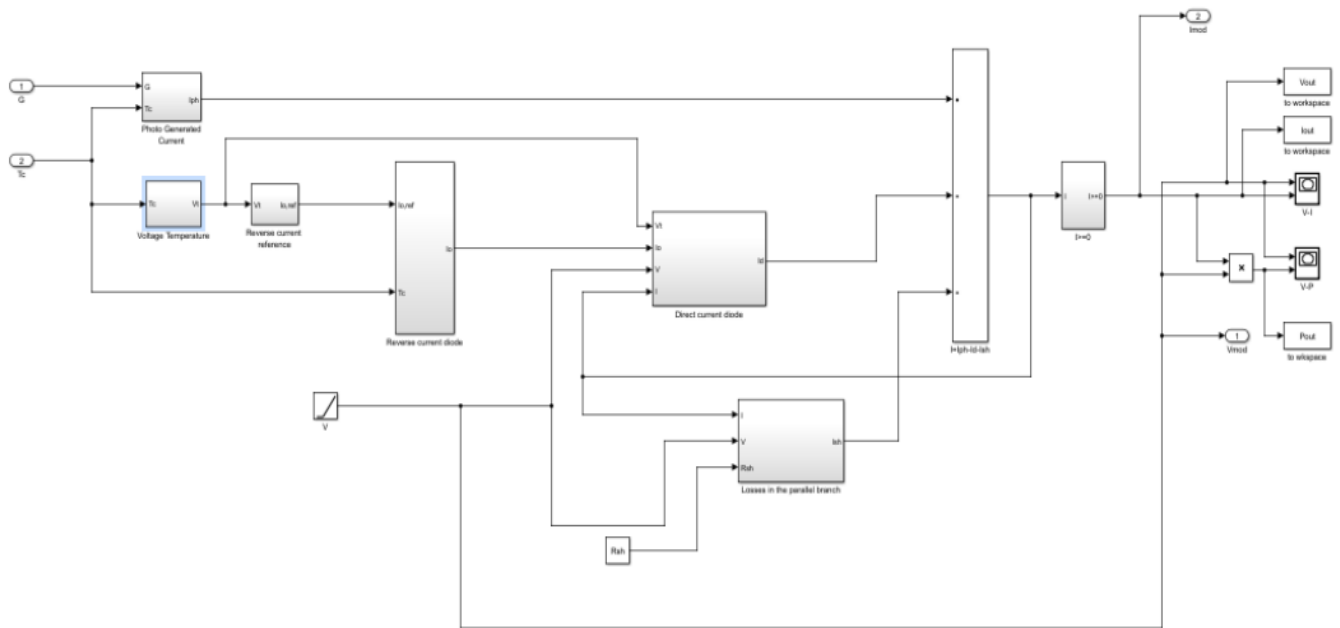
Figure 6.12. Full PV module block model. [eq.41]

6.1.5. Simulation results

The model described in [*Chapter 6.1.4*] is simulated under two different parameters in order to get the characteristic curves and evaluate if it is good for the solar charger. The values of the different constants are:

$$G_{ref} = 1000 \ W/m^2 \quad T_{c,ref} = 25°C \quad V_{oc} = 48 \ V \quad I_{sc} = 1.91 \ A \quad K_{ti} = 0.01 \ \%/°C$$

$$K_{tv} = -0.3 \ \%/°C \quad \eta_d = 1.5 \quad E_g = 1 \ eV \quad R_s = 0.39383 \ \Omega \quad R_{sh} = 313.3991 \ \Omega$$

Simulation under reference conditions – model validation

In this simulation: $G = G_{ref}$, $T_c = T_{c,ref}$

The characteristic curves are plotted in [*Figure 6.13*].

In [*Table 6.3*] the results of the simulation are compared to the characteristics provided by the manufacturer of the PV module, we can observe that the relative error between the computed and the experimental results is small ($\varepsilon_r < 1.5 \ \%$), so the simulation model is validated and can be used to simulate our PV module under any conditions.
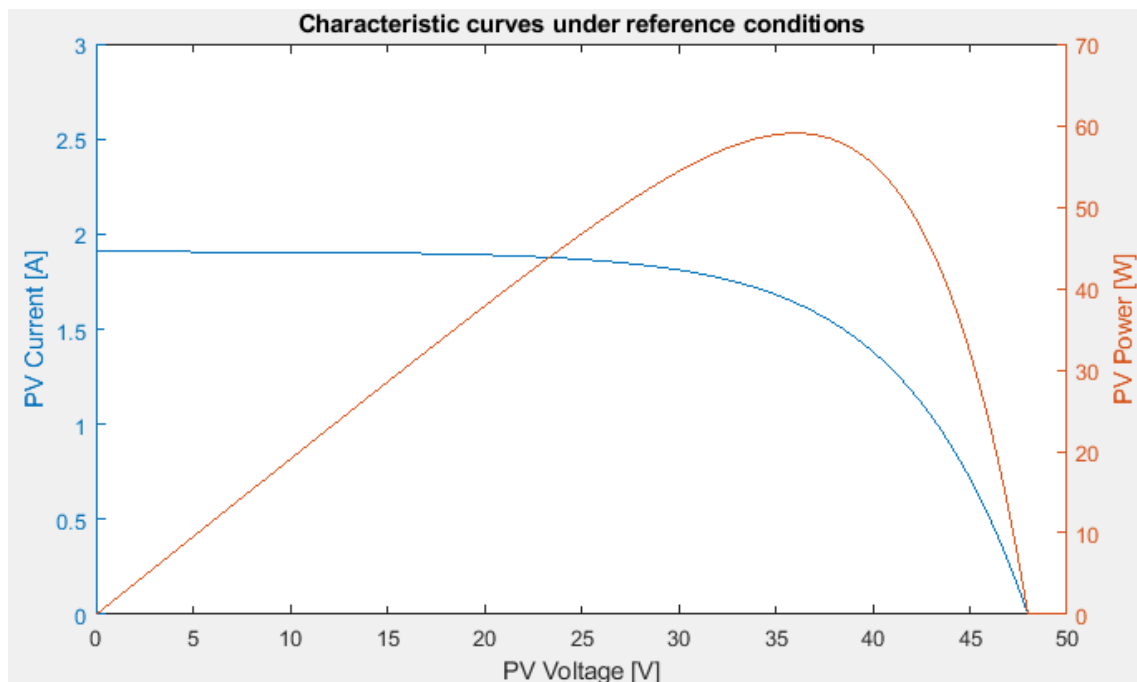
Figure 6.13. Characteristic curves under reference conditions.

	Provided values	*Simulated values*	*Relative error*
$V_{mp}(G_{ref}, T_{c,ref})$	$36\,V$	$36\,V$	$0\,\%$
$I_{mp}(G_{ref}, T_{c,ref})$	$1.66\,A$	$1.64\,W$	$1.2\,\%$
$P_{mp}(G_{ref}, T_{c,ref})$	$59.76\,W$	$59.04\,W$	$1.2\,\%$
FF_{ref}	0.652	0.644	$1.23\,\%$

Table 6.3. Comparison between the values provided by the manufacturer and the simulated values.

Simulation under "normal" conditions – PV module validation

In this simulation: $G = G_n = 430\,W/m^2$, $T_c = T_{c,n} = 20°C$

The characteristic curves are plotted in [*Figure 6.14*] and the simulated characteristic values are presented in [*Table 6.4*]. The maximum power of the PV module under "normal" condition is $P_{mp} = 23.63\,W$, which is very close to the desired value of 24 W defined in [*Chapter 5.1*] ($\varepsilon_r = 1.54\,\%$). Theses results validate the selected PV module for the solar charger.
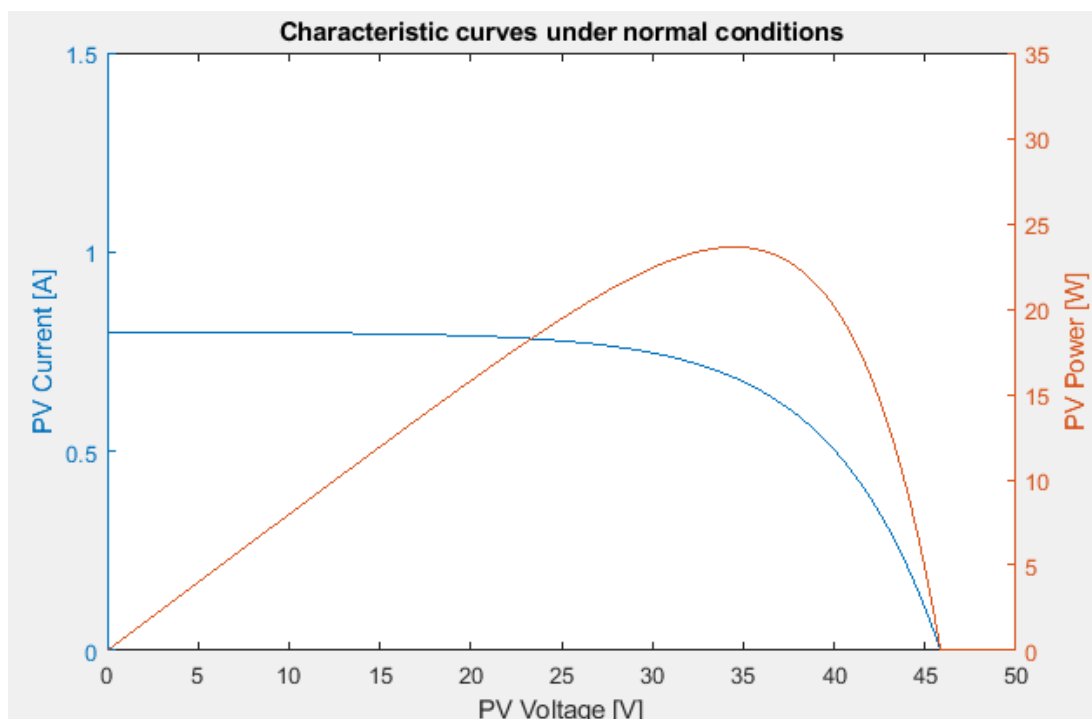
Figure 6.14. Characteristic curves under normal conditions.

$V_{oc}(G_n, T_{c,n})$	$I_{sc}(G_n, T_{c,n})$	$V_{mp}(G_n, T_{c,n})$	$I_{mp}(G_n, T_{c,n})$	$P_{mp}(G_n, T_{c,n})$	FF_n
45.87 V	0.80 A	34.75 V	0.68 A	23.63 W	0.644

Figure 6.4. Simulated values for the selected PV model under normal conditions

6.2. Buck-boost converter: SEPIC + MPPT

This chapter presents Perturb&Observe (P&O) control method for maximum power point tracking (MPPT) of this PV system under varying irradiation and temperature conditions. This algorithm will identify the suitable duty ratio in which the DC/DC SEPIC converter should be operated to maximize the power output. Also, this converter and their control strategies have been analyzed and simulated using Simulink/Matlab software.

6.2.1. Operation Diagram

The MPPT algorithm computes the duty cycle of the converter as explained in [*Chapter 4.2.1*] and generates a pulse signal in a PWM which directly controls the switch of the DC/DC converter, as described in [*Figure 6.15*].

This device (MPPT+SEPIC) has two main objectives:

1- Control the PV module to operate at the maximum power point $[P_{PV} = P_{pm}(G, T_c)]$
2- Control the output voltage to be $V_{out} = 5\,V$

In order to achieve these two objectives, two power stages will be designed:

1- The first stage will have (V_{PV}, I_{PV}) as input and (V_{mp}, I_{mp}) as output
2- The second stage will have (V_{mp}, I_{mp}) as input and $(5\,V, I_{out})$ as output
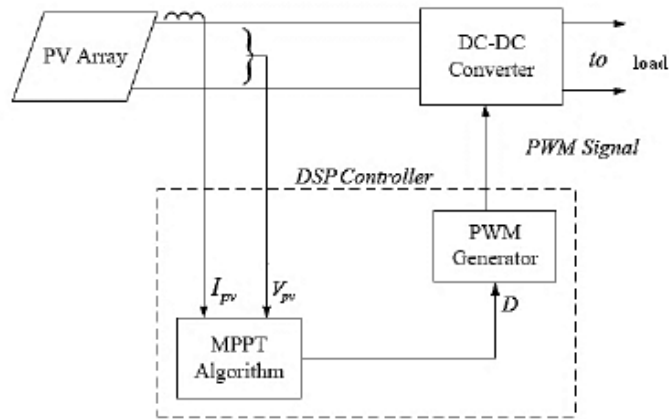
Figure 6.15. Operation diagram of the MPPT+SEPIC device

6.2.2. Selected converter

After an extensive market research, the integrated circuit selected to be used as a SEPIC converter in both power stages is the LT8495 (manufactured by the electronic company LINEAR technology) [*Figure 6.16*]. The datasheet [25] can be found in [*Appendix B*] The main characteristics for which it has been chosen are:

-   Wide range of acceptable input voltage (from 2.5 V to 60 V).
-   Can provide a very stable output voltage signal of 5V
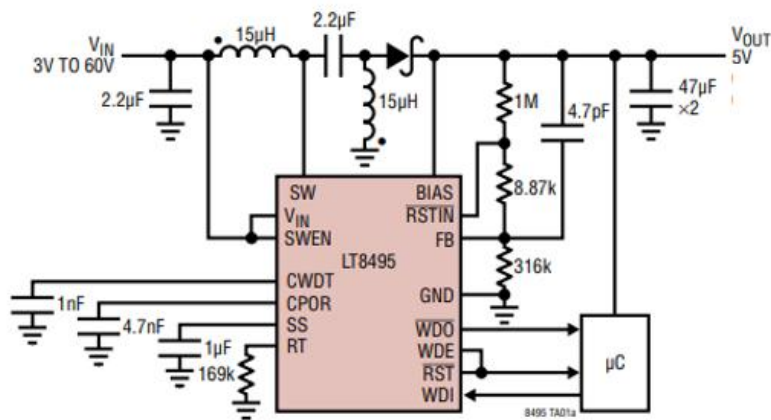
Figure 6.16. 5V output SEPIC LT8495 application.

6.2.3.   Simulation model

The full simulation model is described in [*Figure 6.17*]. It includes the PV module and both power stages of the MPPT+SEPIC power electronics device. The first power stage, which controls the output power of the PV module to reach the maximum [*Figure 6.18*], and the second power stage which controls the output voltage to be 5V [*Figure 6.19*].

The P&O algorithm computed in the MMPT subsystem block follows the flow chart described in [*Figure 4.43*] in [*Chapter 4.2.1*]. The duty cycle computed in the SEPIC subsystem block follows the equation [*eq.59*] in [*Chapter 4.2.1*].
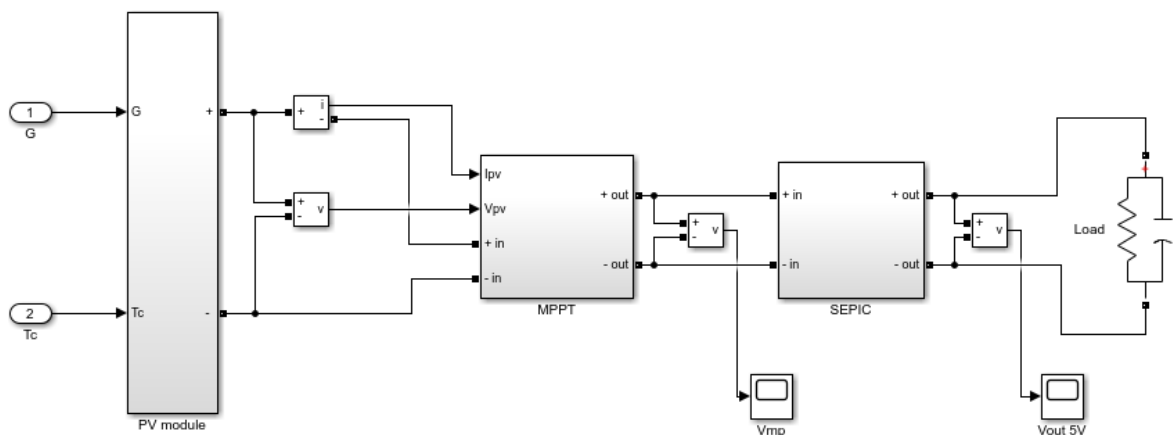
Figure 6.17. Solar charger simulation model.
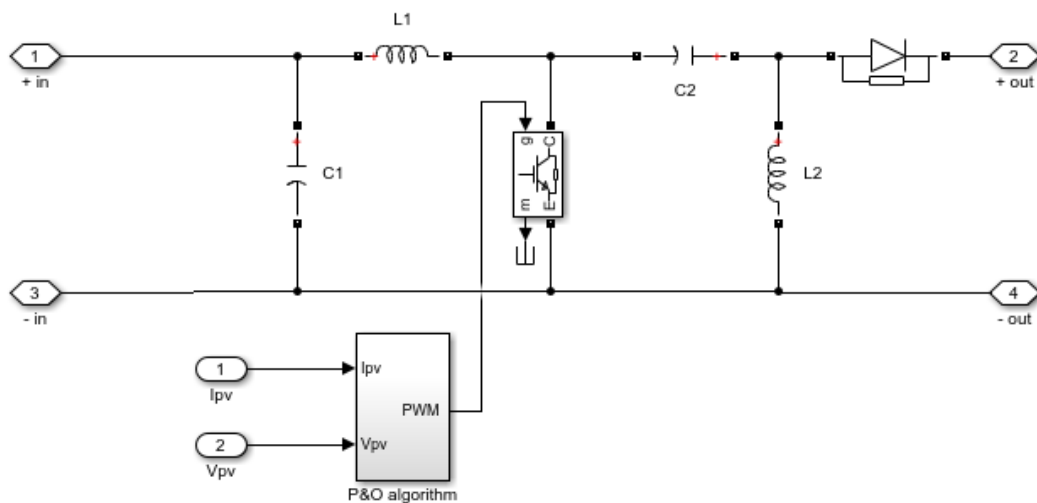
Figure 6.18. MPPT subsystem.
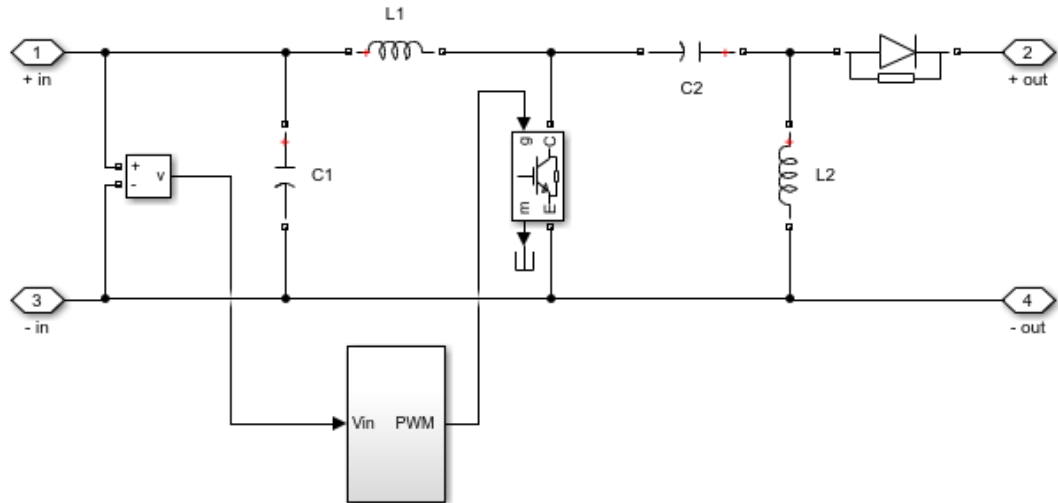
Figure 6.19. SEPIC subsystem.

6.2.4. Simulation results

The different simulations have been done at constant temperature ($T_c = T_{c,n} = 20\ ℃$) and with different values of irradiance. The numerical results are summarized in [*Table 6.5*].

As seen in the table, there is a level of irradiance ($G_{crit} = 530\ W/m^2$) which gives an output current of $I_{out} = 6V$, which means that each USB outlet is receiving a current of 3A. That is maximum current value permitted for 5V fast charging, according to the USB-PD specifications [*Table 4.3*] explained in [*Chapter 4.3*]. So, for irradiance values above the critical irradiance (G_{crit}), the output current will saturate at the values of 3A for each USB outlet.

$G[W/m^2]$	$P_{mp}\ [W]$	$V_{mp}\ [V]$	$I_{mp}[A]$	$V_{out}[A]$	$I_{out}[A]$
200	9.65	31.13	0.31	5	2 x 0.97 A
300	15.55	32.39	0.48	5	2 x 1.56 A
$G_n = 430$	23.63	34.75	0.68	5	2 x 2.36 A
$G_{crit} = 530$	30.08	35.54	0.85	5	2 x 3.01 A
700	41.38	36.83	1.116	5	2 x 4.14 A

Table 6.5. Results of the simulation of the system.

The simulated signals during the MPPT operation are plotted in [*Figure 6.20*] and [*Figure 6.21*]
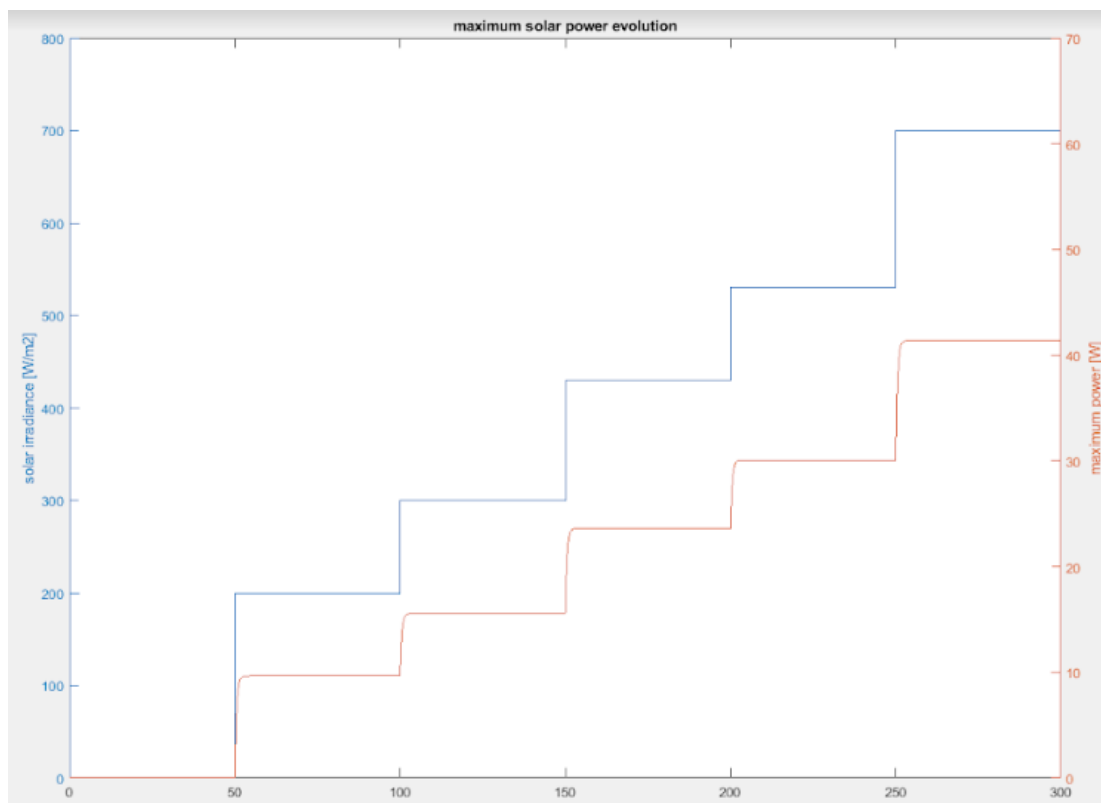
Table 6.20. Maximum solar power evolution for different values of irradiance.
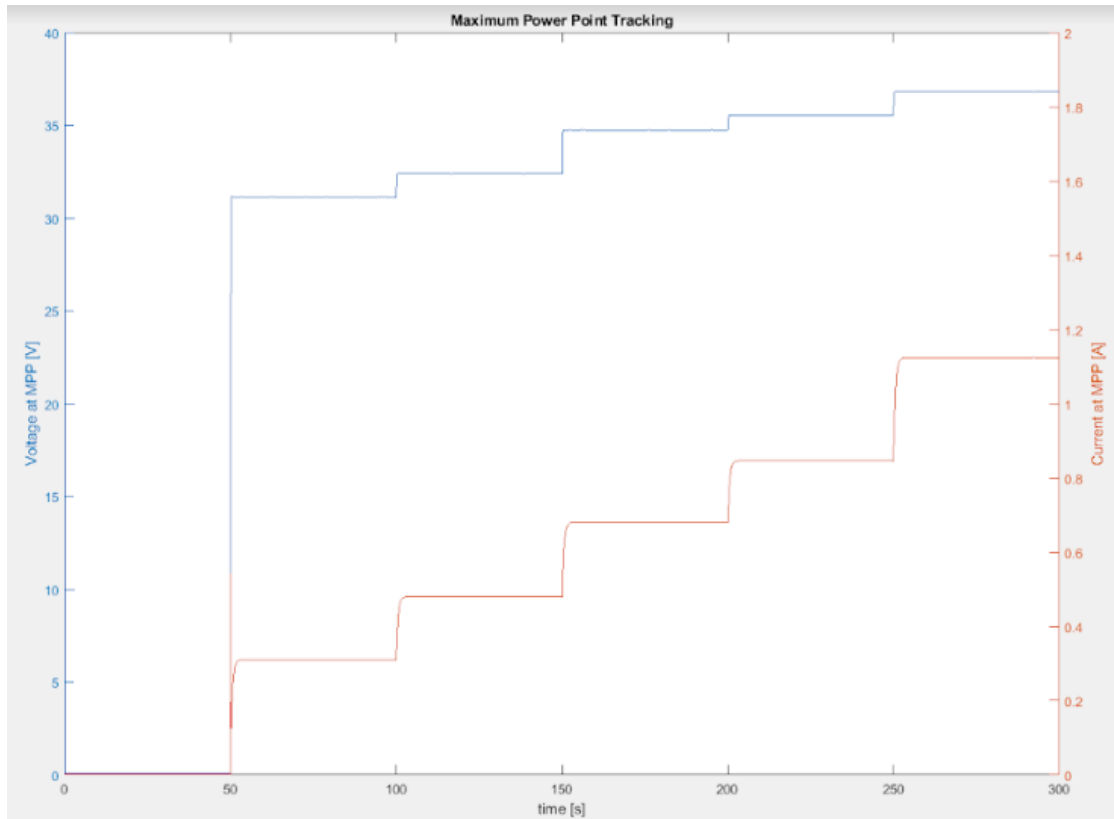
Figure 6.21. Voltage and current evolution during MPPT operation.

In [*Figure 6.20*] and [*Figure 6.21*] the simulated signal may seem smooth, but they are not. As shown in [*Figure 6.22*], the application of the P&O algorithm causes the voltage and current signals to oscillate around the maximum power point.
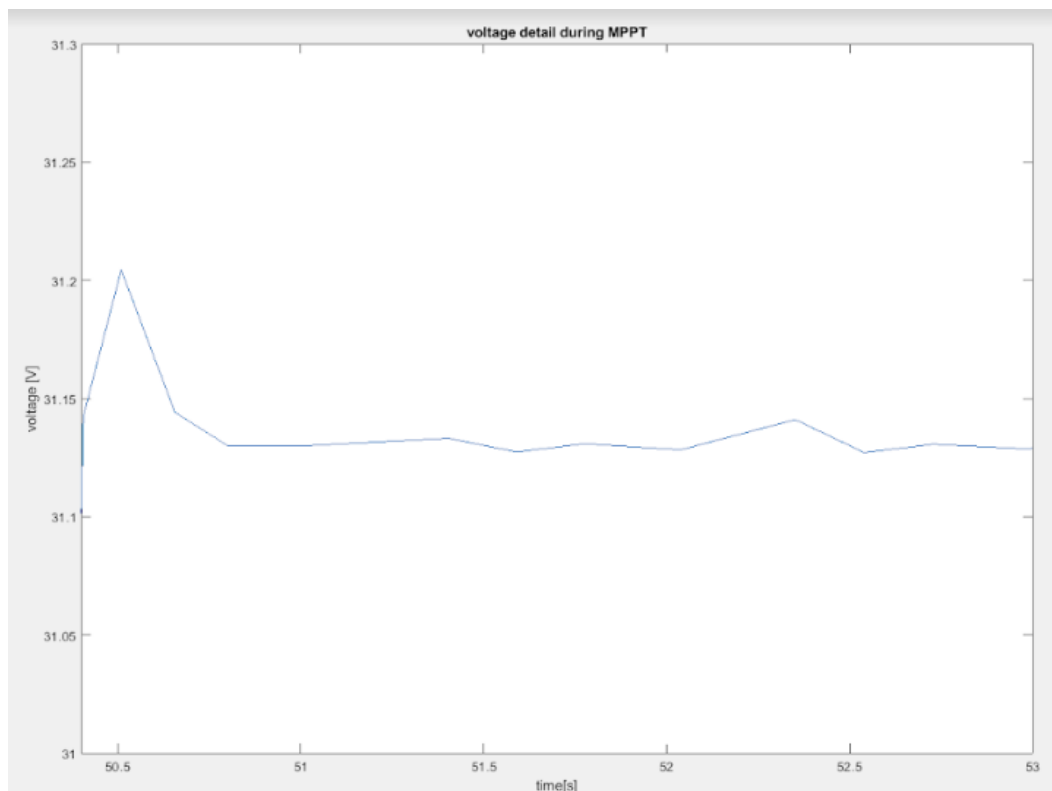
Figure 6.22. Voltage oscillating around the maximum power point.

6.3. Charge management solution

This chapter will select the specific integrated circuit available in the market in order to manage the charging of the lithium-ion system. This integrated circuit will be described but not simulated due to its complexity.

6.3.1. Integrated circuit

In order to manage the different stages during the charging cycle [*Chapter 4.2.1*], it is necessary to add an integrated circuit. As discussed in [*Chapter 5.2*], the selected charging solution is linear in order to reduce complexity and cost, and also to have smoother output signals.

After doing research about different commercial brands of charging management integrated circuits, the MCP73843 (manufactured by the electronic company Microchip Technology Inc.) has been selected. This is an advanced single-or-dual cell lithium-ion/lithium-polymer charge management controller, whose datasheet can be found in [*Appendix C*].

The MCP73843 combine high accuracy, constant-voltage, constant-current regulation, cell preconditioning, cell temperature monitoring, safety timers, automatic charge termination and

charge status indication in space-saving, 10-pin MSOP packages [Figure 6.23].
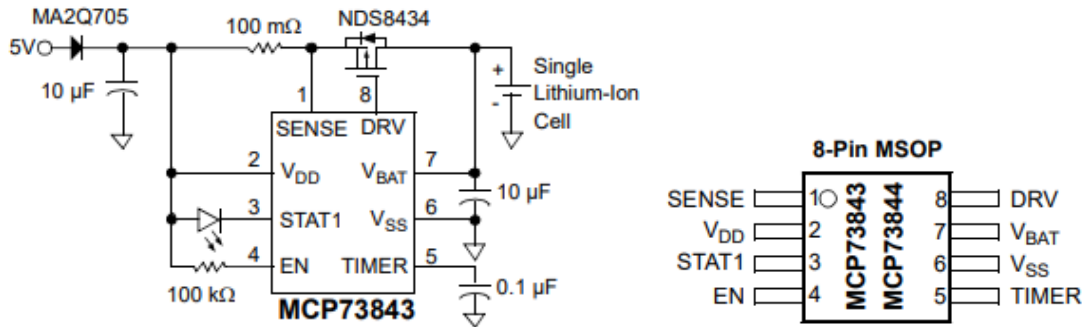
Figure 6.23. Left, MCP73843 typical application circuit for Li-ion battery charger. Right, package type.

6.3.2. Operation

In the datasheet all the details of the MCP73843 integrated circuit are precisely described but, in this chapter, only the most important aspects are remarked.

The charge cycle is described in [*Figure 6.24*] with its important parameters.
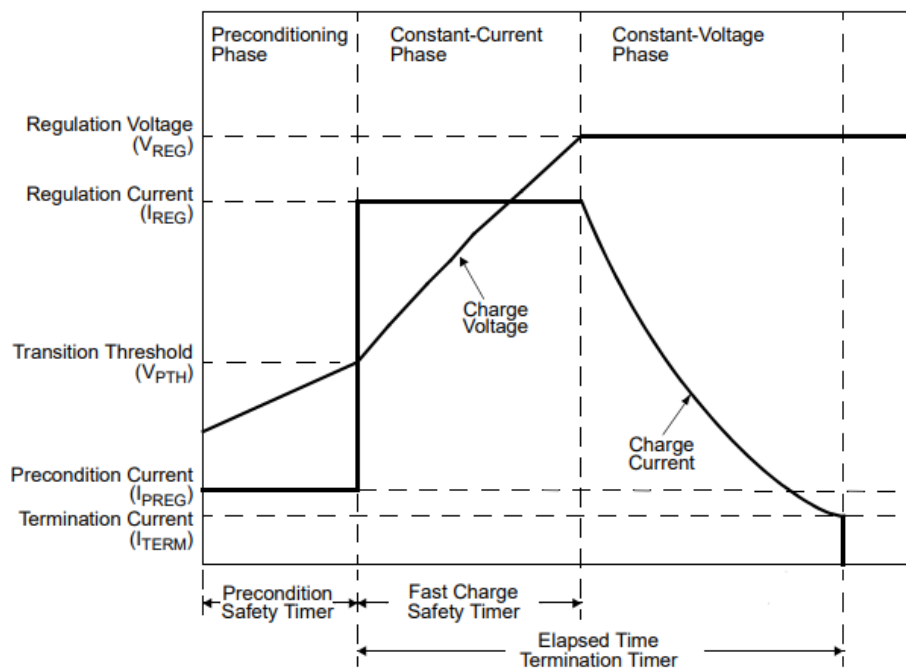
Figure 6.24. Charge cycle operated by MCP73843.

Stage 1 – Charge qualification and preconditioning

the MCP73843 automatically perform a series of safety checks to qualify the charge. The

input source voltage must be above the undervoltage lockout threshold ($V_{DD} > V_{PTH}$; $V_{DD} \cong 5\,V$), the enable pin must be above the logic-high level and the cell temperature monitor must be within the upper and lower thresholds, with the qualification parameters being continuously monitored. Deviation beyond the limits automatically suspends or terminates the charge cycle.

Once the qualification parameters have been met, the MCP73843 initiates a charge cycle. The preconditioning current is set to approximately 10% of the fast charge regulation current ($I_{PREG} \cong 0.1 \cdot I_{REG}$).

Stage 2 – Constant current regulation. Fast charge

When the battery voltage exceeds the preconditioning threshold ($V_{BAT} > V_{PTH}$) preconditioning ends and fast charging begins. Fast charge regulates to a constant-current (I_{REG}) based on the supply voltage (V_{DD}) minus the voltage at the SENSE input (V_{FCS}) developed by the drop across an external resistor (R_{SENSE}). Fast charge continues until the battery voltage reaches the regulation voltage (V_{REG}); or until the fast charge timer expires.

Stage 3 – Constant voltage regulation

When the battery voltage reaches the regulation voltage (V_{REG}), constant-voltage regulation begins. This input is tied directly to the positive terminal of the battery. The MCP73843 gives a fixed voltage of $V_{REG} = 4.1\,V$, which is the proper value for Li-ion batteries.

Stage 4 – Charge cycle completion. Automatic re-charge

The MCP7384X monitors the charging current during the constant-voltage regulation phase. The charge cycle is considered complete when the charge current has diminished below approximately 7% of the regulation current ($I_{TERM} = 0.07 \cdot I_{REG}$) or the elapsed timer has expired. The MCP7384X automatically begins a new charge cycle when the battery voltage falls below the recharge threshold ($V_{RTH} = V_{REG} - 0.2\,V$), assuming all the qualification parameters are met. [26]
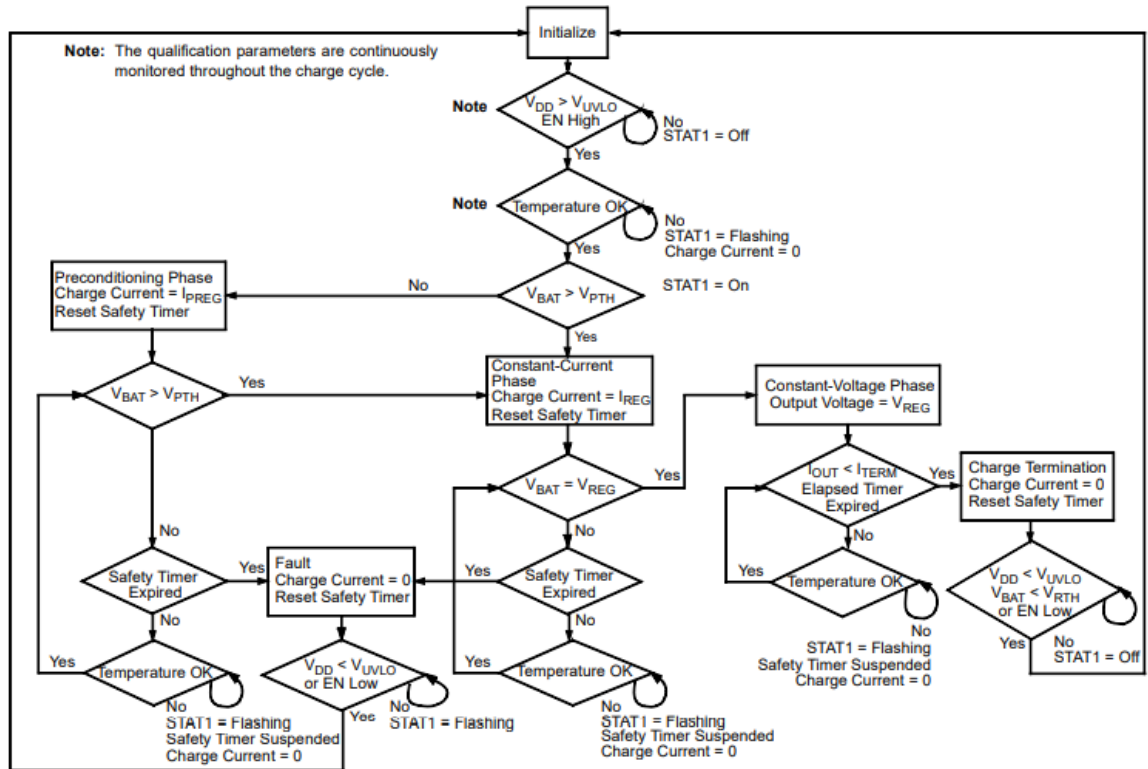
Figure 6.25. Operational Flow Algorithm.

6.3.3. Parameters for correct design

Considering the predesign parameters set in [*Chapter 5.1*]. The suitable parameters for the MCP7384X working at "normal" conditions [*Chapter 6.1.1*] are:

Supply voltage	V_{DD}	5 V	Regulation voltage	V_{REG}	4.1 V
Precond. Threshold Voltage	V_{PTH}	2.8 V	Termination current	I_{TERM}	0.168 A
Regulation current	I_{REG}	2.4 A	Recharge threshold	V_{RTH}	3.9 V
Precondition current	I_{PREG}	0.24 A	External SENSE resistor	R_{SENSE}	0.1 Ω

Table X.X. Design parameters for MCP73843.

Under "normal" conditions the voltage drop across the external SENSE resistor and the voltage at the SENSE input is:

$$\Delta V = V_{DD} - V_{FCS} = I_{REG} \cdot R_{SENSE} = 0.24 \ V \rightarrow V_{FCS} = 4.76 \ V \ [eq. 61]$$

This voltage is in the acceptable range, so the design is correct.

7. Business Plan

As said in the abstract of this paper, the objective of this project is not only to design the product but to create an innovative business plan in order to get revenues and make a positive net profit in the middle term.

In this chapter, the different aspects of the business plan are explained and discussed.

7.1. Value proposition

This business plan is created around the idea of solving a specific need explained in [*Chapter 3.1*]. The main aspects of the value proposition of this business are explained using the conceptual diagram in [*Figure 7.1*].
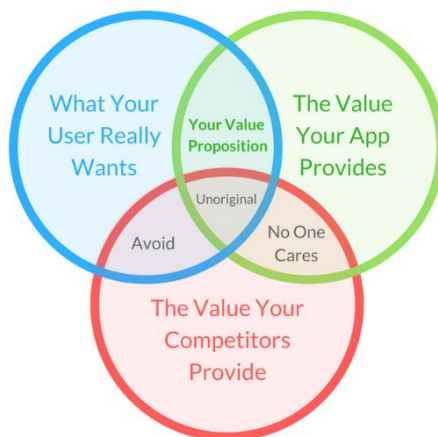
What your user really wants:
The user wants to charge an electronic device during a short period of time (1-3 hours) in a event where acces to electricity is limited or non-existent.

The value proposition your competitors provide:
Our competitors sell good quality solar chargers through different traditional and digital channels (electronic store, Amazon, etc.). Cost is elevated.

Figure 7.1. Value proposition conceptual diagram.

The value your app provides:

Our app provides a pay-per-use service. It delivers solar chargers to the clients on the spot so that they can charge their smartphones during a period of time. Once the electronic device is charged, the solar charger is returned to the company. The cost is low because the client doesn't buy the solar charge.

No one cares	Value proposition
Competitors sell good quality chargers, so our product doesn't stand out in the market.	Innovative business model. Pay-per-use. Service as a product (SaaP). Reduced cost.

Table 7.1. Value proposition summary.

7.2. Business Model

The business model is explained in a Canvas Business Model Chart:

Customer Segments

Principal target:
Young people between 18-30 years old used to go to music festivals.

Secondary target:
People from all ages who usually go to motor sports races during 2-3 days (F1, Moto GP, etc.)

Value Proposition

Satisfy urgent need

Pay-per-use

On the spot delivery

Reduced cost

Service as a Product (SaaP)

Digital environment

Cost Structure

- Solar charger development and manufacturing.
- App creation and development
- R&D
- Operations: stands, delivery, etc.
- Marketing
- Data center

Revenue Streams

- Principal income: charging services with our solar charger
- Secondary income: data selling to business partners

ETSEIB

7.3. Future revenue projections

7.3.1. Solar charger unit cost

The unit cost for each solar charger is calculated as:
- Flisom eFlex 1.6m FF60: 400€
- Linear technology LT8495: 4.26€ (x2) = 8.52€
- Microchip Technology Inc MCP73843: 1.14€ (x2) = 2.24€
- Wire, case and others: 15€

The total cost is estimated to be 426 €/unit. The company will start operating with 100 chargers, which require an expenditure of 43,000€ approximately.

7.3.2. Other costs

Operation costs:
- 5 people salaries: 18,000 €/year (x5) = 90,000 €/year
- Rental costs: 7,200 €/year
- Extra expenditures: 10,000 €/year

Marketing costs
- 2 marketing specialist's salaries: 21,000 €/year (x2) = 42,000 €/year
- Extra expenditures: 10,000 €/year

App development costs
- 3 engineer's salaries: 26,000€ (x3) = 78,000€
- Extra expenditures: 10,000 €/year

Total fix cost: 247,200 €/year

7.3.3. Estimated incomes

For the first three years the company will operate in, at least, 5 music festivals:
- Arenal Sound: 300,000 people in 2019
- Viña Rock: 240,000 people in 2019
- Bilbao BBK Live: 112,800 people in 2019
- FIB Benicàssim: 114,000 people in 2019
- Riverland Festival: 13,000 people in 2019

The estimated potential market is around 780,000 people. Assuming an average conversion rate of 2% during the first year, 3% during the second year and 5% during the third one, we can estimate the future clients as:

- 1st year: 15,600 clients
- 2nd year: 23,400 clients
- 3rd year: 39,600 clients

The charging services will cost 6€/h to the client. It's assumed that the client will use the solar charger an average of 2 hours. The secondary income (data selling) is assumed to be the 20% of the primary income (charging service), so:

	Charging service	Data selling	Total
1st year	187,200 €	37,440 €	224,640 €
2nd year	280,800 €	56,160 €	336,960 €
3rd year	475,200 €	95,040 €	570,200 €

Table 7.2. Estimated incomes for the first three years.

7.3.4. Basic projections for the first three years

An estimation of the company economic growth is summarized in [*Table 7.3*] and [*Figure 7.2*]

	Year 0	Year 1	Year 2	Year 3
Initial expenditure	−43,000 €	no	no	no
Fix costs	no	−247,200 €	−247,200 €	−247,200 €
Turnover	no	224,640 €	336,960 €	570,200 €
Net Benefit (before taxes)	−43,000 €	−22,560 €	89,760 €	323,000 €

Table 7.3. Basic economic projection for the first three years.
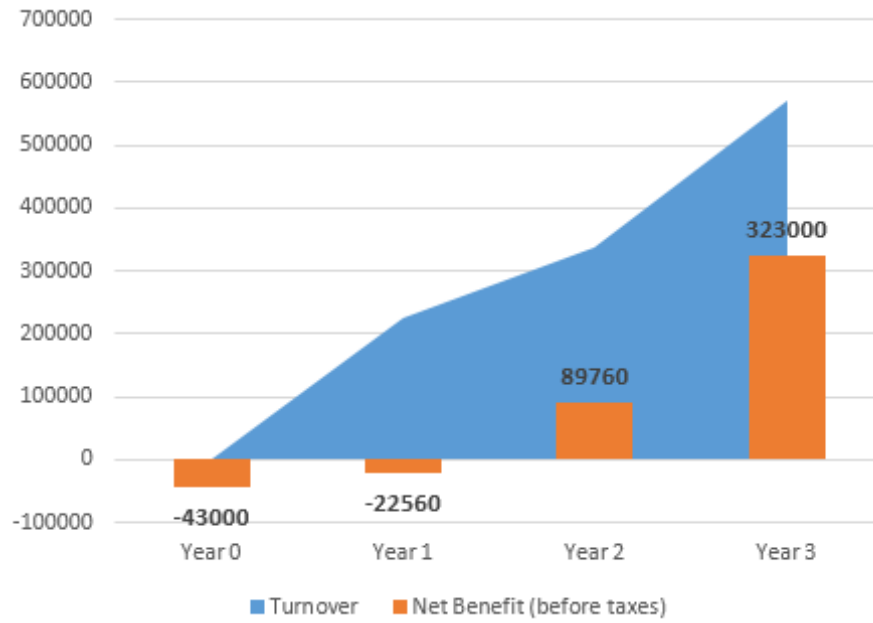
Figure 7.2. Projected growth of the company.

As seen in the figure above, the growth rate of the company seems to be very satisfactory if the desired conversion rates are achieved.

8. Additional information

8.1. Environmental Impact

The designed solar charger provides a nominal power, under "normal" conditions, of 24 W. Assuming that each solar charger will operate 30 days per year during 8 hours per day, the energy that a single solar charger will generate is:

$$E_{gen} = P_{nom} \cdot 30 \, {days}/{year} \cdot 8 \, {hours}/{day} = 5760 \ Wh/year \ [eq. 62]$$

As said in [*Chapter 7.3.1*], there will be 100 solar charger delivering charging services. In Spain, the electrical mix has an estimated emission factor of 321 g CO_2/kWh (2018 data provided by the Climate Change Department - Generalitat de Catalunya). The annual equivalent carbon emissions that will be avoided are:

$$m_{eq,CO_2} = f_{CO_2} \cdot E_{gen,tot} = f_{CO_2} \cdot 100 \cdot E_{gen} = 321 \, {g \ CO_2}/{kWh} \cdot 576 \ kWh$$

$$m_{eq,CO_2} = 184.9 \ {kg \ CO_2}/{year} \ [eq. 63]$$

So, this business project is eco-friendly because it reduces the carbon footprint of its environment $184.9 \ kg \ CO_2/year$.

The average carbon footprint generated by a Spanish citizen is around $7000 \ kg \ CO_2/year$, so the reduction is not too relevant. [27]

8.2. Project Budget

The budget for the completion of this project can be calculated as the sum of the next terms:
- MATLAB Annual License: 800 €
- Microsoft Office 365 Personal Annual License: 55 €
- Laptop, PC Lenovo ideapad 320: 440 €
- Mobility costs: 150 €
- Engineer earnings:

$$Engineer \ earnings = 12 \ ECTS \cdot 25 \ {h}/{ECTS} \cdot 10 \ {€}/{h} = 3000 \ € \ [eq. 63]$$

The total budget is 4,445 €.

8.3. Project Planning

The project planning is described in the Gantt diagram [*Figure 8.1*]. It is important to remark some aspects of the planning:

- I enrolled in the project on February 2019, but I was working full time in an electric company so I considered to deliver the report after the summer vacations, applying for an extension.
- I started to work in the project on June 2019, doing research and looking for good bibliographic material.
- On July I started to select quality information and to write the theoretical aspects of the project, like the State of Art.
- I quitted my job on August 2019 and I started to work full time on the project, focusing my efforts in the design of the solar charger and the simulation models.

Task	feb.-19	mar.-19	abr.-19	may.-19	jun.-19				jul.-19				ago.-19				sep.-19				oct.-19
					W1	W2	W3	W4	W1	W2	W3	W4	W1	W2	W3	W4	W1	W2	W3	W4	
Project Enrollment																					
Definition of the idea																					
Definition of the contents																					
Bibliographical research																					
Information filtering																					
Write a draft of the theoretical concepts																					
Write Chapter 4																					
Predesign of the solar charger																					
Write Chapter 5																					
Create the solar generator simulation model																					
Create the Power Electronics simulation model																					
Generate the simulation results																					
Select real components for the solar charger																					
Write Chapter 6																					
Define the value proposition																					
Define the business model canvas																					
Write Chapter 7																					
Finish the report																					
Delivery of the report																					
Prepare the project presentation																					
Project presentation																					
Working in an electric company																					

Figure 8.1. Gantt diagram of the project.

Conclusions

After working in this project during months designing the electric diagram, creating the simulation models, running them in order to get the results, analyze the results in order to select real components in the market whose characteristics match the desired ones and displaying all these information in this report, I can extract some important conclusions.

The designed product is viable. The solar module is light, small (less than $1m^2$) and flexible, so it can be easily folded in order to optimize the portability of the solar charger. The power electronics is well designed and the simulations provide satisfactory results. Moreover, there are real electronic components whose characteristics match exactly with the ones needed according to the simulation results, so the product should not be developed component by component, because there are commercial components that can be used, which makes us safe time and money. The charger performs well; under normal conditions it should be capable of completely charging a high capacity battery in less than 140 min (even less if there are better irradiance conditions), the charging current is saturated to a maximum value of 3A to protect the Li-Ion battery of the devices (the charge management integrated circuit is the component which performs this) and, in addition, the PV module should perform well when partially shadowed because of the by-pass diodes connected to their cells.

The designed charger has on clear downside, it can't work at night because it can't store energy in a battery. This project could be continued by modifying the product in order to solve this inconvenient and increase its quality without worsen its portability. The project could also be continued by designing the external appearance of the product using a 3D modelling software and even build a real prototype.

I sincerely believe that, to do business with this type of chargers, the proposed business model makes a lot of sense. It is innovative, digital inspired, and can connect very well with young people. The project could also be improved by developing the business model in more detail, and even creating the app.

So, we can finally conclude that the objectives set for this project have been accomplished.

Bibliography

[1] Green, M. A. (11-17-2002). Photovoltaic Principles. Special Research Centre for Third Generation Photovoltaics.

[2] First photovoltaic Devices. From http://www.pveducation.org on 20-06-2019.

[3] Anonymous. (14-09-2018). The Photoelectric Effect. MIT Department of Physics.

[4] The Physics Hypertextbook. From http://www.physics.info/photoelectric/ on 22-06-2019.

[5] Khare, A. (10-2013). One Hundred Years of Boghr Model. Indian Institute of Science, Education and Research (IISER).

[6] Hamza El-Saba, M. (09-2918). Energy Band Theory & Classification of Solids. Ain Shams University.

[7] Neamen, D. A. (08-07-2003). Semiconductor Physics and Devices: Basic Principles. University of New Mexico.

[8] Sze, S. M., Holton, W. C. Semiconductor device, Electronics. From http://www.britannica.com/technology/ on 22-06-2019.

[9] Reig, C. (11-09-2005). Semiconductores intrínsecos y extrínsecos. Universitat de València.

[10] Photoelectric effect, Physics. From http://www.britannica.com/science/ on 27-06-2019.

[11] Sproul, A. (Unknwown). Understanding the p-n junction. The Key Centre for Photovoltaics Engineering, University of New South Wales, Sidney.

[12] Lorenzini, P. (Unknown). PN Junction Theory. Polytech Nice Sophia.

[13] Kalkman, T., Verweg, M. (28-06-2017). The general working of solar cells and the correlation between diffuseness and temperature, irradiance and spectral shape. Physics and Astronomy, University of Amsterdam.

[14] Said, S., Massoud, A., Benammar, M., Ahmed, S. (31-12-2012). A Matlab/Simulink-Based Photovoltaic Array Model Employing SimPowerSystems Toolbox. Journal of Energy and Power Engineering 6.

[15] Shockley, W., Queisser, H. J. (31-10-1960). Detailed Balance Limit of Efficiency of p-n

Junction Solar Cells. Journal of Applied Physics, Volume 32, Number 3.

[16] Koirala, B. P., Sahan, B., Henze, N. (09-2014). Study on MPP mismatch losses in photovoltaic applications. Institute of Solar Energy Technology, Kassel, Germany.

[17] BU-409: Charging Lithium-Ion. From http://www.batteryuniversity.com/learn/article on 03-07-2019.

[18] El Kamouny, K., Laksslr, B., Mahmoudi, H. (01-2015). Smart Solar Battery Charge for PV Application. Journal of Power Electronics. Journal of Power Electronics.

[19] Sarradell, J. (06-2017). Renewable Energy Microgrid: Design and Simulation. Universitat Politècnica de Catalunya.

[20] Cleveland, T., Dearborn, S. Developing Affordable Mixed-Signal Power Systems for Battery Charger Applications. Microchip Technology Inc.

[21] Banaei, M. R., Shirinabady, M. R., Mirzaey, M. (01-2014). MPPT control of Photovoltaics using SEPIC converter to reduce the input current ripples. Journal of Engineering Research and Applications, Volume 4, Issue 1, Version 2, pp.160-166.

[22] Pérez-Burgos, A., Bilbao, J., de Miguel, A., Román, R. (2013). Analysis of Solar Direct Current Irradiance in Spain. 2013 ISES Solar World Congress, Department of Applied Physics, Universidad de Valladolid.

[23] Sendy, A. (06-03-2019). Pros and Cons of Monocrystalline vs. Polycrystalline solar panels. From http://www.solarreviews.com/blog/ on 10-08-2019.

[24] Datasheet: Flisom eFlex 1.6m – for Buildings and Mobility. Flisom.

[25] Datasheet: LT8495. Linear Technology, Analog Devices.

[26] Datasheet: MCP73841/2/3/4. Microchip Technology Inc.

[27] García, R. (07-2013). Estudio de la Huella de Carbono de los hogares españoles: Evolución nacional (1998-2011) y por Comunidades Autónomas (2006-2011). Proyecto de fin de carrera, Universidad Politécnica de Madrid.

ETSEIB

Appendix

A. Datasheet: Flisom e-Flex 1.6m

SWISS ✚ MADE

eFlex 1.6m – for Buildings & Mobility

Description

The eFlex is a flexible and lightweight solar panel designed for integration into roofs, structures with limited load bearing capacity, mobility applications on trailers, RVs, boats and many more demanding applications.

Features

- Most elegant and aesthetic solar module, beautiful uniform design
- High energy yield due to excellent shadow tolerance and temperature stability
- Applicable for curved surfaces – bendable
- Ultra-low weight, < 2kg/m2
- Unbreakable & robust - no glass, no micro cracks
- EL tested
- Made in Switzerland
- Available in 0.8m, 1.6m, 2.3m and 3.1m length

eFlex – for Buildings & Mobility

Flisom
Flexible Solar Modules
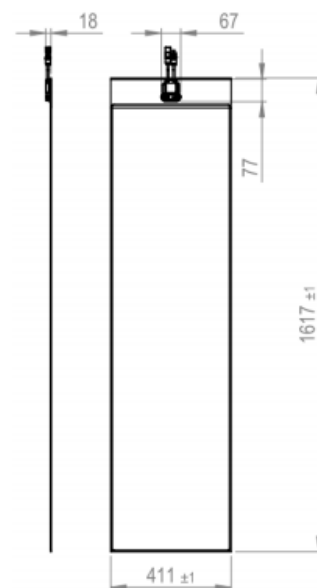
Dimensions				
Length	[mm]	1617		
Width	[mm]	411		
Thickness at module	[mm]	2.2		
Thickness at J-Box	[mm]	21 ± 1		
Weight	[Kg]	1.3		

Electrical characteristics at STC[1] Model number			FF 50	FF 55	FF 60
Nominal power	Pmpp	[W]	50	55	60
Tolerance		[W]	-0/+5	-0/+5	-0/+5
Voltage at nom. power	Vmpp	[V]	34	35	36
Current at nom. power	Impp	[A]	1.47	1.54	1.66
Open circuit voltage	Voc	[V]	46	47	48
Short circuit current	Isc	[A]	1.72	1.82	1.91
Max. system voltage	IEC	[V]	1000		
Max. serial fuse rating		[A]	10		

Thermal characteristics			
Temperature coefficient	Voc	[%/°C]	-0.3
Temperature coefficient	Isc	[%/°C]	0.01
Temperature coefficient	Pmpp	[%/°C]	-0.35

Operating conditions		
Temperature range	[°C]	-40 to +85
Max. mechanical load		2400 Pa, 245 kg/m2

Additional data	
Cell type	Flexible CIGS
Junction box	Front side including bypass diode, IP67, MC4 type / MC4 connectors, 700mm long cable (4 mm2)
Encapsulation	Fluoropolymer front sheet / plastic back sheet
Parallel connection	Y-connector available
Customization	Possible on request for larger volumes / Optional front and back-side junction box

Warranty & certification	
Performance guarantee	10 years on 90% of Pmpp under STC[1] & 20 year on 80% of Pmpp under STC[1]
Warranty	5 years' workmanship after delivery date
Certification	EN IEC 61646; EN IEC 61730-1 &-2
Safety class	II

Notes
[1] STC: 1000 W/m2, AM1.5G, 25°C, stabilized module state
[2] Note covered under current certifications

We continuously develop our products. Electrical and physical properties subject to change without prior notice.

Flisom AG, Gewerbestr 16, CH-8155 Niederhasli   Phone +41 (0) 44 824 3000 Fax +41 (0) 44 824 3001   sales@flisom.ch www.flisom.com

ETSEIB

B.   Datasheet: Linear Technology Inc – LT8495

LINEAR TECHNOLOGY | NOW PART OF **ANALOG DEVICES**

LT8495

SEPIC/Boost Converter with 2A, 70V Switch, 9µA Quiescent Current, POR and Watchdog Timer

FEATURES

- **Wide Input Voltage Range of ~1V to 60V (2.5V to 32V for Start-Up)**
- **Low Ripple Burst Mode® Operation**
  - **9µA I_Q at 12V_{IN} to 5.0V_{OUT}**
  - **Output Ripple (<10mV Typ.)**
- **Dual Supply Pins:**
  - **Improves Efficiency**
  - **Reduces Minimum Supply Voltage to ~1V after Start-Up to Extend Battery Life**
- **Integrated 2A/70V Power Switch**
- **Programmable Watchdog Timer Can Operate When V_{IN} Supply Is Removed**
- **Programmable Power-On Reset Timer (POR) with $\overline{RST}$ Functional for Input Supply Down to 1.3V**
- **FMEA Fault Tolerant in TSSOP Package**
- **Fixed Frequency PWM, SEPIC/BOOST/FLYBACK Topologies**
- **Programmable Switching Frequency: 250kHz to 1.5MHz**
- **UVLO Programmable on SWEN and $\overline{RSTIN}$ Pins**
- **Soft-Start Programmable with One Capacitor**
- **Small 20-Lead QFN or 20-Lead TSSOP Packages**

APPLICATIONS

- Automotive ECU Power
- Power for Portable Products
- Industrial Supplies

DESCRIPTION

The LT®8495 is an adjustable frequency (250kHz to 1.5MHz) monolithic switching regulator with a power-on reset and watchdog timer. Quiescent current can be less than 9µA when operating and is ~0.3µA when SWEN, WDE and $\overline{RSTIN}$ are low. Configurable as a SEPIC, boost or flyback converter, the low ripple Burst Mode operation maintains high efficiency at low output current while keeping output ripple below 10mV. Dual supply pins (V_{IN} and BIAS) allow the part to automatically operate from the most efficient supply. Input supply voltage can be up to 60V for SEPIC topologies and up to 32V (with ride-through up to 60V) for boost and flyback topologies. After start-up, battery life is extended since the part can draw current from its output (BIAS) even when V_{IN} voltage drops below 2.5V.

The reset and watchdog timeout periods are independently adjustable using external capacitors. Using a resistor divider on the SWEN pin provides a programmable undervoltage lockout (UVLO) for the converter. A resistor divider connected to $\overline{RSTIN}$ provides UVLO control that asserts the $\overline{RST}$ pin.

Additional features such as frequency foldback and soft-start are integrated. Fault tolerance in the TSSOP allows for adjacent pin shorts or an open without raising the output voltage above its programmed value. The LT8495

is available in 20-lead QFN and 20-lead TSSOP packages with exposed pads for low thermal resistance.

TYPICAL APPLICATION

450kHz, 5V Output SEPIC Converter

No-Load Supply Current

Efficiency

8495fb

1

ETSEIB
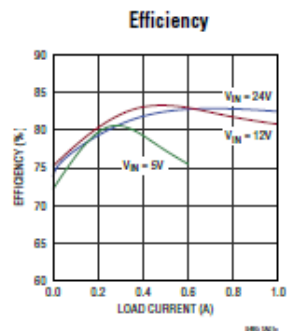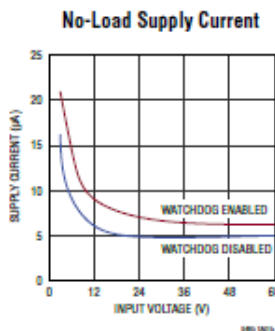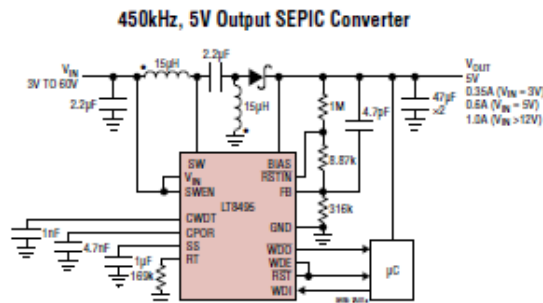
LT8495

ABSOLUTE MAXIMUM RATINGS

(Note 1)

V_{IN}, BIAS Voltage 60V
SWEN, WDE, $\overline{RSTIN}$ Voltage 60V
FB Voltage 60V
SW Voltage 70V
WDI, $\overline{RST}$, $\overline{WDO}$ Voltage 6V
RT Voltage 6V

CPOR, CWDT, SS Voltage 3V
Operating Junction Temperature Range
    LT8495E, LT8495I (Notes 2, 3) .....−40°C to 125°C
    LT8495H (Notes 2, 3) .....−40°C to 150°C
Storage Temperature Range .....−65°C to 150°C
Lead Temperature (Soldering, 10 sec)
    FE Package .....300°C

PIN CONFIGURATION

TOP VIEW

FE PACKAGE
20-LEAD PLASTIC TSSOP
$\theta_{JA} = 38°C/W$
EXPOSED PAD (PIN 21) IS GND, MUST BE SOLDERED TO PCB

BIAS	1	20 SW
FB	2	19 NC
FB	3	18 V$_{IN}$
NC	4	17 NC
CPOR	5	16 WDI
CWDT	6	15 $\overline{WDO}$
$\overline{RST}$	7	14 GND
SS	8	13 WDE
NC	9	12 SWEN
RT	10	11 $\overline{RSTIN}$

21 GND

TOP VIEW

UF PACKAGE
20-LEAD (4mm × 4mm) PLASTIC QFN
$\theta_{JA} = 47°C/W$
EXPOSED PAD (PIN 21) IS GND, MUST BE SOLDERED TO PCB

SS	1	15 GND
RT	2	14 GND
GND	3	13 GND
GND	4	12 SW
$\overline{RSTIN}$	5	11 GND

Top pins: $\overline{RST}$ (20), CWDT (19), CPOR (18), FB (17), BIAS (16)
Bottom pins: SWEN (6), WDE (7), $\overline{WDO}$ (8), WDI (9), V$_{IN}$ (10)

21 GND

ORDER INFORMATION   http://www.linear.com/product/LT8495#orderinfo

LEAD FREE FINISH	TAPE AND REEL	PART MARKING*	PACKAGE DESCRIPTION	TEMPERATURE RANGE
LT8495EUF#PBF	LT8495EUF#TRPBF	8495	20-Lead (4mm × 4mm) Plastic QFN	−40°C to 125°C
LT8495IUF#PBF	LT8495IUF#TRPBF	8495	20-Lead (4mm × 4mm) Plastic QFN	−40°C to 125°C
LT8495EFE#PBF	LT8495EFE#TRPBF	LT8495FE	20-Lead Plastic TSSOP	−40°C to 125°C
LT8495IFE#PBF	LT8495IFE#TRPBF	LT8495FE	20-Lead Plastic TSSOP	−40°C to 125°C
LT8495HFE#PBF	LT8495HFE#TRPBF	LT8495FE	20-Lead Plastic TSSOP	−40°C to 150°C

Consult LTC Marketing for parts specified with wider operating temperature ranges. *The temperature grade is identified by a label on the shipping container.

For more information on lead free part marking, go to: http://www.linear.com/leadfree/
For more information on tape and reel specifications, go to: http://www.linear.com/tapeandreel/. Some packages are available in 500 unit reels through designated sales channels with #TRMPBF suffix.

8495fb

2

ETSEIB

LT8495

ELECTRICAL CHARACTERISTICS

The ● denotes the specifications which apply over the full operating junction temperature range, otherwise specifications are at T_A = 25°C. V_{IN} = V_{SWEN} = 12V, V_{BIAS} = V_{WDE} = 5V, unless otherwise noted (Note 2).

PARAMETER	CONDITIONS		MIN	TYP	MAX	UNITS
$\overline{RSTIN}$ Pin Current (Note 7)	V_{RSTIN} = 1.2V			0	25	nA
	V_{RSTIN} = 5V			35	200	nA
	V_{RSTIN} = 12V			240	550	nA
$\overline{RSTIN}$ Threshold as % of V_{FB} Regulation Voltage		●	86	92	97	%
$\overline{RSTIN}$ Low to $\overline{RST}$ Asserted (t_{UV})	Step V_{RSTIN} from 1.3V to 0.9V	●	8	23	60	µs
Watchdog Timeout and Reset Delay Period (t_{RST}) (Note 8)	C_{POR} = 4700pF, Watchdog Timeout Not Occurring at Same Time as the Reset Delay	●	8.5	9.5	11.85	ms
Watchdog Upper Boundary (t_{WDU}) (Note 8)	C_{WDT} = 1000pF	●	14.9	16.7	20.9	ms
Watchdog Lower Boundary (t_{WDL}) (Note 8)	C_{WDT} = 1000pF	●	580	650	812	µs
$\overline{RST}$ Output Voltage Low	I_{SINK} = 1.25mA	●		33	150	mV
	I_{SINK} = 100µA, V_{BIAS} = 1.3V, V_{IN} = 0V	●		15	150	mV
	I_{SINK} = 100µA, V_{IN} = 1.3V, V_{BIAS} = 0V	●		15	150	mV
$\overline{RST}$ Leakage Current	V_{RSTIN} = 1.2V, $V_{\overline{RST}}$ = 5V (LT8495E, LT8495I)	●		0	0.3	µA
	V_{RSTIN} = 1.2V, $V_{\overline{RST}}$ = 5V (LT8495H)	●		0	1.0	µA
$\overline{WDO}$ Output Voltage Low	I_{SINK} = 1.25mA	●		120	420	mV
$\overline{WDO}$ Leakage Current	$V_{\overline{WDO}}$ = 5V	●		0	0.25	µA
WDI Pin Current	V_{WDI} = 5V			0	0.1	µA
WDI Input Rising Threshold		●	0.4	0.8	1.25	V
WDI Voltage Hysteresis				58		mV
WDI Input Pulse Width		●	300			ns
WDE Pin Current (Note 7)	V_{WDE} = 1.2V			0	25	nA
	V_{WDE} = 5V			35	200	nA
	V_{WDE} = 12V			240	550	nA
WDE Rising Voltage Threshold		●	0.9	1	1.1	V
WDE Voltage Hysteresis				30		mV

Note 1: Stresses beyond those listed under Absolute Maximum Ratings may cause permanent damage to the device. Exposure to any Absolute Maximum Rating condition for extended periods may affect device reliability and lifetime. Voltages are with respect to GND pin unless otherwise noted.

Note 2: The LT8495E is guaranteed to meet performance specifications from 0°C to 125°C junction temperature. Specifications over the −40°C to 125°C operating junction temperature range are assured by design, characterization and correlation with statistical process controls. The LT8495I is guaranteed to meet performance specifications from −40°C to 125°C junction temperature. The LT8495H is guaranteed over the full −40°C to 150°C operating junction temperature range. Operating lifetime is derated at junction temperatures greater than 125°C.

Note 3: This IC includes overtemperature protection that is intended to protect the device during momentary overload conditions. Junction temperature will exceed the maximum operating range when

overtemperature protection is active. Continuous operation above the specified maximum operating junction temperature may impair device reliability.

Note 4: See Power Supplies and Operating Limits in the Applications Information section for more details.

Note 5: Current limit guaranteed by design and/or correlation to static test. Slope Compensation reduces current limit at higher duty cycles.

Note 6: Max duty cycle current limit measured at 1MHz switching frequency.

Note 7: Polarity specification for all currents into pins is positive. All voltages are referenced to GND unless otherwise specified.

Note 8: This specification is guaranteed for only the exact capacitance as listed in the conditions. Variation of the capacitance from the exact listed value will cause proportional variation to t_{RST}, t_{WDU} and t_{WDL}.

8495fb

For more information www.linear.com/LT8495

ETSEIB

LT8495

BLOCK DIAGRAM

2.1V

OVP

SWEN

SS

256k

Q S
SR2
R

1.00V

CHIP
SHUTDOWN

DIE
TEMP
165°C

34V

V_{IN}

2.4V

SUPPLY
SELECT
LOGIC

100mV

DISABLE PSD

VOLTAGE
REFS

2.1V
1.10V
1.00V
OTHERS

34V

BIAS

2.4V

SOFT-
START

I_{LIMIT}
VC_LIMITER

A1

VC

Burst
Mode
DETECT

LOW POWER MODE

1.202V

SW

Q1

FB

FREQUENCY
FOLDBACK

QUADRATIC
RAMP
GENERATOR

Σ

A3

R Q
SR1
S

POWER
SWITCH
DRIVER

RT

ADJUSTABLE
OSCILLATOR

A2

GND

$\overline{RSTIN}$

$\overline{RST}$

$\overline{PGOOD}$

RESET

ADJUSTABLE
RESET PULSE
GENERATOR

$\overline{WDO}$

1.10V

CHIP
SHUTDOWN

WATCHDOG
TIMEOUT

2.3µA

2.3µA

WDE

1.00V

ENABLE

WDI

TRANSITION
DETECT

WATCHDOG
TIMER

CPOR

23µA

23µA

CWDT

8495 BD

10

8495fb

For more information www.linear.com/LT8495

ETSEIB

LT8495

TIMING DIAGRAMS

Start-Up Timing

$\overline{RSTIN}$ Timing
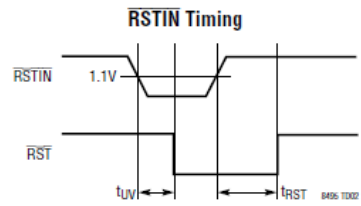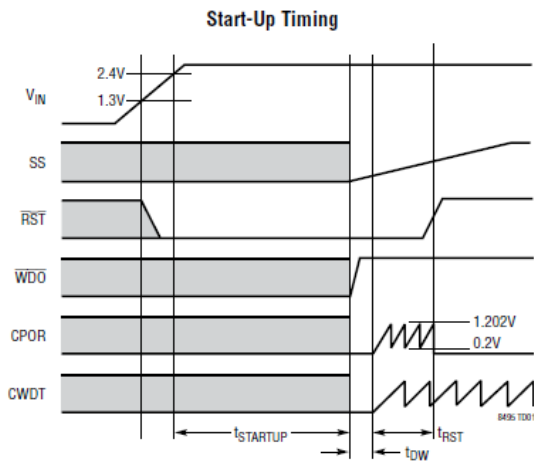
Watchdog Timing, Lower Boundary
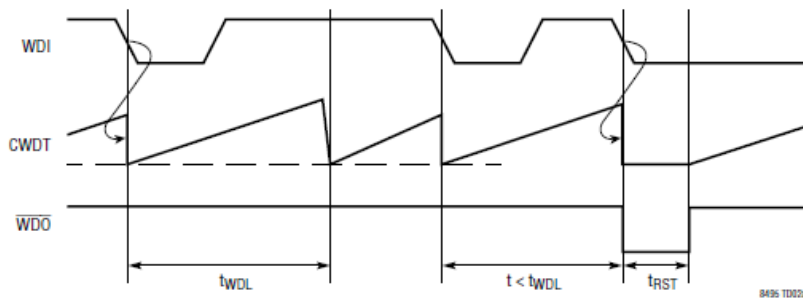
Watchdog Timing, Upper Boundary
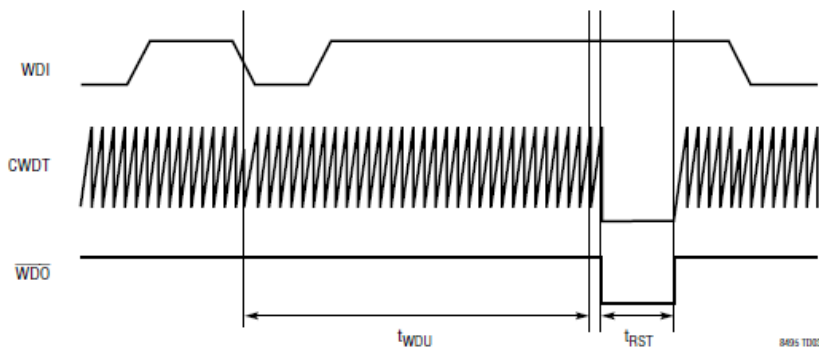
$t_{STARTUP}$ = TIME REQUIRED TO START UP THE CHIP, APPROXIMATELY 1ms
t_{DW} = TIME REQUIRED TO START UP THE WATCHDOG OR POR TIMER, APPROXIMATELY 200µs
t_{UV} = TIME REQUIRED TO ASSERT $\overline{RST}$ LOW AFTER $\overline{RSTIN}$ GOES BELOW ITS THRESHOLD, APPROXIMATELY 23µs
t_{RST} = PROGRAMMED RESET PERIOD
t_{WDU} = WATCHDOG UPPER BOUNDARY PERIOD, APPROXIMATELY 31 RAMPING CYCLES ON CWDT PIN
t_{WDL} = WATCHDOG LOWER BOUNDARY PERIOD, APPROXIMATELY 1 RAMPING CYCLE ON CWDT PIN

8495fb

LT8495

TYPICAL APPLICATIONS

**450kHz, 5V Output SEPIC Converter
(Same as Front Page Application)**

C1, C3: 2.2µF, 100V, X5R, 1206
C2: TAIYO YUDEN, EMK325BJ476MM-T
D1: ONSEMI MBRA2H100
L1, L2: COILTRONICS DRQ125-150-R
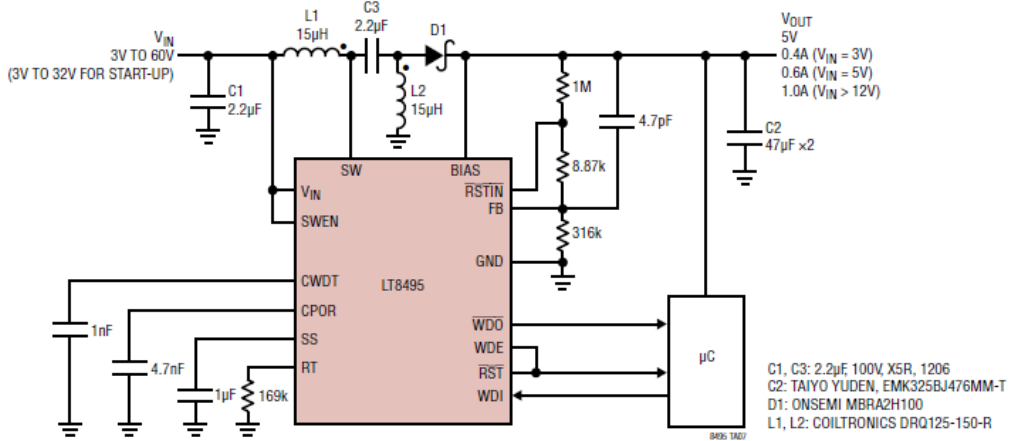
1.5MHz, 12V Output SEPIC Converter

C1, C3: 2.2µF, 50V, X5R, 1206
C2: TAIYO YUDEN, TMK325BJ106MM
D1: CENTRAL SEMI CMMSH2-40
L1, L2: COILTRONICS DRQ74-4R7

Efficiency, V_{IN} = 12V

8495fb
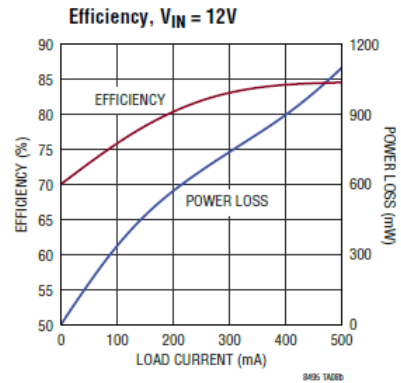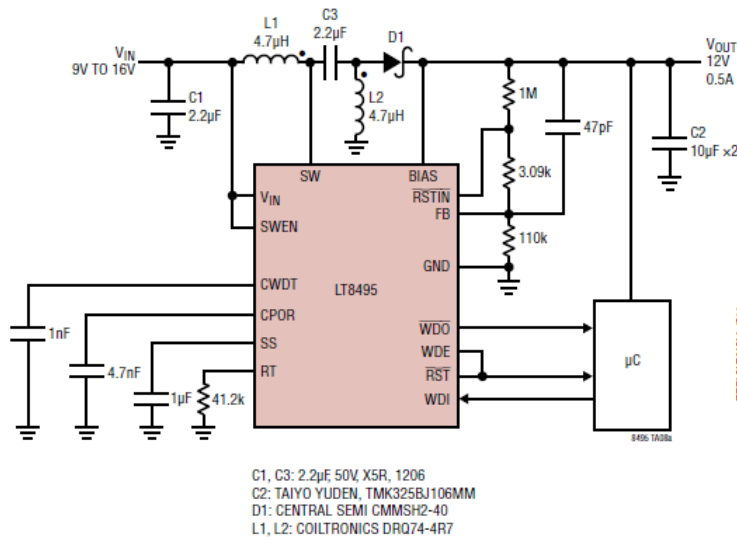
LT8495

PACKAGE DESCRIPTION

Please refer to http://www.linear.com/product/LT8495#packaging for the most recent package drawings.

FE Package
20-Lead Plastic TSSOP (4.4mm)
(Reference LTC DWG # 05-08-1663 Rev L)
Exposed Pad Variation CA
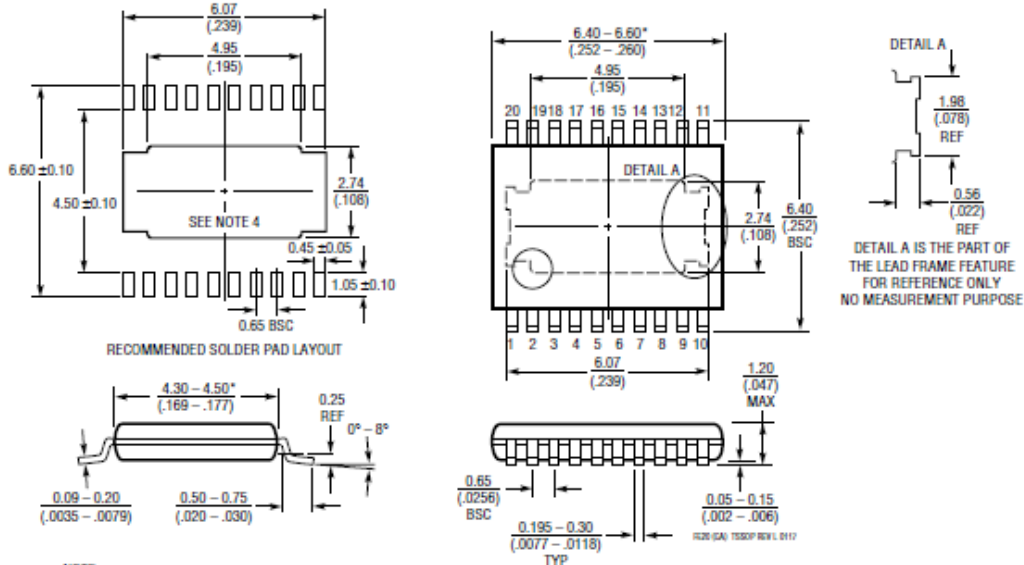
NOTE:
1. CONTROLLING DIMENSION: MILLIMETERS
2. DIMENSIONS ARE IN $\frac{\text{MILLIMETERS}}{\text{(INCHES)}}$
3. DRAWING NOT TO SCALE

4. RECOMMENDED MINIMUM PCB METAL SIZE FOR EXPOSED PAD ATTACHMENT
*DIMENSIONS DO NOT INCLUDE MOLD FLASH. MOLD FLASH SHALL NOT EXCEED 0.150mm (.006") PER SIDE

UF Package
20-Lead Plastic QFN (4mm × 4mm)
(Reference LTC DWG # 05-08-1710 Rev A)

ETSEIB
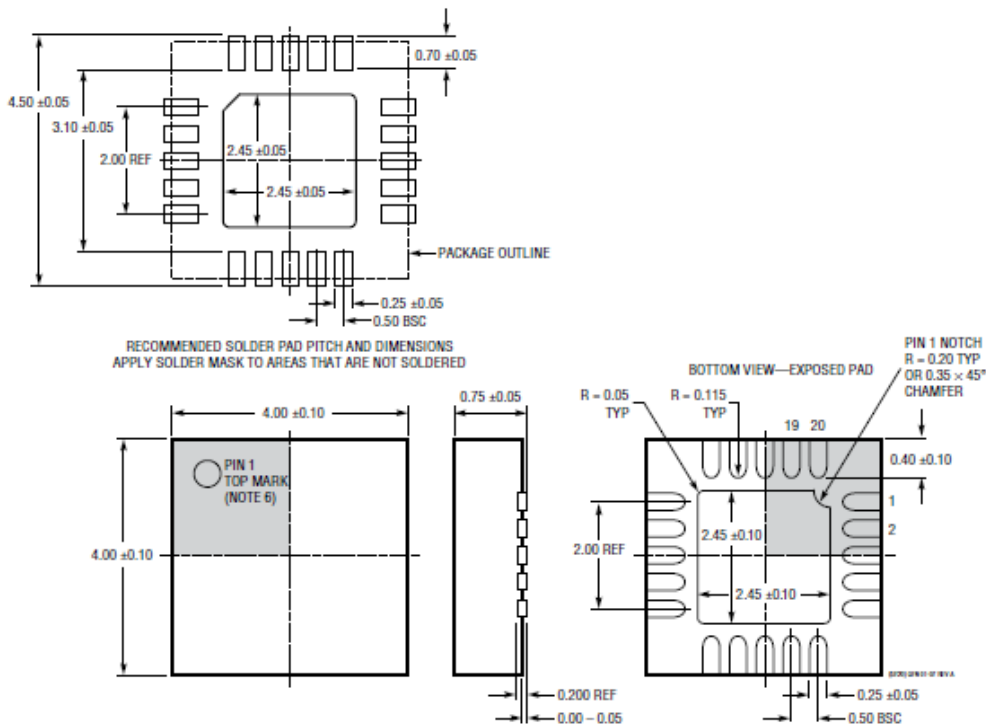
C.   Datasheet: Microchip Technology Inc – MCP73843

MICROCHIP

MCP73841/2/3/4

Advanced Single or Dual Cell Lithium-Ion/ Lithium-Polymer Charge Management Controllers

Features

- Linear Charge Management Controllers
- High-Accuracy Preset Voltage Regulation:
  - $\pm 0.5\%$ (max)
- Four Preset Voltage Regulation Options:
  - 4.1V - MCP73841-4.1, MCP73843-4.1
  - 4.2V - MCP73841-4.2, MCP73843-4.2
  - 8.2V - MCP73842-8.2, MCP73844-8.2
  - 8.4V - MCP73842-8.4, MCP73844-8.4
- Programmable Charge Current
- Programmable Safety Charge Timers
- Preconditioning of Deeply Depleted Cells
- Automatic End-of-Charge Control
- Optional Continuous Cell Temperature Monitoring (MCP73841 and MCP73842)
- Charge Status Output for Direct LED Drive
- Automatic Power-Down when Input Power Removed
- Temperature Range: -40°C to 85°C
- Packaging: MSOP-10 - MCP73841, MCP73842
  MSOP-8 - MCP73843, MCP73844

Applications

- Lithium-Ion/Lithium-Polymer Battery Chargers
- Personal Data Assistants
- Cellular Telephones
- Hand-Held Instruments
- Cradle Chargers
- Digital Cameras
- MP3 Players

Description

The MCP7384X family of devices are highly advanced linear charge management controllers for use in space-limited, cost-sensi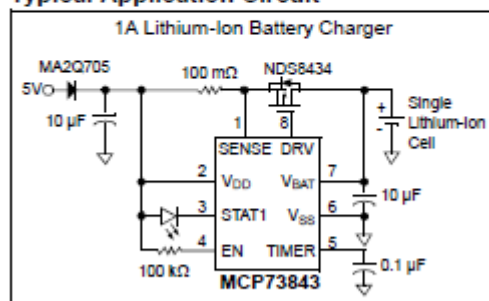tive applications. The MCP73841 and MCP73842 combine high accuracy, constant-voltage, constant-current regulation, cell pre-conditioning, cell temperature monitoring, advanced safety timers, automatic charge termination and charge status indication in space-saving, 10-pin MSOP packages. The MCP73841 and MCP73842 provide complete, fully-functional, stand-alone charge management solutions.

The MCP73843 and MCP73844 employ all the features of the MCP73841 and MCP73842, with the exception of the cell temperature monitor. The MCP73843 and MCP73844 are offered in 8-pin MSOP packages.

The MCP73841 and MCP73843 are designed for applications utilizing single-cell Lithium-Ion or Lithium-Polymer battery packs. Two preset voltage regulation options are available (4.1V and 4.2V) for use with either coke or graphite anodes. The MCP73841 and MCP73843 operate with an input voltage range of 4.5V to 12V.

The MCP73842 and MCP73844 are designed for applications utilizing dual series cell Lithium-Ion or Lithium-Polymer battery packs. Two preset voltage regulation options are available (8.2V and 8.4V). The MCP73842 and MCP73844 operate with an input voltage range of 8.7V to 12V.

The MCP7384X family of devices are fully specified over the ambient temperature range of -40°C to +85°C.

Typical Application Circuit

1A Lithium-Ion Battery Charger

Package Types
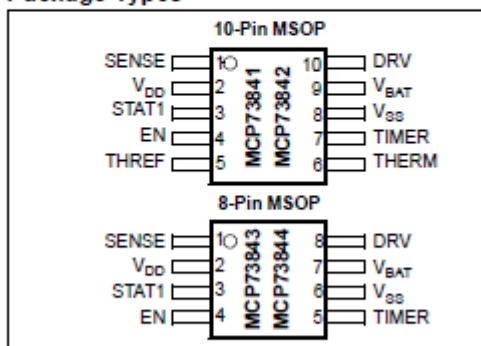
MCP73841/2/3/4

Functional Block Diagram

© 2003-2013 Microchip Technology Inc.

MCP73841/2/3/4

1.0 ELECTRICAL CHARACTERISTICS

Absolute Maximum Ratings †

V_{DD}..13.5V

All inputs and outputs w.r.t. V_{SS} .... -0.3 to (V_{DD}+0.3)V

Current at DRV Pin ....±4 mA

Current at STAT1 Pin ....±30 mA

Maximum Junction Temperature, T_J .... 150°C

Storage temperature ....-65°C to +150°C

ESD protection on all pins:

Human Body Model (1.5 kΩ in Series with 100 pF).......≥ 2 kV

Machine Model (200 pF, No Series Resistance)..............200V

*Notice: Stresses above those listed under "Maximum Ratings" may cause permanent damage to the device. This is a stress rating only and functional operation of the device at those or any 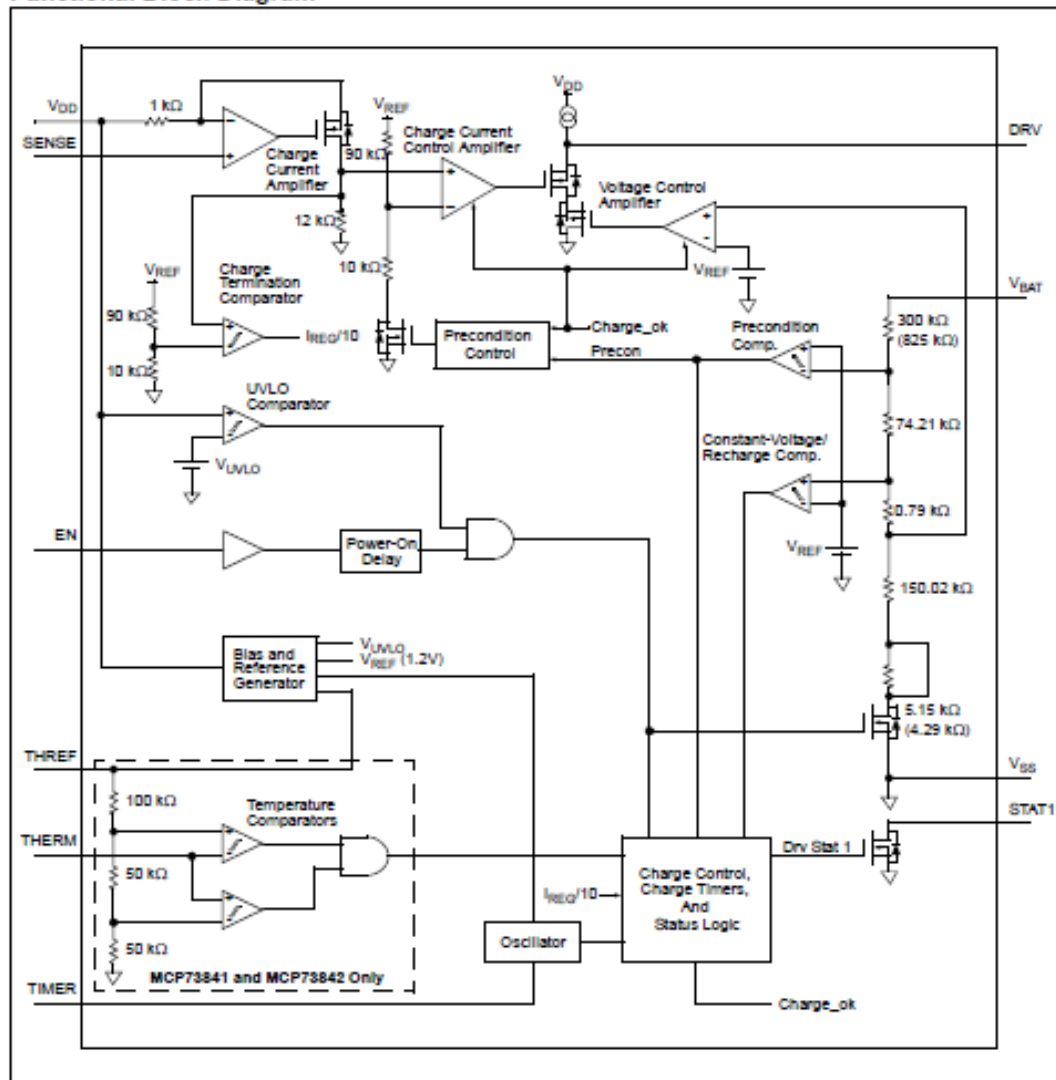other conditions above those indicated in the operational listings of this specification is not implied. Exposure to maximum rating conditions for extended periods may affect device reliability.

DC CHARACTERISTICS

Electrical Specifications: Unless otherwise indicated, all limits apply for V_{DD}= [V_{REG}(Typ)+0.3V] to 12V, T_A = -40°C to +85°C. Typical values are at +25°C, V_{DD} = [V_{REG}(Typ) + 1V].

Parameters	Sym	Min	Typ	Max	Units	Conditions
Supply Input						
Supply Voltage	V_{DD}					
MCP73841, MCP73843		4.5	–	12	V	
MCP73842, MCP73844		8.7	–	12	V	
Supply Current	I_{SS}	–	0.25	4	µA	Disabled
		–	0.75	4	mA	Operating V_{DD} =V_{REG}(Typ)+1V
UVLO Start Threshold	V_{START}					
MCP73841, MCP73843		4.25	4.45	4.60	V	V_{DD} Low-to-High
MCP73842, MCP73844		8.45	8.65	8.90	V	V_{DD} Low-to-High
UVLO Stop Threshold	V_{STOP}					
MCP73841, MCP73843		4.20	4.40	4.55	V	V_{DD} High-to-Low
MCP73842, MCP73844		8.40	8.60	8.85	V	V_{DD} High-to-Low

Voltage Regulation (Constant-Voltage Mode)						
Regulated Output Voltage	V_{REG}					
MCP73841-4.1, MCP73843-4.1		4.079	4.1	4.121	V	V_{DD} = [V_{REG}(Typ)+1V], I_{OUT} = 10 mA, T_A = -5°C to +55°C
MCP73841-4.2, MCP73843-4.2		4.179	4.2	4.221	V	V_{DD} = [V_{REG}(Typ)+1V], I_{OUT} = 10 mA, T_A = -5°C to +55°C
MCP73842-8.2, MCP73844-8.2		8.159	8.2	8.241	V	V_{DD} = [V_{REG}(Typ)+1V], I_{OUT} = 10 mA, T_A = -5°C to +55°C
MCP73842-8.4, MCP73844-8.4		8.358	8.4	8.442	V	V_{DD} = [V_{REG}(Typ)+1V], I_{OUT} = 10 mA, T_A = -5°C to +55°C
Line Regulation	$|(\Delta V_{BAT}/V_{BAT})|/\Delta V_{DD}$	–	0.025	0.25	%/V	V_{DD} = [V_{REG}(Typ)+1V] to 12V, I_{OUT} = 10 mA
Load Regulation	$|\Delta V_{BAT}|/V_{BAT}$	–	0.01	0.25	%	I_{OUT} = 10 mA to 150 mA, V_{DD} = [V_{REG}(Typ)+1V]
Supply Ripple Attenuation	PSRR	–	-58	–	dB	I_{OUT} = 10 mA, 100 Hz
		–	-42	–	dB	I_{OUT} = 10 mA, 1 kHz
		–	-30	–	dB	I_{OUT} = 10 mA, 10 kHz
Output Reverse Leakage Current	$I_{DISCHARGE}$	–	0.4	1	µA	V_{DD} Floating, V_{BAT} = V_{REG}(Typ)
Current Regulation (Fast Charge Constant-Current Mode)						
Fast Charge Current Regulation Threshold	V_{FCS}	100	110	120	mV	$V_{DD} - V_{SENSE}$, T_A = -5°C to +55°C

© 2003-2013 Microchip Technology Inc.

ETSEIB

MCP73841/2/3/4

DC CHARACTERISTICS (CONTINUED)

Electrical Specifications: Unless otherwise indicated, all limits apply for V_{DD}= [V_{REG}(Typ)+0.3V] to 12V, T_A = -40°C to +85°C. Typical values are at +25°C, V_{DD} = [V_{REG}(Typ) + 1V].

Parameters	Sym	Min	Typ	Max	Units	Conditions
Preconditioning Current Regulation (Trickle Charge Constant-Current Mode)						
Precondition Current Regulation Threshold	V_{PCS}	5	10	15	mV	$V_{DD} - V_{SENSE}$, T_A = -5°C to +55°C
Precondition Threshold Voltage	V_{PTH}					
MCP73841-4.1, MCP73843-4.1		2.70	2.80	2.90	V	V_{BAT} Low-to-High
MCP73841-4.2, MCP73843-4.2		2.75	2.85	2.95	V	V_{BAT} Low-to-High
MCP73842-8.2, MCP73844-8.2		5.40	5.60	5.80	V	V_{BAT} Low-to-High
MCP73842-8.4, MCP73844-8.4		5.50	5.70	5.90	V	V_{BAT} Low-to-High
Charge Termination						
Charge Termination Threshold	V_{TCS}	4	7	10	mV	$V_{DD} - V_{SENSE}$, T_A = -5°C to +55°C
Automatic Recharge						
Recharge Threshold Voltage	V_{RTH}					
MCP73841, MCP73843		V_{REG}-300 mV	V_{REG}-200 mV	V_{REG}-100 mV	V	V_{BAT} High-to-Low
MCP73842, MCP73844		V_{REG}-600 mV	V_{REG}-400 mV	V_{REG}-200 mV	V	V_{BAT} High-to-Low

Parameters	Sym	Min	Typ	Max	Units	Conditions
External MOSFET Gate Drive						
Gate Drive Current	I_{DRV}	–	2	–	mA	Sink, CV Mode
		–	-0.5	–	mA	Source, CV Mode
Gate Drive Minimum Voltage	V_{DRVMIN}	–	–	1.0	V	V_{DD} = 4.5V
Gate - Source Clamp Voltage	V_{GS}	-7.0	–	-4.5	V	V_{DD} = 12.0V
Thermistor Reference - MCP73841, MCP73842						
Thermistor Reference Output Voltage	V_{THREF}	2.475	2.55	2.625	V	T_A = +25°C, V_{DD} = V_{REG}(Typ)+1V, I_{THREF} = 0 mA
Temperature Coefficient	TC_{THREF}	–	±50	–	ppm/°C	
Thermistor Reference Source Current	I_{THREF}	200	–	–	µA	
Thermistor Reference Line Regulation	$|(\Delta V_{THREF}/V_{THREF})|/\Delta V_{DD}$	–	0.1	0.25	%/V	V_{DD}=[V_{REG}(Typ)+1V] to 12V
Thermistor Reference Load Regulation	$\Delta V_{THREF}/V_{THREF}$	–	0.01	0.10	%	I_{THREF} = 0 mA to 0.20 mA
Thermistor Comparator - MCP73841, MCP73842						
Upper Trip Threshold	V_{T1}	1.18	1.25	1.32	V	
Upper Trip Point Hysteresis	V_{T1HYS}	–	-50	–	mV	
Lower Trip Threshold	V_{T2}	0.59	0.62	0.66	V	
Lower Trip Point Hysteresis	V_{T2HYS}	–	80	–	mV	
Input Bias Current	$|I_{BIAS}|$	–	–	2	µA	
Status Indicator						
Sink Current	I_{SINK}	4	7	12	mA	
Low Output Voltage	V_{OL}	–	200	400	mV	I_{SINK} = 1 mA
Input Leakage Current	I_{LK}	–	0.01	1	µA	I_{SINK} = 0 mA, V_{STAT1} = 12V

ETSEIB

MCP73841/2/3/4

DC CHARACTERISTICS (CONTINUED)

Electrical Specifications: Unless otherwise indicated, all limits apply for V_{DD}= [V_{REG}(Typ)+0.3V] to 12V, T_A = -40°C to +85°C. Typical values are at +25°C, V_{DD} = [V_{REG}(Typ) + 1V].

Parameters	Sym	Min	Typ	Max	Units	Conditions
Enable Input						
Input High-Voltage Level	V_{IH}	1.4	-	–	V	
Input Low-Voltage Level	V_{IL}	–	-	0.8	V	
Input Leakage Current	I_{LK}	–	0.01	1	µA	V_{ENABLE} = 12V

AC CHARACTERISTICS

Electrical Specifications: Unless otherwise indicated, all limits apply for V_{DD}= [V_{REG}(Typ)+0.3V] to 12V, T_A = -40°C to +85°C. Typical values are at +25°C, V_{DD}= [V_{REG}(Typ)+1V].

Parameters	Sym	Min	Typ	Max	Units	Conditions
UVLO Start Delay	t_{START}	–	–	5	msec	V_{DD} Low-to-High
Current Regulation						
Transition Time Out of Preconditioning	t_{DELAY}	–	–	1	msec	V_{BAT}< V_{PTH} to V_{BAT} > V_{PTH}
Current Rise Time Out of Preconditioning	t_{RISE}	–	–	1	msec	I_{OUT} Rising to 90% of I_{REG}
Fast Charge Safety Timer Period	t_{FAST}	1.1	1.5	1.9	Hours	C_{TIMER} = 0.1 µF
Preconditioning Current Regulation						
Preconditioning Charge Safety Timer Period	t_{PRECON}	45	60	75	Minutes	C_{TIMER} = 0.1 µF
Charge Termination						
Elapsed Time Termination Period	t_{TERM}	2.2	3.0	3.8	Hours	C_{TIMER} = 0.1 µF
Status Indicators						
Status Output turn-off	t_{OFF}	–	–	200	µsec	I_{SINK} = 10 mA to 0 mA
Status Output turn-on	t_{ON}	–	–	200	µsec	I_{SINK} = 0 mA to 10 mA

TEMPERATURE SPECIFICATIONS

Electrical Specifications: Unless otherwise specified, all limits apply for V_{DD}= [V_{REG}(Typ)+0.3V] to 12V. Typical values are at +25°C, V_{DD}= [V_{REG}(Typ)+1.0V].

Parameters	Sym	Min	Typ	Max	Units	Conditions
Temperature Ranges						
Specified Temperature Range	T_A	-40		+85	°C	
Operating Temperature Range	T_A	-40		+125	°C	
Storage Temperature Range	T_A	-65		+150	°C	
Thermal Package Resistances						
Thermal Resistance, MSOP-10	θ_{JA}		113		°C/W	4-Layer JC51-7 Standard Board, Natural Convection
Thermal Resistance, MSOP-8	θ_{JA}		206		°C/W	Single-Layer SEMI G42-88 Board, Natural Convection

MCP73841/2/3/4

2.0   TYPICAL PERFORMANCE CURVES

> **Note:** The graphs and tables provided following this note are a statistical summary based on a limited number of samples and are provided for informational purposes only. The performance characteristics listed herein are not tested or guaranteed. In some graphs or tables, the data presented may be outside the specified operating range (e.g., outside specified power supply range) and therefore outside the warranted range.

Note: Unless otherwise indicated, V_{DD} = [V_{REG}(Typ) + 1V], I_{OUT} = 10 mA and T_A = +25°C.
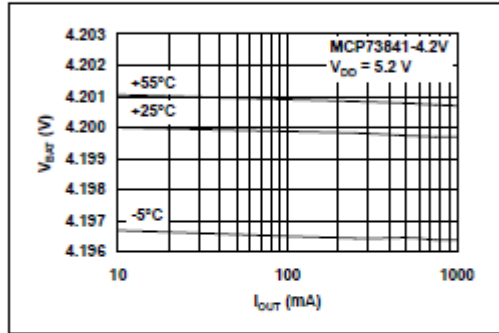

FIGURE 2-1:   Battery Regulation Voltage (V_{BAT}) vs. Charge Current (I_{OUT}).
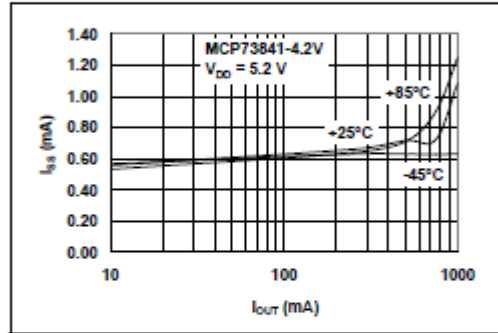

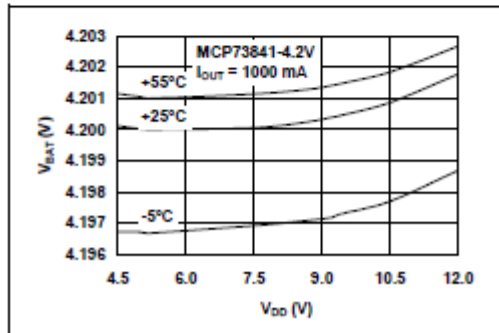**FIGURE 2-4:**   Supply Current (I_{SS}) vs. Charge Current (I_{OUT}).

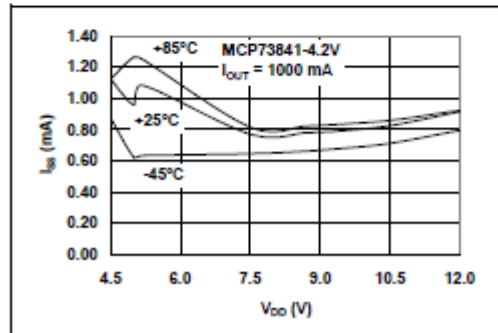**FIGURE 2-2:**   Battery Regulation Voltage (V_{BAT}) vs. Supply Voltage (V_{DD}).

FIGURE 2-5:   Supply Current (I_{SS}) vs. Supply Voltage (V_{DD}).
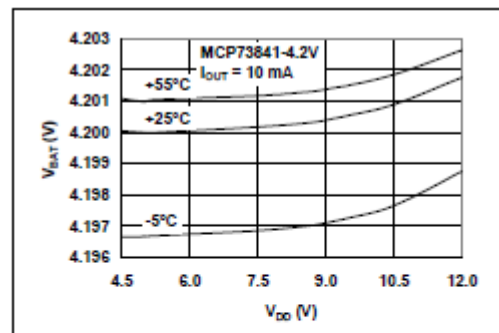

FIGURE 2-3:   Battery Regulation Voltage (V_{BAT}) vs. Supply Voltage (V_{DD}).
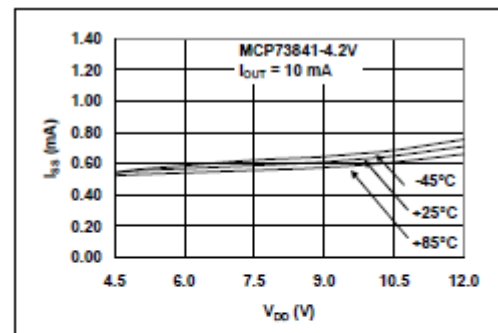

FIGURE 2-6:   Supply Current (I_{SS}) vs. Supply Voltage (V_{DD}).

MCP73841/2/3/4

3.0   PIN DESCRIPTIONS

The descriptions of the pins are listed in Table 3-1.

TABLE 3-1:   PIN DESCRIPTION TABLE

MCP73841, MCP73842 Pin No.	MCP73843, MCP73844 Pin No.	Name	Function
1	1	SENSE	Charge Current Sense Input
2	2	V_{DD}	Battery Management Input Supply
3	3	STAT1	Charge Status Output
4	4	EN	Logic Enable
5	—	THREF	Cell Temperature Sensor Bias
6	—	THERM	Cell Temperature Sensor Input
7	5	TIMER	Timer Set
8	6	V_{SS}	Battery Management 0V Reference
9	7	V_{BAT}	Battery Voltage Sense
10	8	DRV	Drive Output

3.1   Charge Current Sense Input (SENSE)

Charge current is sensed via the voltage developed across an external precision sense resistor. The sense resistor must be placed between the supply voltage (V_{DD}) and the external pass transistor (Q1). A 220 mΩ sense resistor produces a fast charge current of 500 mA, typically.

3.2   Battery Management Input Supply (V_{DD})

A supply voltage of [V_{REG}(Typ) + 0.3V] to 12V is recommended. Bypass to V_{SS} with a minimum of 4.7 µF.

3.3   Charge Status Output (STAT1)

Current limited, open-drain drive for direct connection to a LED for charge status indication. Alternatively, a pull-up resistor can be applied for interfacing to a host microcontroller.

3.4   Logic Enable (EN)

Input to force charge termination, initiate charge, clear faults or disable automatic recharge.

3.5   Cell Temperature Sensor Bias (THREF)

Voltage reference to bias external thermistor for continuous cell temperature monitoring and prequalification.

3.6   Cell Temperature Sensor Input (THERM)

Input for an external thermistor for continuous cell-temperature monitoring and pre-qualification. Apply a voltage equal to 0.85V to disable temperature-sensing.

3.7   Timer Set (TIMER)

All safety timers are scaled by C_{TIMER}/0.1 µF.

3.8   Battery Management 0V Reference (V_{SS})

Connect to negative terminal of battery.

3.9   Battery Voltage Sense (V_{BAT})

Voltage sense input. Connect to positive terminal of battery. Bypass to V_{SS} with a minimum of 4.7 µF to ensure loop stability when the battery is disconnected. A precision internal resistor divider regulates the final voltage on this pin to V_{REG}.
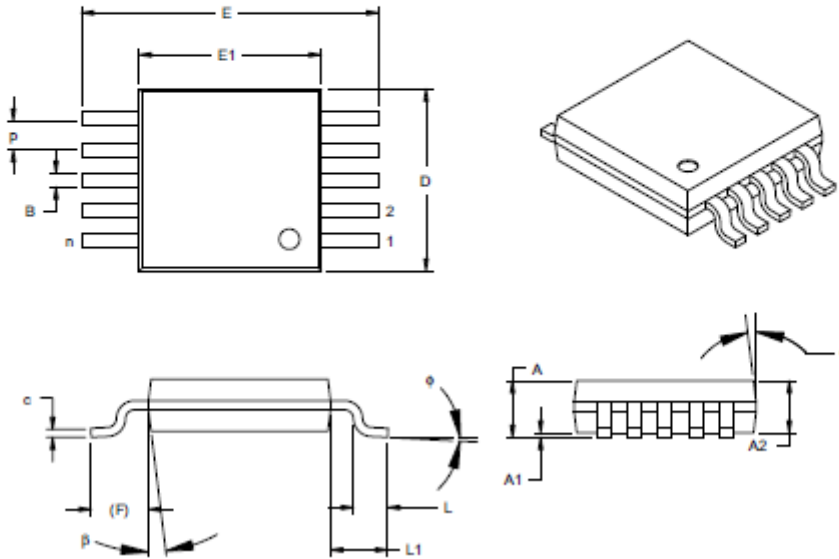
3.10   Drive Output (DRV)

Direct output drive of an external P-channel MOSFET for current and voltage regulation.

ETSEIB

MCP73841/2/3/4

10-Lead Plastic Micro Small Outline Package (UN) (MSOP)

Note: For the most current package drawings, please see the Microchip Packaging Specification located at http://www.microchip.com/packaging

	Units	INCHES			MILLIMETERS*		
Dimension Limits		MIN	NOM	MAX	MIN	NOM	MAX
Number of Pins	n		10			10	
Pitch	p		.020 TYP			0.50 TYP.	
Overall Height	A	-	-	.043	-	-	1.10
Molded Package Thickness	A2	.030	.033	.037	0.75	0.85	0.95
Standoff	A1	.000	-	.006	0.00	-	0.15
Overall Width	E		.193 BSC			4.90 BSC	
Molded Package Width	E1		.118 BSC			3.00 BSC	
Overall Length	D		.118 BSC			3.00 BSC	
Foot Length	L	.016	.024	.031	0.40	0.60	0.80
Footprint	F		.037 REF			0.95 REF	
Foot Angle	φ	0°	-	8°	0°	-	8°
Lead Thickness	c	.003	-	.009	0.08	-	0.23
Lead Width	B	.006	.009	.012	0.15	0.23	0.30
Mold Draft Angle Top	α	5°	-	15°	5°	-	15°
Mold Draft Angle Bottom	β	5°	-	15°	5°	-	15°

*Controlling Parameter

Notes:
Dimensions D and E1 do not include mold flash or protrusions. Mold flash or protrusions shall not exceed .010" (0.254mm) per side.

JEDEC Equivalent: MO-187
Drawing No. C04-021

ETSEIB